Title
Effects of Hydrogen-Oxygen Torch Igniter Combustion Applied to an ABS/GOx Hybrid Rocket System

Author
Ochi, Kellen Kazuaki

Publication Date
2022

Peer reviewed|Thesis/dissertation

Effects of Hydrogen-Oxygen Torch Igniter Combustion Applied to an ABS/GOx Hybrid Rocket System

By

Kellen Kazuaki Ochi

Thesis

Submitted in partial satisfaction of the requirements for the degree of

Master of Science

in

Mechanical and Aerospace Engineering

in the

Office of Graduate Studies

of the

University of California

Davis

Approved:

Paul Erickson, Chair

Nesrin Sarigul-Klijn

Marti Sarigul-Klijn

Committee in Charge

2022

To my parents Natolie and Kaz, brother Ian, and girlfriend Jayce ...

this one is for you.

Contents

List of Figures

List of Tables

Abstract

Effects of Hydrogen-Oxygen Torch Igniter Combustion Applied to an ABS/GOx Hybrid Rocket System

In this work, a hydrogen-oxygen torch igniter was developed and utilized to study the combustion of gaseous oxygen (GOx) and solid acrylonitrile butadiene styrene thermoplastic (ABS) in conjunction with gaseous hydrogen (GH_2) in application to hybrid rocket motors. The effects thereof are not presently found in literature. Initial pyrolysis of the ABS fuel grain was accomplished via products of GH_2 and GOx combustion from a spark initiated torch igniter. In order to isolate the effects of hydrogen to the overall combustion, the mass flow rate of hydrogen and its duration was varied in a factorial design of experiment. It was found that an increase of the hydrogen mass flow rate at constant GOx mass flow rate led to an increase in the average linear regression rate for lean to stoichiometric operating conditions of the torch igniter. Additionally, extending the duration of hydrogen flow, from 10% to 50% of the total burn time, led to an increase in the regression rate. The author posits that the increases in average linear regression rate are due to the hydrogen-oxygen flame applying high heat and mass flux to the surface of the fuel grain, helping to overcome the rate-limiting, endothermic pyrolysis step. However, an increase in the hydrogen mass flow rate, from stoichiometric to rich operating conditions, led to decreases in the average linear regression rate. It is posited that at the fuel-rich operating condition, the hydrogen consumes most of the available oxidizer molecules. This resulted in a competition between the hydrogen gas and the ABS fuel grain for available oxidizer molecules. This theory is further supported by the turbulent boundary layer combustion model presented by Marxman and Gilbert[1]. These results suggest that the hydrogen-oxygen torch igniter can be used not only as a reliable starter, but also for regression rate enhancement that targets the rate-limiting step, pyrolysis, for hybrid rocket combustion at stoichiometric to fuel-lean operating conditions of the torch igniter.

Acknowledgments

I want to thank Professor Paul Erickson for his constant support and care for both me and this project. His mentorship has been invaluable to my growth as a scientist and a human.

Special thanks to my colleagues Garrett Robertson, Michael Horton, Kyle Heinzman, Samar Malhotra, and the entire ERL lab for their time, effort, and friendship.

I also want to thank my family for their constant support and love. From working multiple jobs, Japanese-American internment, and lifetimes of hard work, I am incredibly grateful for those who have laid down the foundation for me to become who I am today.

Lastly, I want to thank my friends who have blessed me with their support and companionship. Countless times of studying, laughing, and support have given me memories that are truly priceless.

Nomenclature

$\dot{m}$	Mass Flow Rate, $\frac{kg}{s}$
$\dot{q}$	Heat Flux, $\frac{kJ}{kg}$
$\dot{r}$	Regression Rate, $\frac{cm}{s}$
λ	Equivalence Ratio = $\frac{O/F_{actual}}{O/F_{stoichiometric}}$
ϕ	Fuel-Air Equivalence Ratio = $\frac{F/A_{actual}}{F/A_{stoichiometric}}$
ρ	Density, $\frac{kg}{m^3}$
τ_{ign}	Characteristic Ignition Time, s
$\vec{F}$	Force, N
$\vec{v}$	Velocity, $\frac{m}{s}$
A_t	Area of the Nozzle Throat, m^2
ABS	Acrylonitrile Butadiene Styrene
AP	Aluminum Perchlorate
c^*	Characteristic Exhaust Velocity of Propellants, $\frac{m}{s}$
c_p	Specific Heat, $\frac{kJ}{kgK}$
CEA	NASA Chemical Equilibrium Application
CH_4	Methane
CO_2	Carbon Dioxide
D	Inner Diameter of a Fuel Grain Port
E_i	Effect of Independent Variable i

FDM Fused-Deposition Modeling

G_{ox} Oxidizer Mass Flux, $\frac{kg}{m^3 s}$

GH_2 Gaseous Hydrogen

GOx Gaseous Oxygen

h Specific Enthalpy, $\frac{kJ}{kg}$

$HTPB$ Hydroxyl-Terminated Polybutadiene

$I_{i,j}$ Interaction of Independent Variables i and j

$L.O.time$ Light-off Time, s

L Length, m

LOx Liquid Oxygen

m Mass, kg

NOx Nitrogen Oxides

O/F Oxidizer to Fuel Ratio

P Pressure, Pa

PE Polyethylene

PLA Polylactic Acid

$PMMA$ Poly-methyl Methacrylate

Pr Prandtl Number

Re Reynolds Number

S_E Standard Error

St Stanton Number

T	Temperature, K
t	Time, s
t^*	Signal-to-Noise Ratio
TEA	Tri-ethylaluminum
TEB	Triethylborane
u_∞	Fluid Velocity, $\frac{m}{s}$

Chapter 1

Introduction

Rockets in general employ Newton's second and third laws of motion. The second law of motion gives the force relation, $\vec{F} = m\vec{a}$, however more pertinently to rockets is the equation for thrust force: $\vec{F}_{thrust} = \dot{m}\vec{v}$. Rockets create thrust through large pressure gradients which can originate from various sources such as pressurized tanks of fluid and/or combustion. These fluids are expelled away from the rocket from the high pressure combustion chamber to the low pressure environment. As a result, the system moves in the opposite direction as governed by Newton's third law which states that all forces have an equal and opposite reactive force. This effect is illustrated in Figure 1.1, where the gaseous products of combustion apply thrust force to the right which induces a reaction force that propels the rocket in the opposite direction. However, if the rocket allows gasses to simply exit the combustion chamber, there will be massive losses in thrust force since the gasses will tend toward any areas of low pressure. Therefore, a nozzle is necessary in order to control the unrestrained expansion of the sonic gasses (gases moving at the speed of sound). Particularly, a converging-diverging nozzle is used in order restrict the rapid expansion of the gasses and focuses the flow in a more singular direction which accelerates the flow past the speed of sound, resulting in a greater exhaust velocity $\vec{v}$ and thus greater thrust force.

By looking at the equation for thrust, increasing the mass flow rate of expelled fluids or increasing the velocity of the fluid particles is necessary to increase the thrust force. Since rockets are usually launched from the Earth's surface, a large amount of thrust force is

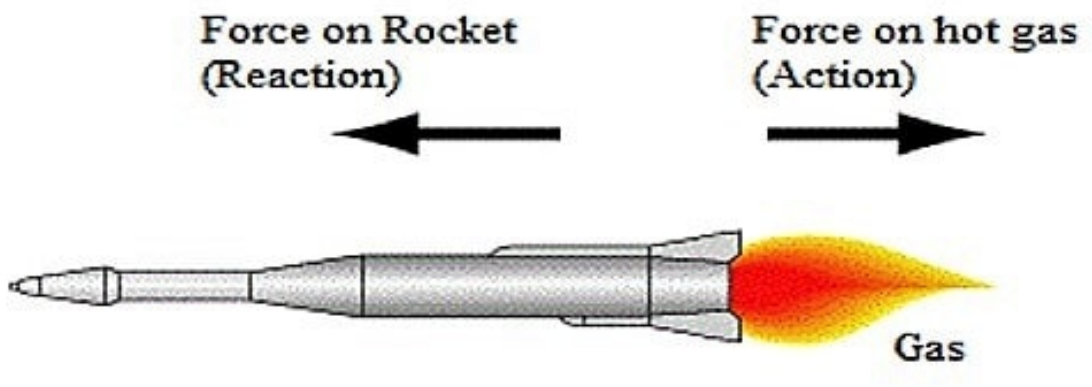

Figure 1.1. Newton's 3rd law of motion applied to rockets.

[2]

required to overcome gravity and aerodynamic drag in order to reach the required apogees or orbital insertion trajectories. In order to reach the thrusts required, combustion is the primary method to achieve both high mass flow rates and exit velocities. Combustion is an exothermic chemical reaction whose reactants are a fuel source, commonly hydrocarbon based, and an oxidizer such as oxygen or air. A series of complex and rapid chemical reactions occur within the combustion chamber which results in a large release of energy. In rockets, the reactants for the combustion process are a part of the overall system mass, thus it is important to have energy dense fuels with the desired chemical reactions to release an adequate amount of usable energy.

Combustion itself is very general and encompasses many chemical combinations. The combustion methods by which rockets generate thrust vary from mission to mission and by manufacturer to manufacturer. Currently there are four main types of rocket propulsion that are used: monopropellant engines, bipropellant engines, solid motors, and hybrid motors. Each have their own strengths and weaknesses and it is up to the mission designers to determine which system is most suitable for the mission requirements. Mission requirements can include: multiple relights, variable thrust profiles, landing, heavy payloads, and

reaction control systems.

1.1 Hybrid Rockets

Hybrid rocket motors are an amalgamation of solid rocket motors and liquid propellant engines. They are a class of rocket motors that usually consist of a solid fuel grain and a fluid oxidizer. Hybrid rockets are meant to marry the benefits of solid and liquid propellant systems while also addressing their detriments. In a hybrid rocket, the oxidizer is no longer incorporated in the solid fuel matrix, as is done in a solid rocket motor, therefore the oxidizer must have its own piping and storage system similar to the bipropellant motor. However, unlike bipropellant systems, hybrid rocket motors usually require only one storage tank and therefore smaller amounts of piping. This results in significant decreases in the overall flight weight and complexity compared to the bipropellant system while still retaining structural strength, rigidity, and simplicity similar to solid rocket motors. Another example of how hybrid rocket motors combine advantages of liquid propulsion and solid propulsion is its ability to throttle its thrust similar to liquid propulsion systems. Throttling is accomplished by controlling the oxidizer mass flow rate which also controls the rate of pyrolysis, also known as gasification, of the solid fuel whereas in a solid rocket motor the rate of pyrolysis is mostly fixed to one predetermined rate. In addition, hybrids are also able to fully stop and restart combustion by controlling the oxidizer mass flow rate. These abilities expand the mission flexibility and capabilities of the hybrid rocket system, making it a worthwhile consideration for propulsion designers.

Traditionally, hybrid rocket motors employ a thermosetting polymer material called hydroxyl-terminated polybutadiene (HTPB) which is a common binding agent for solid rocket fuel grains [3]. However, the solid fuel grains can be practically any hydrocarbon based chemical such as polyethylene (PE), acrylonitrile butadiene styrene (ABS), or polymethyl methacrylate (PMMA). The solid fuel grains used in hybrid rockets are almost always inert at normal room environments, not readily reactive until adequate heat and oxidizer are available, and can be stored for a long duration of time [4–7]. In contrast, since solid rocket propellants have oxidizer incorporated into the chemical structure, they

inherently present a significant fire hazard where greater safety precautions are required in all facets of fabrication, transportation, and installation [8]. However, the benefit of inertness brings the added difficulty of initiating combustion. Since hybrid rockets can fully stop and restart operation, a reliable ignition source that is able to supply enough activation or ignition energy numerous times is required. This is in contrast to solid rocket motors where a single use ignition source such as a pyrotechnic device or a hypergolic combination of di-nitrogen tetra oxide (N_2O_4) and hydrazine (N_2H_4) can be utilized. Due to the importance of ignition for hybrid rocket motors, ignition methods are a significant research interest in the literature.

1.2 Hydrogen and the Hydrogen-Oxygen Torch Igniter

Hydrogen has been the subject of many recent studies due to its promise as a clean energy source. Hydrogen fuel cell electric vehicles (FCEV), such as the Toyota Mirai, utilize an on-board tank of hydrogen to feed a proton exchange membrane (PEM), or more commonly referred to as the fuel cell, in order to produce electricity that powers the motor(s). This process results in electric power with water as the other byproduct. Hydrogen is also commonly used in process called hydrogenation in order to create other chemicals such as ammonia (NH_3) where diatomic hydrogen and nitrogen are combined in the Haber-Bosch process. Another important use for hydrogen, particularly for this research, is its usage in rocket propulsion. Hydrogen, usually as a cryogenic liquid at temperatures of about 20.28K or -423.17 °F, is used in combination with an oxidizer, such as liquid oxygen, to produce highly exothermic reactions that can produce large amounts of thrust force. In addition, the liquid hydrogen can also be used simultaneously both as a fuel and as a coolant in examples such as the Space Shuttle Main Engine (SSME).

First created by NASA Lewis in the late 1970's after NASA eliminated the use of fluorine, the hydrogen-oxygen torch igniter is another example of hydrogen's versatility [9]. Prior to the hydrogen-oxygen torch igniter, NASA Lewis utilized the hypergolic

combination of hydrogen and fluorine as a method of ignition. Other NASA testing facilities mainly used di-nitrogen tetra oxide (N_2O_4) and hydrazine (N_2H_4) as the ignition source, but NASA Lewis never used the hypergolic combination due to their toxicities.

The hydrogen-oxygen torch igniter is a simple system where oxygen and hydrogen combine within a small chamber which has a spark plug fixed to it. The spark applies the activation energy necessary to achieve a rapid exothermic chain reaction between the two gases. If the torch igniter is operated at stoichiometric proportions, the product is steam, but when operated at fuel lean conditions the product stream can be mostly oxygen while maintaining stable combustion [10]. Hydrogen is unique compared to other fuels since it can support combustion until the lower flammability limit of 4% hydrogen by volume in oxygen is reached [11]. This allows a steady stream of unreacted, heated oxygen to enter the main combustion chamber while simultaneously supplying enough activation energy for the main combustion event. This torch igniter was capable of withstanding hundreds of ignitions before needing to be replaced.

As previously stated, hybrid rockets motors are able to both throttle and fully stop and restart operation similar to a liquid propellant rockets while also retaining the structurally strong and energy dense solid fuel grains. Because the oxidizer is not incorporated within the solid fuel grain, a myriad of options for fuel grains that are inherently safer to handle and produce are available. However, the benefits seen are not without their challenges. The method of ignition with high enough repeatability, durability, and activation energy being the central challenge. Therefore, a device such as the hydrogen-oxygen torch igniter is seen to be a good solution to the ignition problem. Hydrogen is extremely reactive in the presence of an oxidizer and with the appropriate activation energy it can produce a fast and hot flame. As proven by NASA Lewis, the hydrogen-oxygen torch igniter exhibits all the key desires for a hybrid rocket motor ignition. This body of work looks to investigate the application of the hydrogen-oxygen torch igniter to a hybrid rocket and to document its effects thereof which is not presently found in the literature. To accomplish this, a review of previous investigations relevant to the subject, a summary of the Energy Research Lab hybrid rocket build, an explanation of the design of experiment, review and

discussion of the collected data, and recommendations for future works will be presented.

Chapter 2

Literature Review

In this section, a comprehensive literary review was conducted in order to demonstrate how the current work seeks to contribute to the literature. An overview of the various rocket propulsion types, hybrid rockets, hybrid rocket ignition systems, ABS, and hydrogen is presented.

2.1 Rocket Propulsion Types

2.1.1 Monopropellant Rockets

Monopropellant rockets are a class of rocket engines that utilize the decomposition of a singular propellant which has its oxidizer and fuel built into its chemical matrix. Monopropellants commonly utilize catalytic decomposition or heating to produce a large exothermic reaction, thus creating a large pressure gradient between the combustion chamber and the nozzle exit. A common monopropellant that easily demonstrates this is hydrazine (N_2H_4). Hydrazine is stored as a liquid within a tank and in order to access the energy that is required to propel the rocket, the hydrogen and nitrogen must be separated from each other. To do this, the hydrazine passes over a catalyst which provides sites where decomposition reactions occur to break the intermolecular bonds [12]. This decomposition reaction forms ammonia (NH_3) and nitrogen (N_2) exothermically, therefore increasing temperatures and pressures within the combustion chamber.

Monopropellants are advantageous because of their lower complexity and lower weight cost as compared to bipropellants [13]. However, monopropellants usually require cat-

alysts which can add significant weight and can also limit the total run time due to catalyst degradation. Similar to bipropellant rockets, monopropellants can be throttled by adjusting the mass flow rate of propellant and can be restarted from a full shut down. However, monopropellants pose a significant risk as well. Because the fuel and oxidizer are chemically mixed together, the mixture can be extremely explosive which makes handling and transportation expensive and dangerous. Therefore, monopropellants need to be thermally and chemically stable in order to store and transport.

2.1.2 Bipropellant Rockets

Bipropellant rockets differ from monopropellant rockets because instead of using one fluid as the fuel and oxidizer, the bipropellant system has the fuel and oxidizer separated as different fluids. Most bipropellant systems use propellants that are in the liquid phase such as liquid methane (LNG: Liquid Natural Gas) or RP-1 and a liquid oxidizer such as oxygen (LO_x). This system is similar to the monopropellant in construction except there are two tanks rather than one which increases the system complexity and size.

Bipropellant rockets typically possess high performance characteristics while using less volatile propellants as the monopropellant system requires. They generally have the best thrust-to-weight ratio and specific power making them more ideal for ground launches [3]. In addition, bipropellant rockets are able to throttle its thrust to around 10% of full thrust which expands its mission capabilities [14–16]. For this reason, it is common to see large scale operations such as SpaceX and NASA utilize this system in rockets such as the Space Shuttle Main Engine (SSME) and the recent SpaceX Falcon 9.

While transportation and storage of propellants is less dangerous as compared to monopropellants, it is still a costly process to utilize the full benefits of bipropellant systems. Because many of the propellants are in the liquid phase, storage and transportation commonly require cryogenic cooling solutions. This is an energy intensive process that commonly utilizes other cryogenic fluids to keep propellants at storage temperatures. In addition, cryogenic fluids require thicker and more expensive containers and piping since the temperatures of cryogens may cause structural failures to common metals [17]. Another complication is that propellants must be pumped into the run tanks only a few

moments before liftoff in order to avoid boiling of the cryogenic fluids.

The combustion chamber volumes of liquid propellant rockets are among the smallest since a large mixing volume is not required. However, since monopropellant and bipropellant engines do not have a fuel grain to act as a thermal sink for the hot combustion temperatures, active cooling is usually required. This is commonly accomplished by flowing one of the fluids around the combustion chamber and nozzle. This cools the hot areas while also increasing the enthalpy of the fluid prior to combustion which can increase the energy released. Additionally, in order to achieve high mass flow rates required for high thrust applications, turbopumps must be utilized [3]. This increases the system complexity and cost significantly and therefore bipropellant systems are usually reserved for large rockets and large operations with the resources capable of meeting these requirements.

2.1.3 Solid Rockets

As the name suggests, solid rockets employ solid phase fuel with oxidizer mixed in the chemical matrix. Solid propellants are commonly combined with a binder material such as HTPB. Examples include ammonium perchlorate (AP) (NH_4ClO_4) which was used for the Space Shuttle Rocket Booster or octogen (HMX) ($C_4H_8N_4(NO_2)_4$) [18, 19]. Solid rockets have been employed for over 800 years dating back to Chinese black powder rockets. Solid fuel grains generally have excellent chemical and thermal stability which allow for easier and less costly transportation considerations unlike mono/bipropellants [20]. In addition, the propellants generally can be stored for extended periods of time without concerns of fuel degradation. Solid rocket motors are among the simplest propulsion systems as the fuel and the oxidizer are neatly packaged together with little to no pipe work explicitly necessary for the combustion. However, solid rocket propellants require some kind of activation energy in order to start the exothermic chain-propagation steps which result in gas-phase heat release and radiation [21]. Pyrotechnic charges and electroexplosive devices (EED) are commonly used for ignition of solid rockets [22]. Since multiple restarts are not required, these ignition systems are generally simple and do not significantly increase the overall mass of the rocket. Solid rockets also do not require active cooling as many liquid propulsion systems do since the solid fuel grain itself acts as a heat sink that helps protect

the surrounding motor case. For these reasons, modern solid rockets are commonly used in missiles such as the Minuteman III and the Sidewinder and in launch vehicles like the Space Launch System (SLS) and the Atlas V.

Despite its advantages, solid rocket motors are primarily limited by its inability to easily throttle and perform restarts. This means that solid rocket motors are not used in situations where unplanned, variable pulses of thrust are required such as reaction control systems and landing vehicles. Additionally, solid rocket motors' combustion chamber volumes are the largest among common propulsion types where the fuel grains typically constitute 80-94% of the total rocket motor mass [3]. Within the combustion chamber, the solid fuel grains can be susceptible to fractures and cracks which can lead to combustion instabilities or even catastrophic detonations that can lead to motor case failure [3].

2.1.4 Hybrid Rockets

Hybrid rocket motors are a class of rockets that are a combination of the solid rocket motor and the liquid rocket engine. The most common configuration of the hybrid rocket motor is a solid phase fuel and a liquid or gaseous oxidizer; however, a small amount of research has been done on a solid oxidizer, liquid fueled hybrid rocket motor [3, 23]. As seen in Figure 2.1, the classic hybrid uses the fluid oxidizer such as LO_x from a liquid bipropellant system and a solid fuel similar to a solid rocket motor in order to create thrust. The oxidizer feed operates similarly to a liquid rocket engine where the oxidizer is held in a tank upstream of the combustion chamber. Since the oxidizer depletes from the tank during operation, a method to maintain adequate tank pressure is required in order to have consistent and usable mass flow rates. This is usually accomplished by bladders or injection of another gas into the tank [3].

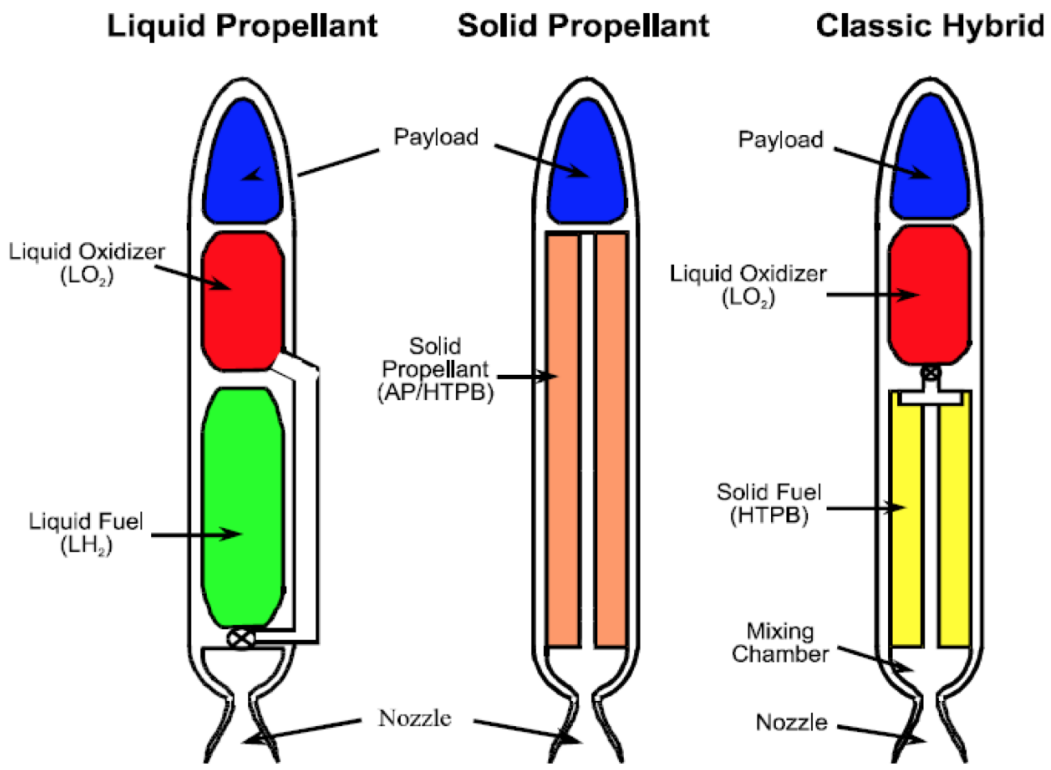

Figure 2.1. Comparison between liquid, solid, and hybrid rocket systems.

[8]

The combustion chamber for a hybrid rocket motor is more similar to a solid rocket since the combustion happens primarily within the solid fuel grain. This is dissimilar to a bipropellant rocket engine where the combustion chamber volume is significantly smaller since the volume required for mixing and combustion between two liquids is small. In addition, the solid fuel grains of both the solid and hybrid rocket motors act as pressure vessels whereas the bipropellant rocket engine's combustion chamber needs to be able to withstand both high pressures and temperatures without any internal solid support structures. Therefore, active cooling is usually required for large thrust bipropellant engines since the material performance of the combustion chamber can decrease under high thermal stress.

Unlike the solid rocket motor, the solid fuel grain of a hybrid rocket motor does not

have an oxidizer as part of the chemical matrix since the oxidizer is supplied by a separate tank. The most common fuel for hybrid rocket motors has traditionally been hydroxyl-terminated poly-butadiene, or HTPB. HTPB is a legacy binding agent for solid rocket motor fuel production and is a hard rubber like substance. However, hybrid rocket fuel selection is vast. Virtually any hydrocarbon solid could be potentially used [24]. This includes the use of thermoplastics such as ABS, PMMA, and PLA.

Hybrid rocket combustion can be seen as working similarly to a wood burning fire since they are both qualified as diffusion flames. As demonstrated in Figure 2.2, a diffusion flame is a type of combustion event where the fuel and oxidizer molecules are independent of each other prior to burning, whereas a premix flame has its fuel and oxidizers well mixed. Diffusion flames inherently have fuel rich and fuel lean zones, however a flame is established when the local conditions reside within its flammability limits. These flammability limits vary with fuel and oxidizer combination, but are generally dictated by the oxidizer to fuel ratio (O/F) in the presence of an adequate ignition source at a certain temperature and pressure. With solid fuels, it is necessary to first liberate combustible products, namely lower order hydrocarbons ($C_nH_m, n < 3$) and other volatile products from the chemical matrix of the fuel. These fuel and oxidizer molecules must be in a gaseous state in order to combust. For hybrid rocket motors, the fuel molecules are liberated by a mechanism called pyrolysis, or high temperature thermal decomposition.

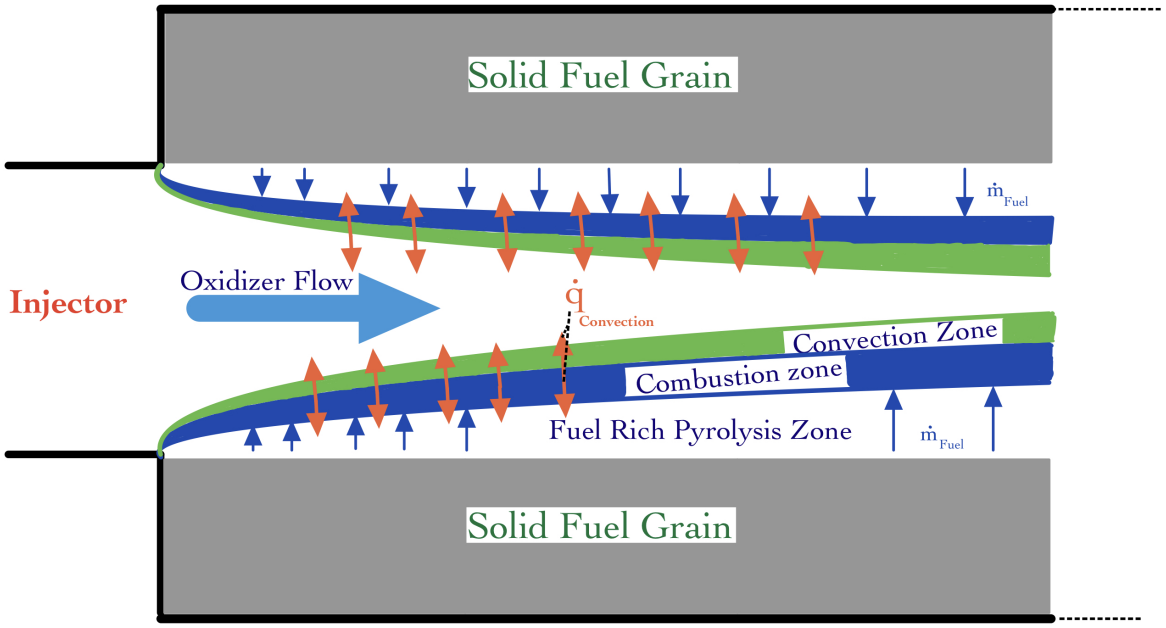

Figure 2.2. Turbulent boundary layer combustion mechanism of a hybrid rocket, adapted from [1].

In Figure 2.2, a model of hybrid rocket combustion is presented. From the left, an oxidizer stream enters the combustion chamber where a solid fuel grain resides. Convective heat is transferred to the surface of the fuel grain from the combustion zone, liberating volatile organic compounds, inducing a fuel-rich region. Additionally, convective heat from the combustion zone also heats the oxidizer-rich stream within the convection zone. The unbounded hydrocarbon molecules then mix with the preheated oxidizer stream and combust within the combustion zone [25–28]. As the fuel pyrolyzes, the fuel-rich layer pushes boundary layer of the combustion zone radially away from the fuel surface due to a mass flow rate emanating from the fuel. This 'wall blowing effect' is a well known phenomena in hybrid rocketry and can cause a decrease in convective heating to the surface and inadequate mixing of oxidizer and fuel molecules. As shown by Marxman and Gilbert, Equation 2.1 [1, 29], the regression rate $[\frac{cm}{s}]$ of a hybrid rocket can be modeled using turbulent boundary layer theory:

$$\dot{r} = \frac{StG_{ox}(h_{comb} - h_{wall})}{\rho_{fuel} h_{vap}} \tag{2.1}$$

where St is the Stanton number, G_{ox} is the oxidizer mass flux $[\frac{kg}{m^2 s}]$, $h_{comb} - h_{wall}$ is the enthalpy transfer by convection from the flame to the surface of the fuel grain $[\frac{kj}{kg}]$, and h_{vap} is the enthalpy of vaporization of the fuel grain$[\frac{kj}{kg}]$. The Stanton number is a dimensionless quantity describing the ratio of enthalpy transferred into a fluid versus the fluid's thermal capacity, shown in Equation 2.2:

$$St = \frac{h_{coeff}}{\rho u_{\infty} c_p} = \frac{Nu}{RePr} \tag{2.2}$$

where h_{coeff} is the heat transfer coefficient, ρ is the density $[\frac{kg}{m^3}]$, u_{∞} $[\frac{m}{s}]$ is the fluid velocity, and c_p $[\frac{kj}{kgK}]$ is the specific heat. The Stanton number can also be represented as a function of other dimensionless numbers: Nusselt number, Reynolds number, and Prandtl number. From Equation 2.1, for a given propellant selection, the regression rate can be increased by an increase in the oxidizer mass flux, G_{ox}, or by increasing the enthalpy transfer from the flame to the surface, $h_{comb} - h_{wall}$.

Compared to other rocket propulsion types, hybrid rockets are generally seen as among the safest and most cost effective [24, 30]. Since the solid fuel grain used in hybrid rockets does not incorporate an oxidizer as part of its chemical matrix and they are separated into different phases (solid and fluid), it is inherently safer than a solid fuel grain in a solid rocket motor. The fuel grain remains inert until it is ignited within the rocket combustion chamber where sufficient amount of heat flux and oxidizer can be applied to liberate and combust the volatile combustible compounds. Therefore, the hybrid rocket solid fuel grain have little to no explosion risk and imperfections on the fuel grain surface will not cause deflagration to detonation transitions [5]. This results in the reduced costs in almost all phases of the fuel grains' lifetime. For these reasons, hybrids have been used in private space ventures such as the Virgin Galactic SpaceShipOne and SpaceShipTwo (shown in Figure 2.3) where space tourists' safety is paramount.

Figure 2.3. Virgin Galactic's SpaceShipTwo.

[31]

In general, the production of hybrid rocket fuel grains will not require severe safety precautions whereas hypergols, cryogens, and solid rocket fuels do. Hypergolic propellants are extremely reactive, toxic, carcinogenic, and corrosive which necessitates the need for specialized piping and handling equipment, production, and strict safety procedures [32]. Cryogenic propellants require robust, specialized piping and storage containers in order to withstand the extremely cold temperatures to maintain liquid phase. Additionally, cryogenic propellants can be explosive as is the case of liquid natural gas. Lastly, solid rocket fuel grains are also reactive and can combust or explode in the presence of an ignition source. This is mostly due to the oxidizer selected such as aluminum perchlorate (AP) which is considered explosive for diameters less than 15 microns and can burn if contaminated with combustible material, or explode when exposed to prolonged heat [33]. In contrast, hybrid rocket fuel grains do not require many of the safety precautions and specialized equipment in order to produce, transport, and store. They are solid at room temperatures, do not incorporate an oxidizer in the fuel matrix, and are nonreactive until

its specific ignition criteria are met.

Similar to liquid rocket engines, the hybrid rocket motor is able to throttle and fully stop and restart operation. By controlling the oxidizer mass flow rate, the thrust and rate of pyrolysis can be controlled. Furthermore, with a reliable ignition method the hybrid rocket motor can restart operation numerous times allowing it to perform pulse fires and other strategic maneuvers. This is a great advantage over the solid rocket motor where the combustion time and thrust profiles are fixed by the fuel grain prior to launch. Additionally, the complexity of throttling is decreased as compared to the liquid bipropellant rocket engine since the liquid bipropellant requires precise control of two depleting tanks rather than one tank.

Hybrid rockets are not without their detriments. As explained earlier, the solid fuel grain used by hybrid rockets can be virtually any hydrocarbon solid and is inherently safer to produce, handle, transport, and store than most other rocket fuels. However, these positive aspects actually lead to inherent struggles and detriments. Hybrid rocket fuel grains, in general, achieve lower performance as compared to cryogenic liquids propellants, where specific impulses for HTPB and GOx is 300-350 seconds and LH_2 and LOX is 400-450 seconds [3, 5, 14]. However, hybrid rockets generally have higher specific impulses than solid rocket motors, HTPB and AP 190-230 seconds [18]. Hybrid rockets also suffer from low fuel regression rates which is usually due to limits in heat transfer from the diffusion flame to the surface of the fuel grain. This is a large area of interest within the hybrid rocket propulsion literature covering potential solutions including: swirl injectors, complex fuel geometries, particle additives, radial-flow configurations, and more energetic compounds [34–44]. In addition, hybrid rockets are also susceptible to lower performance due to O/F ratio shifting. This is due to the increasing burn surface area as the fuel pyrolyzes which increases the amount fuel is exposed to the diffusion flame's heat transfer, causing the overall decrease in the O/F ratio for constant oxidizer mass flux [45–47]. As illustrated by Figure 2.4, low O/F ratios have a steep drop-off in combustion temperatures whereas higher O/F's gradually decrease in temperature. Therefore, a decrease in the O/F ratio can be detrimental to the overall performance in the hybrid rocket. Another critical

problem in hybrid rocket propulsion is that ignition can be more difficult to achieve as compared to liquid and solid rocket motors, however this will be discussed in more detail in a future section.

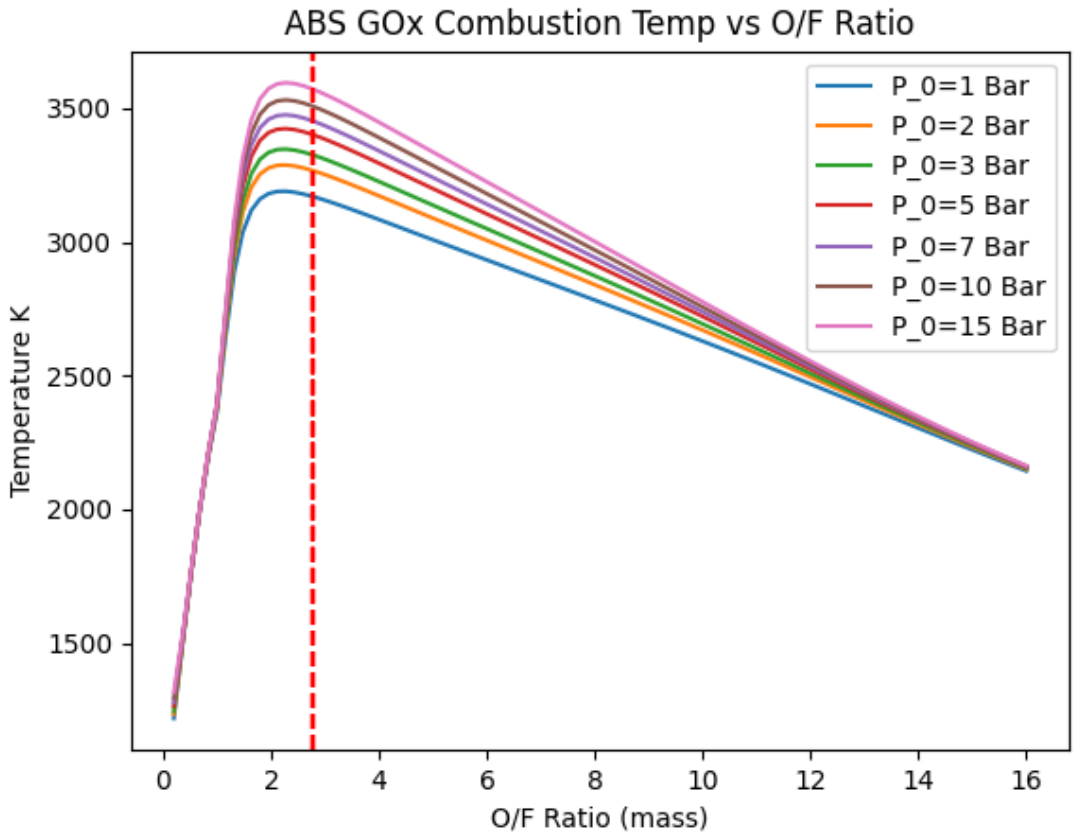

Figure 2.4. ABS GOx combustion temperature as a function of O/F Ratio; red line is stoichiometric O/F ratio.

[10]

2.2 Hybrid Rocket Ignition Systems

In order to initiate the chain of exothermic reactions required to propel the hybrid rocket motor, the following conditions are required: heat to liberate fuel molecules from solid to gas phase, mixing between gaseous oxidizer and fuel molecules, and an ignition source supplying the required activation energy for the chain initiating reactions. Ignition for hybrid rocket motors are generally more difficult than liquid rocket engines and solid rocket motors since hybrid rocket fuel grains are more stable, less readily reactive, and usually

require restart operation. Ignition for solid rockets can be accomplished by one time use methods such as hypergolic squibs or solid propellants that provides high heat flux and high gas evolution to the main fuel grain [20]. Liquid rocket engine ignition methods include hypergols, torch igniters, laser ignition, and spark ignition [48–50]. Despite sharing many of the same technologies, hybrid rocket ignition is more difficult to achieve since the fuel grain is in the solid phase and not in the same phase as liquid rocket engines. In this section, various types of ignition systems investigated in rocket literature will be discussed.

2.2.1 Hypergolic Ignition

Traditionally, hypergolic ignition systems have been the preferred choice for many missions including the Nike Ajax, Titan 2, and Ariane 1-4 [48]. Hypergolic ignition refers to a room temperature self-ignition between the combination of two propellants. The major advantage to hypergolic ignition systems is the lack of external activation energy required to carry out the chain initiation and propagation steps, where impingement and mixing of the two propellants is sufficient. For hypergolic propellant rockets, a dedicated ignition system is no longer necessary which allows for simple and reliable ignition solutions with the added benefit of reduced weight. Common hypergolic combinations used are: triethylaluminum and triethylborane (TEA-TEB), Aerozine 50/50 and nitrogen tetraoxide, unsymmetrical dimethylhydrazine and nitrogen tetroxide [48]. TEA-TEB is a pyrophoric, which means it will achieve self-ignition in the presence of oxygen or air. TEA-TEB is currently used for ignition on the SpaceX Falcon 9 and was used on the Saturn V.

Hypergolic propellants are inherently dangerous due to their corrosive, toxic, carcinogenic, and reactive properties. Thus significant amount of planning, equipment, and safety precautions in all stages of development and testing are required. In a technical report detailing hypergolic propellant incidents published by NASA [32], in 23 oxidizer related incidents: 3 led to a fire, 3 led to an explosion, 8 led to injuries or death, and 12 led to hardware damage. In the same report, for 25 fuel related incidents: 8 led to a fire, 2 led to an explosion, 7 resulted in injuries or death, and 12 led to hardware damage. They reported that most of the incidents (23) had a root cause in improper design of ground

support equipment or improper vehicle design and most (42) occurred during hypergolic propellant operation. Because of the inherent dangers of these propellants, other ignition methods are currently in development.

Although working with hypergolic propellants presents an extreme danger, there are still on-going studies despite growing interest in other ignition methods. Among them are ignition delay testing methods, modeling hydrazine based hypergols, and reducing hydrazine toxicity by gelation or by using non-hydrazine based propellants [48]. Additionally, since the . Interestingly, there is on-going research in hybrid rocket hypergolic combustion. In [23], researchers utilized a hypergolic reaction between a solid phase propellant, sodium amide in a paraffin based fuel, and a liquid oxidizer, mixed oxides of nitrogen (MON). They were able to ignite and reignite four fuel grains with average regression rates of 1.65 and 1.95 $\frac{mm}{s}$.

2.2.2 Laser Ignition

The laser ignition system presented in [51] is a novel and promising concept for hybrid rockets in order produce a reliable and compact ignition source. Laser ignition is an area of academic research for internal combustion engines and its technologies are extending to rocketry [52]. Generally, laser ignition operates by utilizing a diode laser to create a focused beam of light that supplies the required activation energy for chain initiation reactions. Among its potential benefits for internal combustion engines are: the ability to ignite from particular locations within the chamber, lack of flame kernel quenching, possibility of simultaneous multi-location ignition energy application, and precise temporal control [52]. A particular benefit for rockets is that the laser ignition system does not require any additional propellants, however it will require an electrical power source.

Similar to using a magnifying glass to focus the Sun's light to create a fire, the laser ignition system for the hybrid rocket uses its focused laser to heat the surface of the fuel grain. The energy from the beam heats and pyrolyzes the fuel grain which then mixes with the oxidizer and ignition can occur. The system presented in [51] operates by using a diode laser capable of 16 W at 1064 nm. However, this ignition system is limited to small-scale motors as the reliability of ignition comes into question as the fuel regresses

further away from the beam source. As the heat sink location moves further away from the laser diode, the beam radius increases leading to a decrease in intensity. The authors suggest that the laser ignition system with commercially available diode lasers is limited to beam ignition energies no larger than $10^7 \frac{W}{m^2}$. The investigation is on-going and data for this particular setup has yet to be published at the time of writing.

2.2.3 Plasma Torch

Plasma torches are a type of ignition method that utilize gas flow over an electrical arc. As the gas passes through the arc, it ionizes the gas, creating free radicals of positive and negative charges, creating a plasma. Plasma torches are of particular interest for supersonic combustion such as a scramjet engine because combustion in supersonic and hypersonic regimes is difficult. These regimes suffer from extremely low residence time of fuels, difficulty in flameholding, and difficulty in flame stabilization [53]. Gases that have been used for plasma ignition include hydrogen, argon, or a mixture of both argon and hydrogen [54].

One of the main difficulties of plasma torch ignition for hybrid rockets is the incredibly high electrical power required to operate, ranging in power input form 1 kW to above 2 kW [54, 55]. This energy would have to come from a large battery or other on-board electrical generator whereas other torch igniter concepts produces ignition energy from chemical reactions of already on-board propellants.

2.2.4 Pyrotechnic Ignition

Pyrotechnic igniters are one of the simplest and most reliable methods for ignition. It uses an easily ignitable, usually solid phase substance in order to ignite a more difficult material such as a solid fuel grain. Pyrotechnic ignition is commonly used in solid and hybrid rocket motors and comprises of materials such as zirconium potassium perchlorate (NASA's Standard Initiator), magnesium-Teflon, and boron potassium nitrate [22, 56, 57]. The process usually starts with electrical current flowing through a wire which heats up and then thermally decomposes the pyrotechnic material which supplies enough energy for chain initiation and propagation.

A central problem with pyrotechnic ignition is that it is almost always a single use system. This defeats the purpose of using a hybrid rocket motor as one of the central defining benefits of a hybrid rocket motor is its ability to stop and restart operation. If multiple restarts were necessary, several pyrotechnic charges would be required. Similarly to solid rocket motors, the pyrotechnic charges also require careful safety precautions in production, handling, storage, and transportation which further deflates the benefits of the hybrid rocket motor.

2.2.5 Direct Electrical Arc Ignition

The Direct Electrical Arc igniter was developed at Utah State University where it was found that fused-deposition modeled (FDM) ABS thermopolymer would create an arc when high voltage was applied to the surface, causing it to char [58, 59]. They found it to only work for the FDM-formed ABS despite efforts to create a similar phenomena in extruded ABS, HTPB, acrylic, and paraffin. The igniter requires voltages in the range of 10-400 volts for FDM ABS whereas the extruded ABS required voltages greater than 10 kV. As demonstrated in Figure 2.5, the Direct Electrical Arc Igniter operates by utilizing a electrical arcing through the air between two embedded electrodes, where ABS material near the electrodes begin to heat and pyrolyze. The charring induces the arc to create a path on the surface of the ABS where it continues to create volatile hydrocarbon gas that are ignited when mixed with oxidizer. The system is used as a pyrotechnic-like ignition, but with the ability to reliably restart.

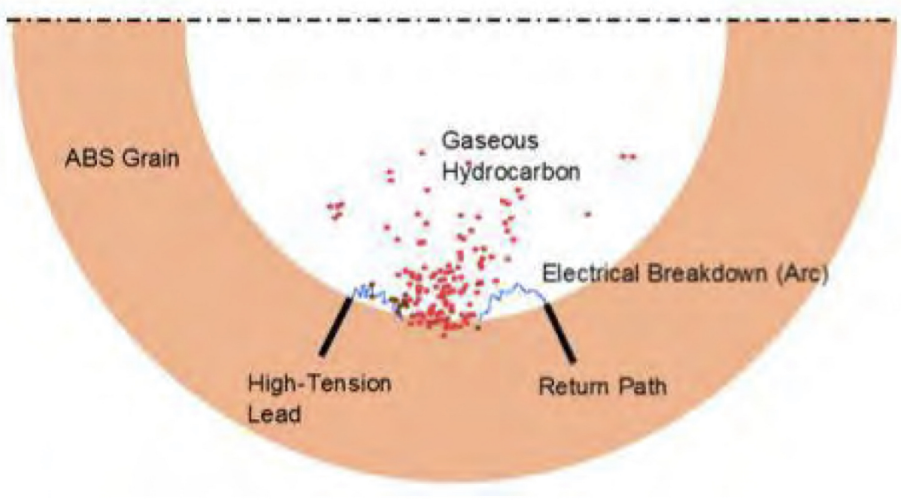

Figure 2.5. Direct Electrical Arc Igniter mechanism.

[58]

This method of ignition is promising, but it is currently limited to a selection of thermopolymers. In addition, the Direct Electrical Arc Igniter requires an on-board power source, but luckily the power draw is low enough that the power source can still be small. Additionally, this method of ignition is less toxic and less dangerous to work with than systems such as pyrotechnic igniters and hypergolic propellants for the same reasons that hybrid rocket motors are safer than the solid and liquid rocket systems; the fuel source is inert until a heat source and oxidizer are applied.

2.2.6 Methane Torch

The methane torch igniter is an ignition system utilizing the combustion of methane and usually oxygen to apply the required heat to pyrolyze the hybrid rocket fuel grain. As shown in Figure 2.6, the two propellants flow into a separate ignition body attached to the main combustion chamber or into an injector assembly where the igniter is integrated within [60, 61]. Ignition between the two propellants is achieved by a spark plug.

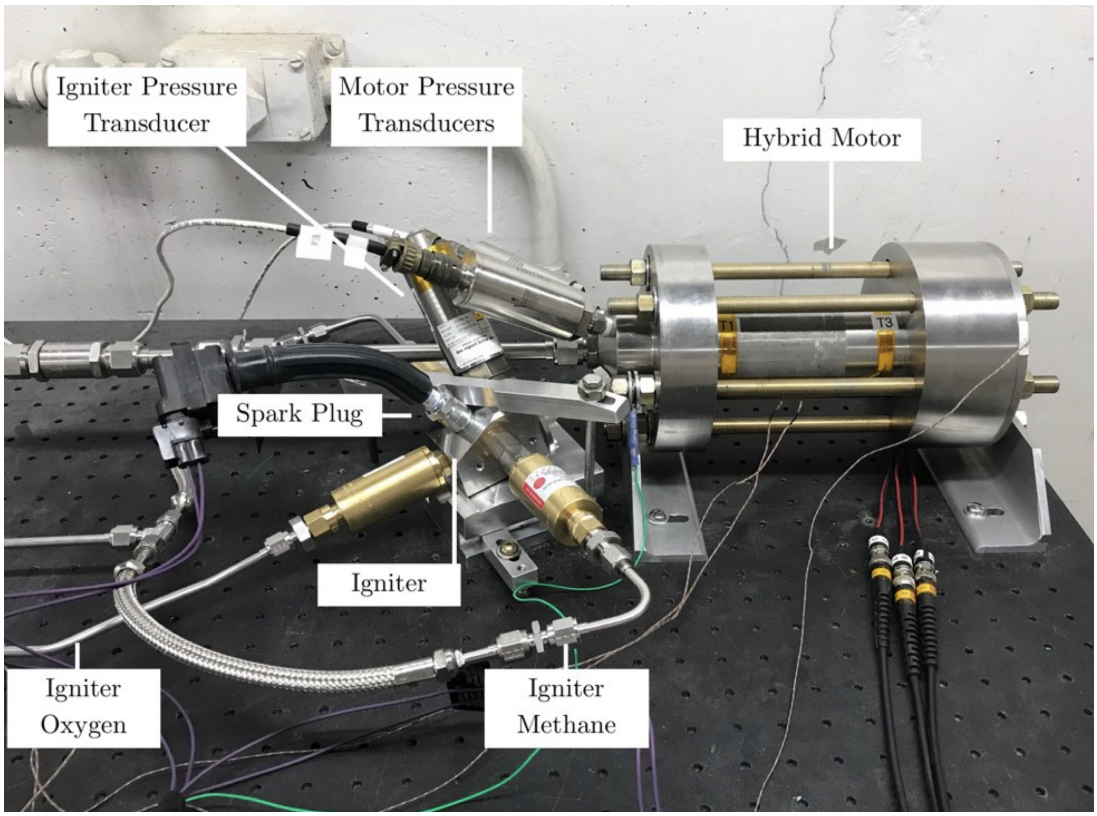

Figure 2.6. NASA methane torch ignition system.

[61]

The methane torch is a method that is derived from liquid rocket engines as liquid methane and liquid oxygen are increasingly common propellant combinations [62]. It has been shown that the methane torch igniter is reliable, repeatable, and able to perform under a variety of O/F ratios and igniter body temperatures.

A key difference between its usage in liquid engines and hybrid motors is that in order to use the methane torch, the hybrid motor requires an additional tank and pipe work, thus increasing the overall motor weight and complexity. This is in contrast to liquid engines where the methane and oxygen are fed from the main propellant storage tanks. This is particularly disadvantageous for hybrid rockets in terms of weight and build complexity, however this disadvantage may be offset by the benefits of a reliable ignition system that can be used for many ignition cycles as hybrid rockets often perform during the course of its mission.

2.2.7 Hydrogen-Oxygen Torch Igniter

The hydrogen-oxygen torch igniter uses the same principles as the methane torch except instead of methane, hydrogen is used. It was first developed at NASA Lewis for research rocket engines as a replacement for hypergolic ignition of hydrogen and flourine [9]. As shown in Figure 2.7, the igniter is installed on the side of a liquid bipropellant engine.

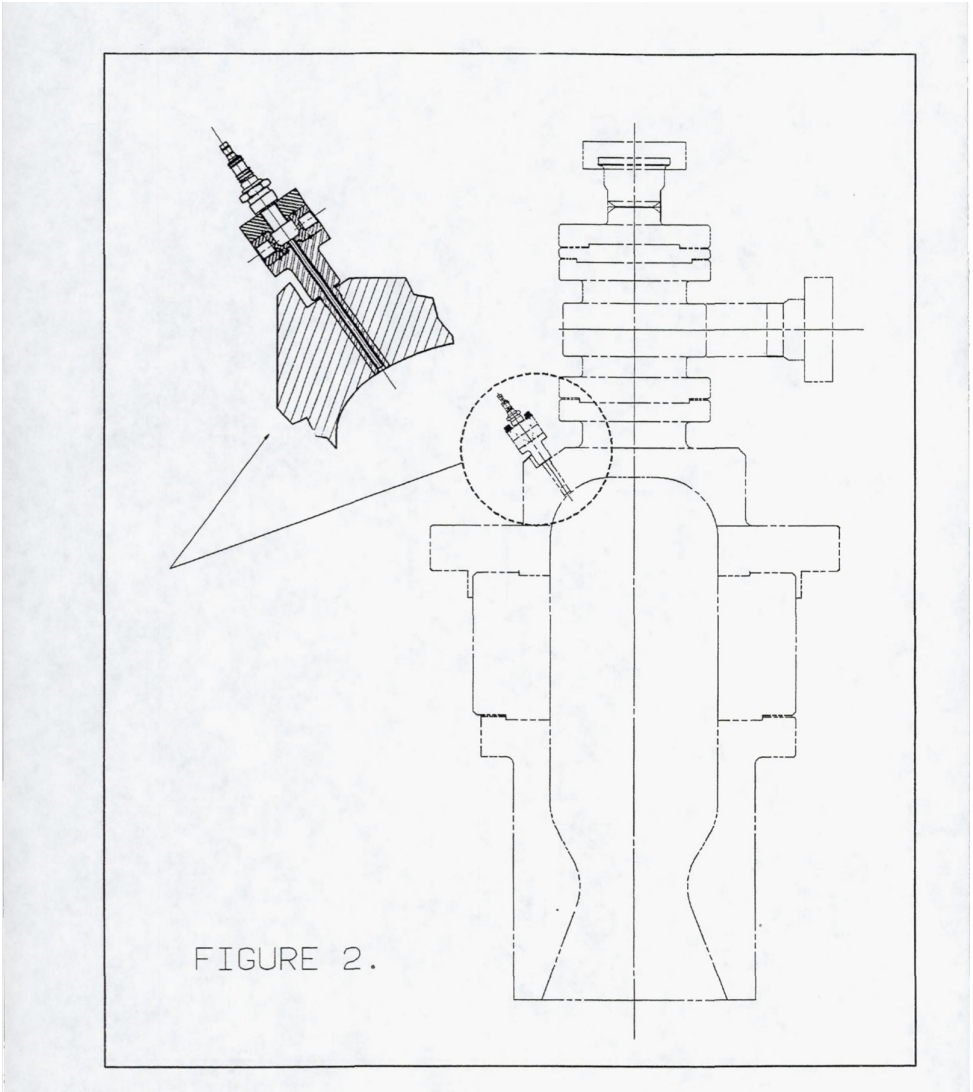

Figure 2.7. An example configuration of NASA Lewis hydrogen-oxygen torch igniter, igniter is within the dotted circle.

[9]

The hydrogen and oxygen enter through the sides of the igniter where the two streams meet at a spark plug which supplies the required activation energy to induce combustion.

The resultant product stream then enters the main combustion chamber where it ignites the main propellant stream.

The hydrogen-oxygen torch igniter was a reliable source of ignition for a variety of propellant combinations including RP-1/LOx, methane/GOx, and carbon monoxide/GOx. Due to the properties of hydrogen-oxygen combustion, an extremely lean flame, O/F equal to 40, is possible. At these lean flame conditions, the combustion temperature is about 2050 K. With a low flame temperature and combined with short igniter run times, the igniter combustion chamber does not need to be externally cooled. Additionally, the igniter used at NASA Lewis was able to produce ignition 400 times before being replaced, a testament to its reliability.

As discussed with the methane torch, for hybrid rockets, it may be disadvantageous to increase the system complexity and weight by adding an additional propellant like hydrogen. However, the advantage of an extremely reliable ignition source for systems that require many restarts may offset the disadvantages. In addition, hydrogen and oxygen combustion has among the fastest flame speeds resulting in low ignition times and it allows for extremely lean O/F ratios which enables another level of mission flexibility [63, 64]. Similarly, hydrogen has high energy density which can allow for lower flight weights for the same amount of energy.

2.3 Hydrogen

Hydrogen is the lightest element on the periodic table consisting of 1 proton and 1 electron for a total of 1.008 atomic unit of mass or 1 gram per mole. It is commonly found in its diatomic state of H_2 which has a weight of 2 grams per mole. Hydrogen was among the first elements to be formed after the Big Bang and is the most abundant element in the universe. It is a main component of stars and is the fuel stock for nuclear fusion, which involves high temperatures and pressures to fuse hydrogen nuclei together to form helium in the Sun producing massive amounts of energy.

On Earth, hydrogen is not as freely abundant as it is in the celestial bodies of the universe. It is commonly found bonded together with carbon atoms, forming chains of

hydrocarbons (organic compounds) which are a fundamental building block of life as we know it. Because hydrogen is not "simply found growing on trees", methods of extraction from hydrocarbons is necessary. Currently, hydrogen is formed through industrial scale process utilizing reactions such as steam methane reformation (SMR), methanol steam reformation (MSR), auto-thermal reformation (ATR), and electrolysis. Approximately 95% of hydrogen is created through SMR which utilizes natural gas, a hydrocarbon gas mixture containing mostly methane [65].

In rocketry, hydrogen has been used extensively in engines starting from the RL-10 and J-2 in the 1960's to the Space Shuttle Main Engine (SSME) and Aerojet's M-1. Hydrogen is among the highest performing propellants, owing to its low molecular weight and high energy density (119.96 $\frac{MJ}{kg}$), it can achieve ISP's of 450 seconds [66]. Furthermore, hydrogen is frequently used as a cooling fluid as it has a high thermal conductivity, high heat capacity, and low dynamic viscosity. A benefit that is receiving more recognition is that hydrogen is a 'green' propellant. When combusted with oxygen, the majority of its combustion products is water, a less harmful product than other rocket propulsion types where metal additives, CO_2, and NOx emissions are frequently present. As alluded to in a previous section, hydrogen burning flames are the fastest as compared to other hydrocarbon mixtures [11], illustrated by Figure 2.8. The flame speeds, S_L, are a function of the fuel-air equivalence ratio, ϕ, which is the ratio of actual fuel to air (F/A) ratio to stoichiometric F/A ratio for a given fuel and oxidizer combination. $\phi > 1$ is fuel-rich and $\phi < 1$ is fuel lean.

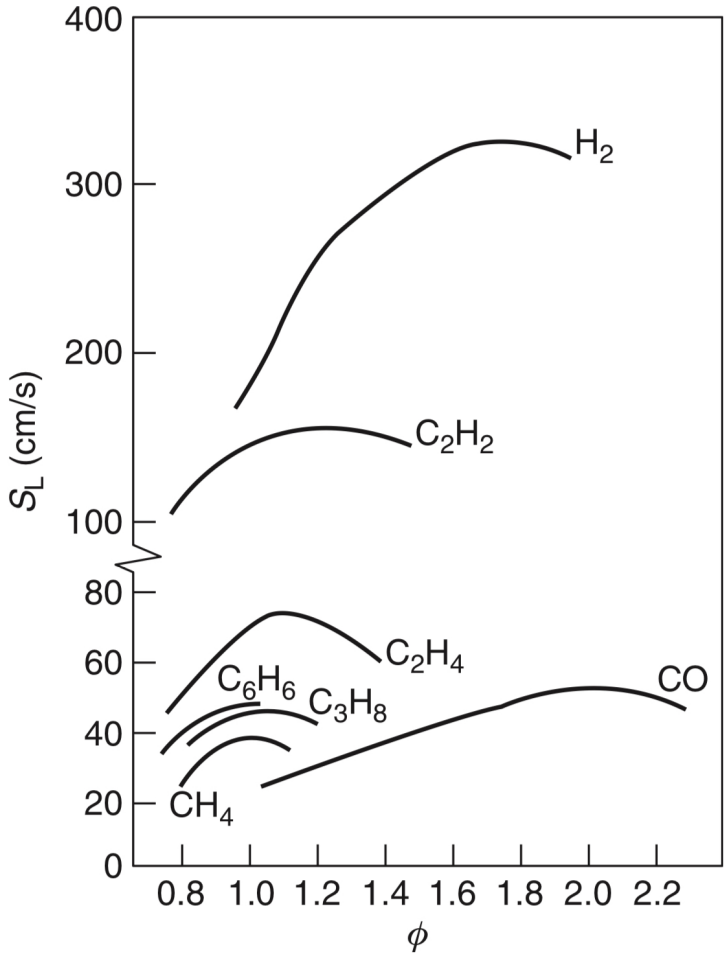

Figure 2.8. Flame speeds as a function of equivalence ratio ϕ for various fuel-air combinations at P=1 bar, T=298K.

[11]

The high flame speed, high diffusion coefficient in air of hydrogen, and low activation energy to break hydrogen-hydrogen bonds contribute to improvements in the combustion processes when used as a supplement to other hydrocarbon mixtures in machinery such as gas turbines and internal combustion engines [64, 67, 68]. It has been shown that enrichment of hydrogen decreases ignition delays, increases the reactivity of other hydrocarbons, and can help extend the lean operating limit of other hydrocarbon combustion [64, 68–70].

As seen in Figure 2.9, on a mass basis hydrogen has almost 3 times the energy content

than other long chain hydrocarbons like gasoline, 119.96 $\frac{MJ}{kg}$ and 42.8 $\frac{MJ}{kg}$ respectively, but hydrogen suffers from low volumetric energy density: about 1 $\frac{kWh}{L}$ for pressurized gaseous hydrogen and about 2.5 $\frac{kWh}{L}$ for liquid hydrogen. In comparison, liquid methane has a volumetric density of about 6 $\frac{kWh}{L}$ [66, 71].

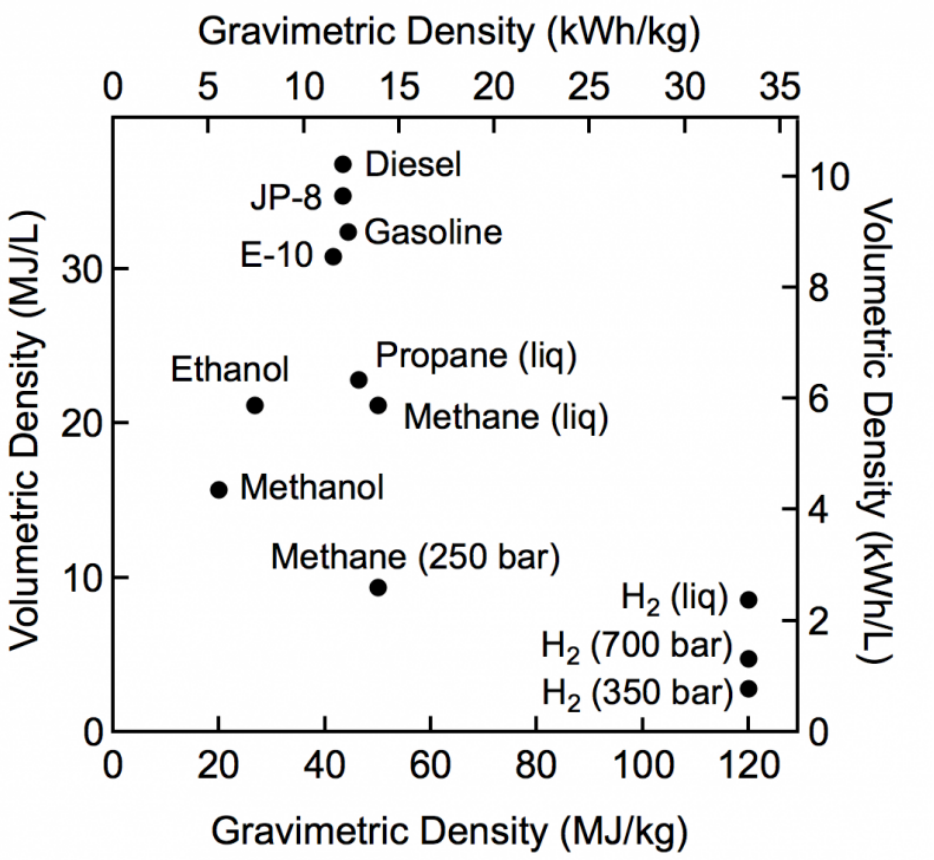

Figure 2.9. Energy densities and volumetric energy densities of common fuels. [71]

Therefore, when hydrogen is used in rocketry, it is most commonly found as a cryogenic liquid rather than as compressed gas in order to increase its volumetric energy density. In addition, hydrogen's high reactivity and low activation energy poses a danger for explosion. Accordingly, this increases the overall mission and design complexity since precautions are needed in order to handle, transport, store, and keep the hydrogen as a liquid without boiling prior to launch. Because of this, liquid hydrogen is usually used in large thrust rockets with large budgets and resources.

2.4 Acrylonitrile Butadiene Styrene (ABS)

Acrylonitrile butadiene styrene (ABS) is a thermoplastic that is comprised of repeating chains of hydrocarbons called monomers. ABS is comprised of acrylonitrile, butadiene, and styrene monomers in varying ratios that vary from producer to producer to create the polymer. ABS was first patented by the Borg-Warner (now General Electric) in 1948 in which ABS was grafted onto free-radical sites on a macromolecule in a process called free-radical polymerization. Today, ABS is commonly formed by a process called emulsion polymerization which mixes the monomers with other ingredients including initiators, molecular weight regulators, emulsifiers, and water in a solution where complex chemical reactions form the polymer [72]. The amounts of ingredients and in which ratios are usually proprietary intellectual property of the producer. Like other polymers, ABS is an amorphous solid which means it has no distinct melting point. Instead, it has a glass transition temperature of roughly 105°C where the ABS becomes soft and melted [72, 73]. This allows ABS to be used in processes such as injection molding, extrusion, fused deposition modeling (FDM, commonly known as 3D printing). Because of the manufacturing flexibility and favorable physical properties, ABS is a common polymer that is used in a wide variety of areas including toys, plumbing, car interiors, and structural materials. A common example of ABS is shown in Figure 2.10. In 2018, the world produced about 11.2 million metric tons of ABS and is projected to increase to 12.49 million metric tons by 2023 making it one of the most common thermoplastics in use [74].

Due to ABS's ability to be used in FDM, it has recently picked up interest within hybrid rocket motors [35, 37, 41, 75, 76]. ABS feedstock is generally inexpensive since it is very common and can be purchased from a variety of vendors, in a variety of shapes and sizes. Conversely, the components that make up HTPB are more difficult to procure and can be expensive. In addition, HTPB is a thermosetting material that requires mixing of its two components, polybutadiene resin and methylene diphenyl diisocyanate (MDI) curative. It is then cast into a mold, then heat cured until the correct hardness is achieved. As previously mentioned, hybrid rocket motors can suffer from low regression rates which can be solved by implementing more complex grain geometries in order to increase the

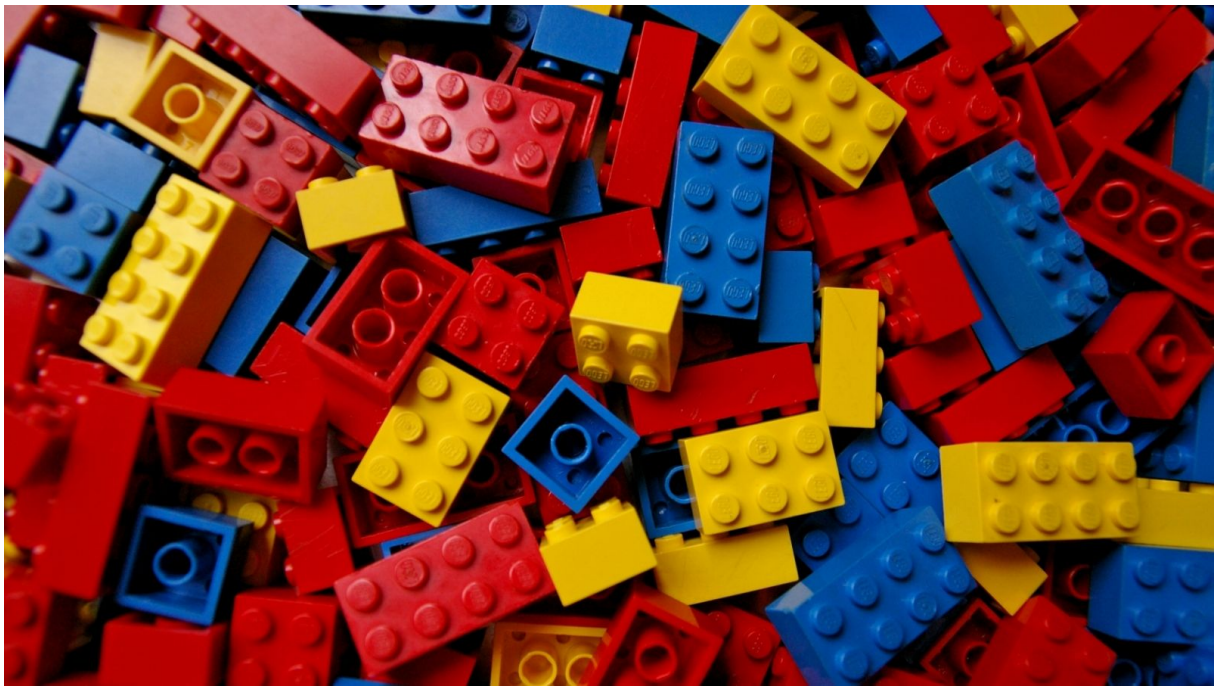

Figure 2.10. Common example of ABS use: Legos.

burn surface area. The thermosetting process causes HTPB to be limited in possible grain geometries and therefore less ways to mitigate low regression rates. Since ABS is one of the most common materials used in FDM, it has been of particular interest to solve low regression rates by complex grain geometries. In addition, ABS has a number of mechanical properties that make it a popular choice among designers and engineers alike. Its tensile strength of 41.1 MPa and elongation percentage of 5% shows that ABS is both strong and resistant to warping [73]. The properties of ABS allow it to sustain high pressures and temperatures without material failure. It is then possible to decrease the material of the combustion chamber since the ABS is able to absorb significant internal load.

ABS has been shown to have comparable performance characteristics to the most widely used hybrid rocket fuel grain, HTPB. In the experiments produced by Whitmore et al. [5], HTPB and FDM produced ABS were compared for a simple single port configuration. They found that HTPB/N_2O produced a ISP of 225.1 seconds and ABS/N_2O ISP was 215.9 seconds, a difference of about 4%. In addition, ABS had a higher burn rates than HTPB, 0.086 $\frac{kg}{s}$ and 0.082 $\frac{kg}{s}$ respectively.

Chapter 3

Theoretical Approach and Design of Experiment

This body of work seeks to utilize a hydrogen-oxygen torch igniter as a source of ignition and performance enhancement for a hybrid rocket using ABS thermoplastic as the fuel grain, a novel presentation of the hydrogen-oxygen torch igniter. By creating a factorial design of experiments, the effects of the duration of hydrogen flow, hydrogen mass flow rate, and oxygen mass flow rate on the hybrid rocket combustion will be examined. The goal is to create and demonstrate a reliable ignition system capable of working at various O/F ratios, decrease ignition delays, and increase the overall regression rate. In this chapter, the theory of the experiment is discussed. Models from NASA CEA and information from the literature are used to develop a theory of the mechanisms involved with the hydrogen-oxygen torch igniter combustion and its potential effects on the combustion of the ABS and GOx. The design and development of the factorial experiment will also be discussed. Lastly, the methods of calculation for the regression rate and the characteristic ignition time will be defined.

3.1 Theoretical Approach

From previous studies conducted both in the Energy Research Lab and outside have shown that hydrogen flame speeds are among the fastest, have high diffusivity, can increase the reactivity of other hydrocarbon combustion processes, and can decrease ignition delays[64,

68, 70, 77]. The ABS fuel grain requires an endothermic pyrolysis step and activation energy prior to combustion since combustion requires the reactants to be in the gas phase. In contrast, hydrogen and oxygen are already gasses and therefore require only an activation energy to combust. Therefore, as separate mechanisms, hydrogen and oxygen combustion should have a lower ignition delay as compared to ABS and oxygen. However, in this experiment the two combustion mechanisms are together in the same system where the hydrogen and oxygen combustion is used to apply the energy required for ABS's endothermic pyrolysis and subsequent combustion activation energy.

Thus, if the hydrogen and oxygen torch igniter is upstream of the ABS combustion chamber, it is believed that the torch igniter operation will affect the performance of the ABS combustion. As evidenced by previous studies, it is believed that hydrogen can influence other hydrocarbon reactions thus similar effects should be seen in the hydrocarbon combustion of ABS and oxygen. For a given oxygen mass flow rate, the allowable changes in the operation of the hydrogen-oxygen torch igniter are the O/F ratio and the duration of the combustion.

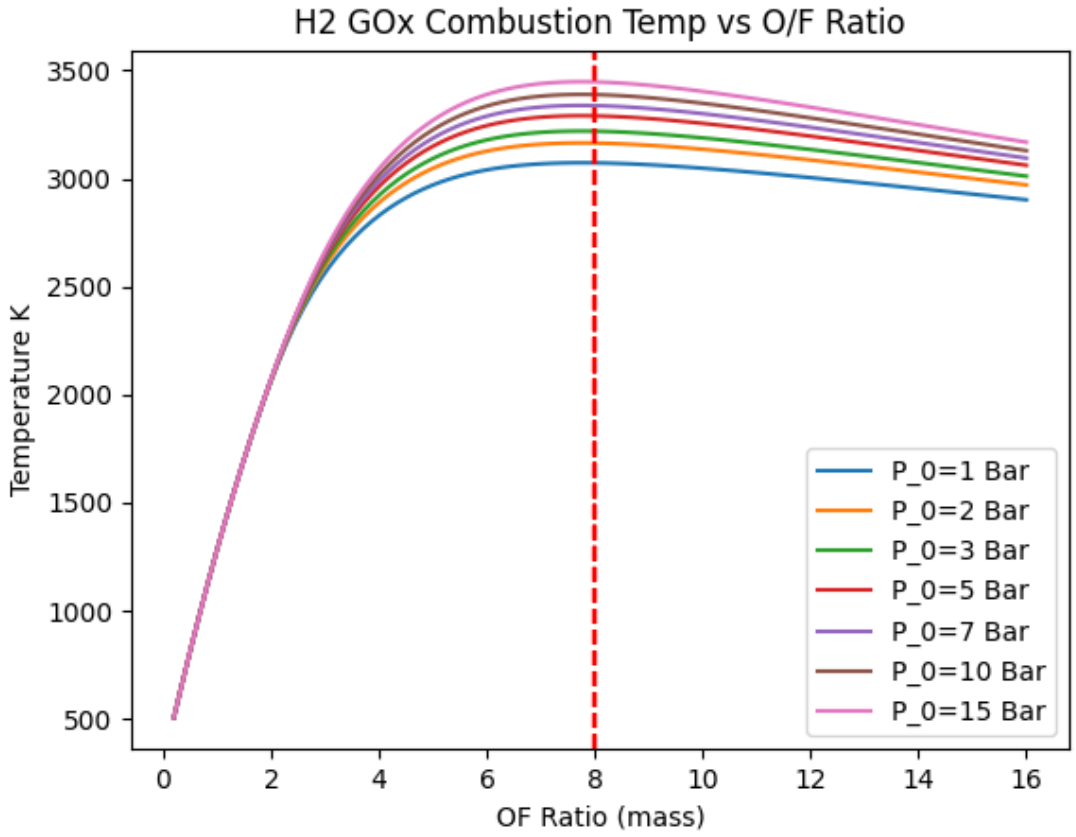

Figure 3.1. GH_2 and GOx combustion temperature as a function of O/F ratio (mass) at different pressures, red dashed line is stoichiometric proportion.
[10]

In Figure 3.1, the combustion temperatures of a hydrogen-oxygen flame with respect to O/F ratio on a mass basis is presented. It can be seen that the hydrogen and oxygen combustion peak temperature is at an O/F equal to 8, at stoichiometric proportions. However, the temperatures stay within 100K of each other within the range of 4-16 O/F. Thus, within the range of O/F's 4-16, the ABS fuel grain should receive high total heat to the surface which would supply the energy required for the endothermic pyrolysis step.

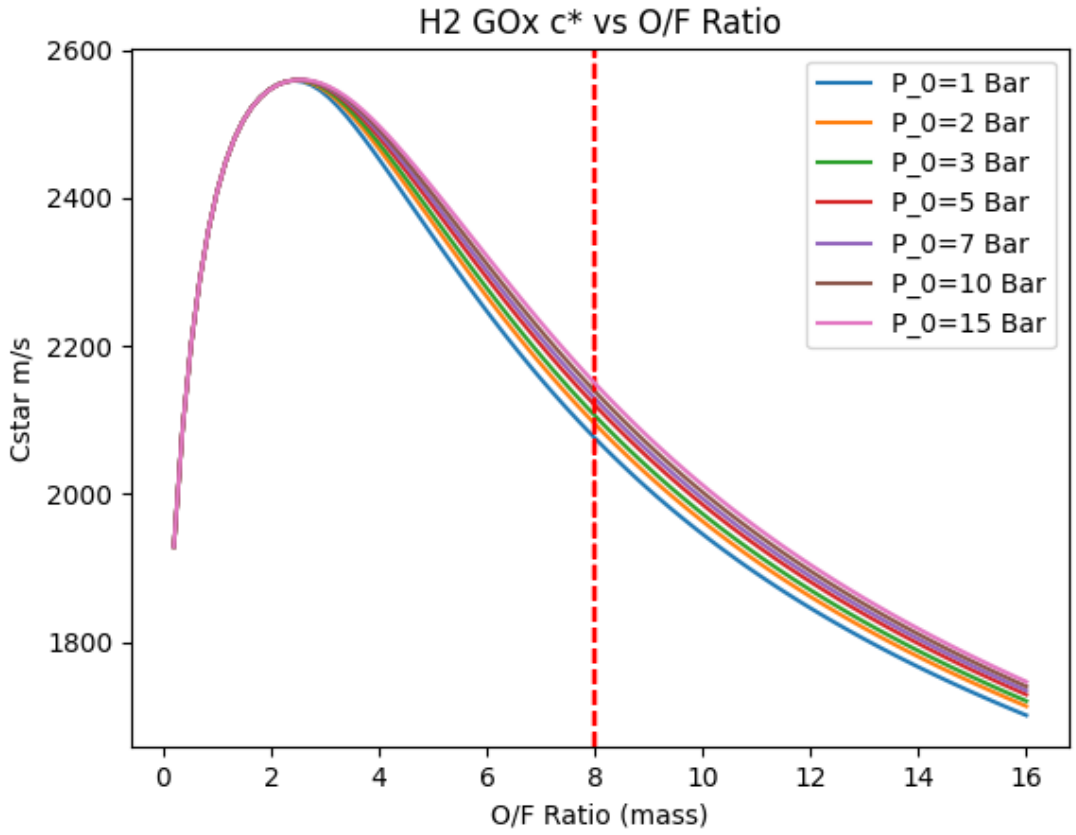

Figure 3.2. GH_2 and GOx c^* as a function of O/F ratio (mass) at different pressures, red dashed line is stoichiometric proportion.
[10]

However, in rocketry, performance values such as the characteristic exhaust velocity are also used to help characterize combustion performances. This characteristic exhaust velocity, c^*, is an important measurement since it describes the relationship between pressure and mass flow rates. Ideally, a high pressure is desired at low mass flow rates, resulting in high c^*. As seen in Figure 3.2, the maximum c^* values occur around O/F equal to 2.5, an equivalence ratio, λ, equal to 0.5. At this O/F ratio, the combustion temperature is still high, but about 500K less than the 4-16 O/F ratio range. Thus, if a higher average c^* value is desired while still applying temperatures around the optimal range, an O/F of 4 appears to be ideal. Additionally, using a rich torch stoichiometry may lead to an increase in the reactivity of the pyrolyzed hydrocarbon combustion since

hydrogen is extremely reactive and is more available in the rich regime. Because of these reasons, this work experiments with O/F ratios (mass basis) of 4, 8, and 16 representing rich, stoichiometric, and lean operating conditions, respectively.

In addition to the hydrogen-oxygen torch igniter operating conditions, the operating conditions for ABS-oxygen combustion must also be accounted for. The combustion temperatures and c^* values for an ABS-gaseous oxygen flame as a function of O/F ratio by mass at different pressures are presented in Figure 3.3 and Figure 3.4. From these figures, it can be seen that the maximum values tend towards stoichiometric proportions, O/F equal to 2.8, for ABS and oxygen combustion.

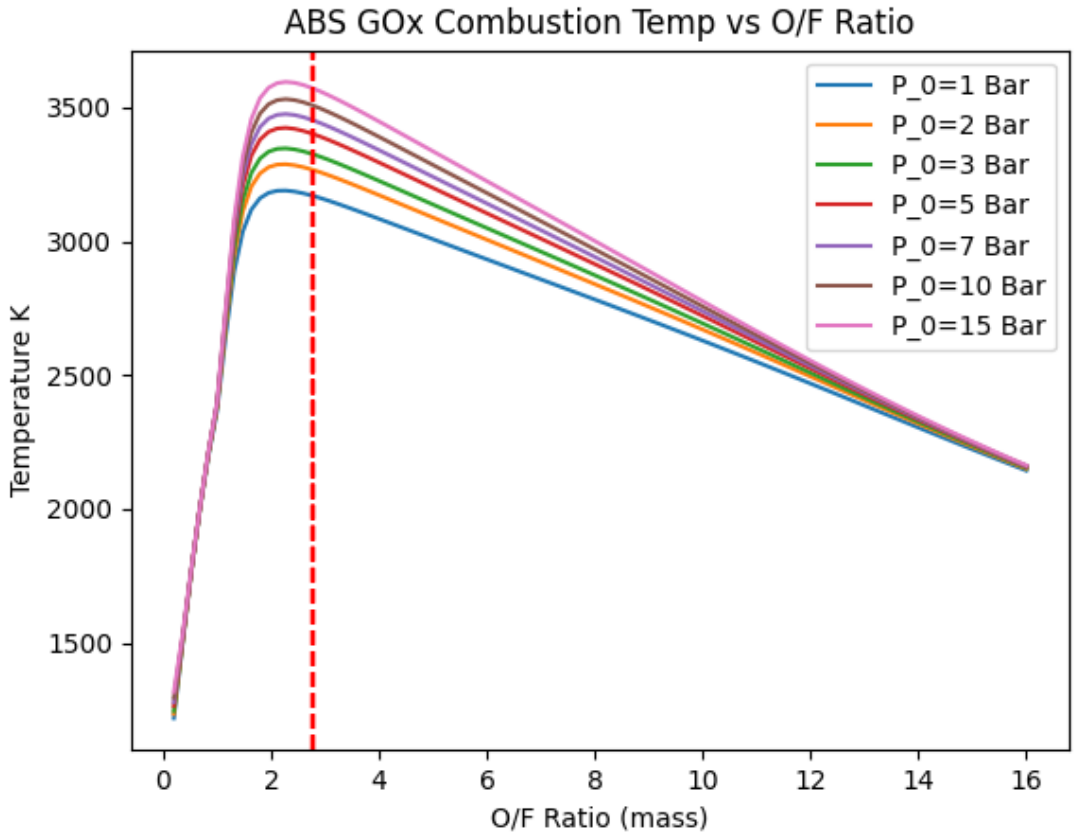

Figure 3.3. ABS and GOx combustion temperature as a function of O/F ratio (mass) at different pressures, red dashed line is stoichiometric proportion.
[10]

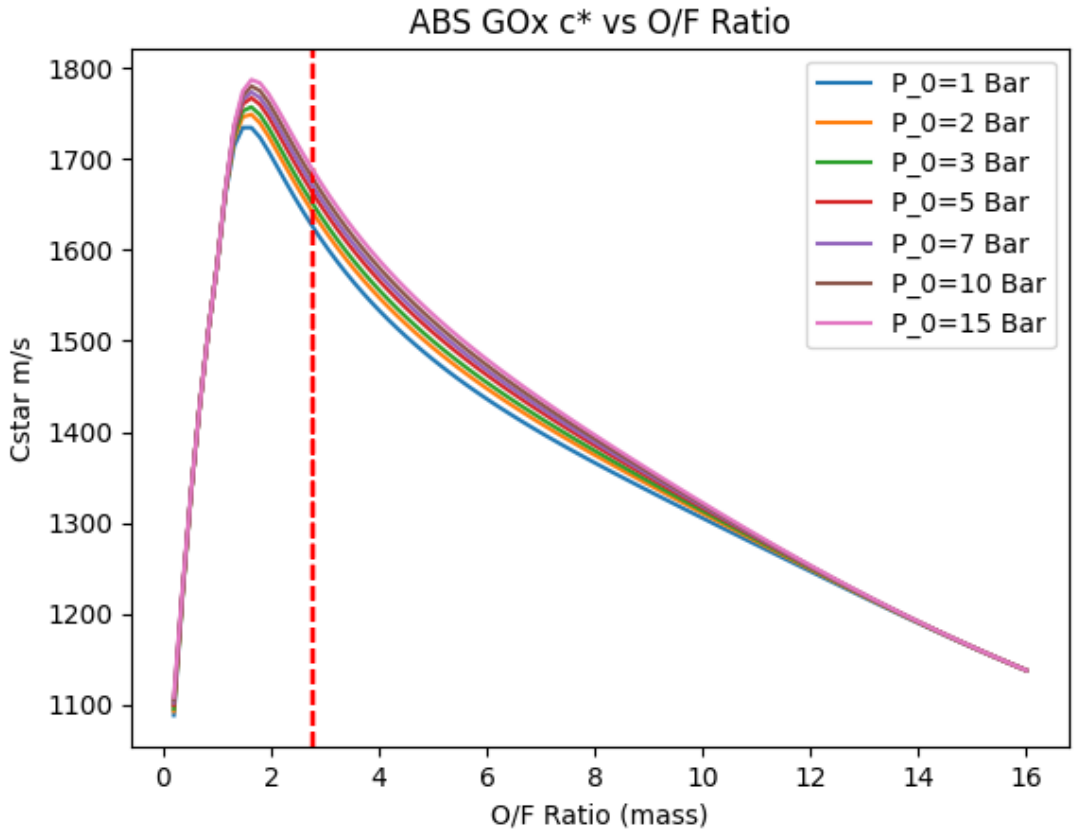

Figure 3.4. ABS and GOx c^* as a function of O/F ratio (mass) at different pressures, red dashed line is stoichiometric proportion.
[10]

At stoichiometric proportions, the ABS and GOx combustion temperatures are about the same as hydrogen, 3000-3500K, but the characteristic exhaust velocity is significantly less, about 800 $\frac{m}{s}$ difference. Thus, the operation of the hydrogen-oxygen torch igniter may affect the performance of the ABS/GOx hybrid rocket by: increasing regression rate by increased heat application and/or increasing the characteristic exhaust velocity by running a more fuel rich torch combustion.

An additional component to the torch igniter is the duration of operation. Inherently, the longer the hydrogen-oxygen torch igniter operates, the more hydrogen propellant is used. In rocketry, the total initial amount of propellants is fixed and is apart of the total mass of the rocket. Therefore, it is generally desirable to have a rocket that uses its

propellants as efficiently as possible. The hydrogen-oxygen torch igniter inherently adds more mass through additional piping and the additional propellant mass, but the system can benefit from using a reliable and repeatable ignition system that may increase the overall performance of the hybrid rocket. Thus it is necessary to analyze and understand the effect of the duration of hydrogen-oxygen torch operation, which for this experiment is called 'Light-Off' time (L.O. time). The L.O. time for this experiment was chosen to have a low condition of 1 second and a high condition of 5 seconds, 10% and 50% of the total burn time respectively. These were chosen in order to try to elucidate the effects of minimal hydrogen utilization and significant hydrogen utilization on the overall ABS-oxygen combustion. Since this experiment is for a hybrid rocket, a full 10 second L.O. time (100% of total burn time) was not tested as this may qualify the rocket as a tri-brid (3 propellant rocket) rather than a hybrid.

3.2 Design of Experiment

A standard 2^k factorial design of experiment is used for the identification of the effects for individual independent variables[78, 79]. This type of experiment is used in order to cover a wide design space while minimizing the amount of runs required. The input variables were selected based on the previous analysis of hydrogen and oxygen combustion and how it may affect the ABS oxygen combustion. Since the goal of this experiment is to elucidate the effects of hydrogen at fuel rich, stoichiometric, and fuel lean proportions, the independent variables chosen are the light-off time (duration of hydrogen-oxygen operation), hydrogen mass flow rate, and oxygen mass flow rate. This yields a 2^3 factorial experiment with 8 unique run configurations. The factorial input matrix is shown in Table 3.1.

Exp. Config.	L.O. Time (s)	$\dot{m}_{H_2}$	$\dot{m}_{O_2}$
A	+	+	+
B	-	+	+
C	+	-	+
D	-	-	+
E	+	+	-
F	-	+	-
G	+	-	-
H	-	-	-

Table 3.1. Factorial experiment design matrix.

Each input has a high (+) and a low (-) state. Run to run variations are inevitable so replication is necessary. Here each experiment was replicated for a total of 16 runs where the run order was randomized in order to prevent biased results due to repetition. The outputs for the factorial design of experiment are: regression rate ($\frac{cm}{s}$), characteristic ignition time (s), and characteristic exhaust velocity ($\frac{m}{s}$).

In order to determine whether or not a change in independent variable causes a statistically significant change in the outputs, a series of mathematical expressions must be solved. After finding the output values for all the runs, the mean and standard deviation are calculated. The values for the effects (E) and interactions (I), known as correlation factors, are then calculated via Equations 3.1 and 3.2:

$$E_i = \frac{\sum_{run=1}^{8} Y_{run} \cdot X_{i,run}}{4} \tag{3.1}$$

The effect of each independent variable, X_i, to each dependent variable, Y_{run}, is calculated by summing the average dependent variable value over all the runs, multiplying by X_i which is equal to 1 or -1 for high or low configurations respectively, and dividing by 4. This equation changes slightly when calculating the interactions between variables because an additional independent variable is added:

$$I_{i,j} = \frac{\sum_{run=1}^{8} Y_{run} \cdot X_{i,run} \cdot X_{j,run}}{4} \tag{3.2}$$

Then the standard error (S_E) is calculated by using the pooled standard deviation and the number of factorials (3 for this experiment):

$$S_E = \frac{2\sigma_P}{\sqrt{n_f}} \tag{3.3}$$

The standard errors calculated in Equation 3.3 show how much sampling fluctuation will occur for a given statistic.

The calculated values from Equations 3.1 and 3.2 elucidate the importance of the effect or interaction to the output values and the directionality of that change. However, these values have to be calculated as statistically significant in order to be considered. In order to determine statistical significance, the Student's t-distribution value is compared with the signal-to-noise t-ratio (t^*). The signal-to-noise t-ratio is calculated in Equation 3.4 using previously calculated values:

$$t^* = \frac{EorI}{S_E} \tag{3.4}$$

The Student's t-distribution used is at a 95% confidence interval with 8 degrees of freedom. For these conditions, the Student's t-distribution value is 2.306 and is used for predicting the mean value of a Gaussian population for small sample sizes. If t^* is greater, then the effect or interaction is considered as statistically significant. For effects and interactions that are deemed statistically insignificant, the values are not analyzed.

3.3 Key Equations and Data Processing

The raw data acquired by the NI-DAQ includes temperatures of the gasses at the inlet, timing, mass flow rates, and pressures. Pressure data for the transducers are inherently noisy and must be processed in order to evaluate further. The data collected is processed in Python language, where a moving average curve fit is applied. The mass flow rates are known at every data acquisition point so the mass flow rates of both the hydrogen and oxygen for the entirety of the burn are known.

3.3.1 Regression Rate

The regression rate is a measurement of the rate of change in inner radius of a solid fuel grain with units in $[\frac{cm}{s}]$. Here, it was determined by two methods: by direct measurement of the inner diameters of the fuel grains and by weight. The direct measurement of the inner diameters was performed by first measuring the end diameters. Then the fuel grains were cut in half axially. After the fuel grain was cut, a measurement of the inner half circumference was performed to each side of the fuel grain. However because the cutting method removed a significant amount of material, an average circumference of material lost was found by comparing the initially measured end diameters with the newly calculated end diameters. The average circumference of material lost was added to each of the calculated circumferences and the regression rate was calculated. Unfortunately, this method introduces a significant amount of error both in the cutting process as well as in the measurement of the circumferences. This led to the use of the average regression rate based on mass, presented in Equation 3.5:

$$\dot{r} = \frac{\frac{\Delta M_{fuel}}{t_{burn}}}{\pi \rho L \sqrt{D_o^2 + (4\frac{\Delta M_{fuel}}{\pi \rho L})}} \tag{3.5}$$

The average regression rate based on mass uses the overall change in mass of the fuel grain ΔM_{fuel} $[g]$, the fuel grain density ρ $[\frac{g}{m^3}]$, time of burn t_{burn} $[s]$, initial diameter D_o $[cm]$, and the length of the fuel grain, L, to calculate a linear regression rate that is space-time averaged [80]. This method has less introduced error since the linear regression rate changes via the change in mass of the ABS fuel grain, rather than making several measurements of the inner diameter along the fuel grain.

3.3.2 Characteristic Ignition Time

The characteristic ignition time is the amount of time it takes the rocket to pressurize to 63.2% of the maximum pressure achieved during the light-off stage. This value is used in order to compare the pressurization rates of each run configuration. It is calculated from a linear ordinary differential equation:

$$\tau\dot{P} + P = P_\infty \tag{3.6}$$

where τ is an exponent and P_∞ is the maximum pressure [Pa] achieved during the light-off stage. After solving for pressure as a function of time:

$$P(t) = (1 - e^{\frac{-t}{\tau}})\Delta P + P_o \tag{3.7}$$

where P_o is the initial pressure at t=0 and ΔP is the difference of the maximum pressure P_∞ and P_o. When the exponent in 'e' is equal to -1 (t=τ), the expression becomes:

$$P(t) = (1 - \frac{1}{e})\Delta P + P_o = 0.632\Delta P + P_o \tag{3.8}$$

Figure 3.5 depicts representative pressure data that has a moving average curve fit applied for a high L.O. time, high GH_2, high GOx mass flow rate configuration.

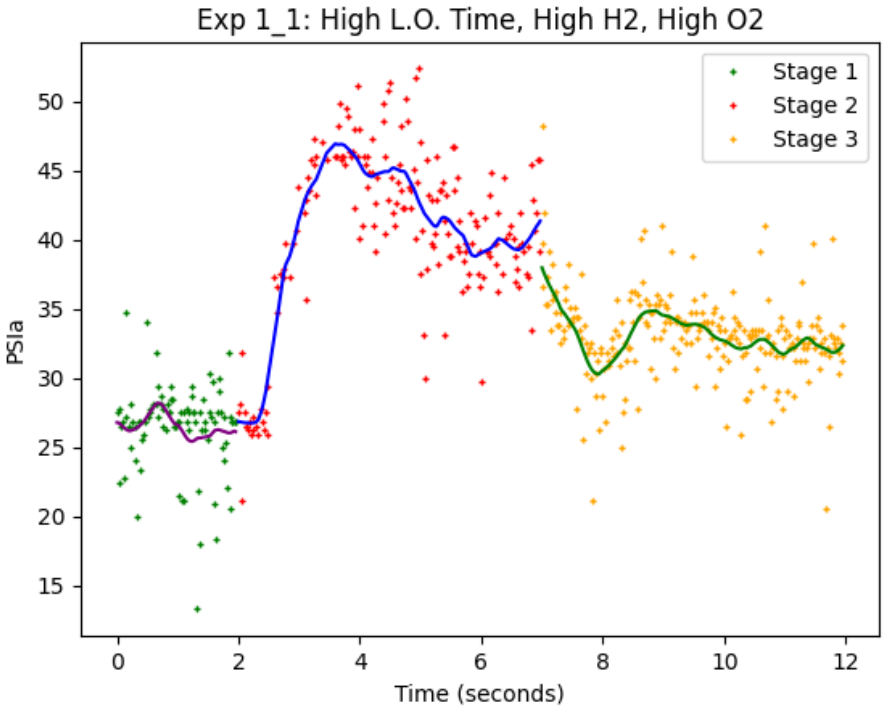

Figure 3.5. Pressure data with applied curve fit for a high L.O. time, high GH_2, high GOx mass flow rate configuration.

Stage 1, is the initial lag period prior to ignition of the torch igniter associated with the opening of the GOx solenoid valve. Here, the Python script automatically finds the point at which the pressure slope starts to increase above 27.579 $\frac{kPa}{s}$. This is the initial point for the characteristic time ignition, t_o and P_o. At this point, all the variables are known and P(t) can be solved. Once P(t) is found, the global run time at P(t) is solved for by linear interpolation between two points on the moving average pressure curve. The difference is taken between the solved global time and the initial global time for the point P_o to find the characteristic ignition time, or the amount of time it takes to pressurize to 63.2%.

Chapter 4

Experimental Setup

4.1 Design of the ABS/GOx/GH_2 Rocket

In this chapter, an overview of the ABS/GOx/GH_2 rocket design is presented. This is a non-flying experimental hybrid rocket that is situated on a linear guide rail to allow thrust measurements. The hydrogen-oxygen torch igniter has 4 inlet ports for the gaseous oxygen, gaseous hydrogen, pressure transducer, and a spark plug. At startup, the hydrogen and oxygen combine within the hydrogen-oxygen torch igniter and are ignited by the spark plug. The fluids then flow into the main combustion chamber where the nominal combustion of ABS and GOx occurs and the products of combustion exit out of the nozzle. After a period of time, defined by the L.O. time, the hydrogen flow is closed, leaving just the oxygen flow on.

4.1.1 Hydrogen-Oxygen Torch Igniter/Injector

The ABS/GOx/GH_2 hybrid rocket presents an interesting design challenge that deviates from normal hybrid rocket design. Normally hybrid rockets employ only one fluid oxidizer which allows for direct injection into the main combustion chamber. However, since this project investigates the hydrogen-oxygen torch igniter as well as how the hydrogen effects the burn characteristics, a standard injector is not optimal. Additionally, because the torch igniter operates for a longer period of time than what is conventionally done, temperature is of concern. Of particular concern is where the flame kernel is projected to reside, near the point of hydrogen and oxygen contact. This means that the surrounding

body and any piping connections will need to be able to withstand a significant amount of heat and pressure.

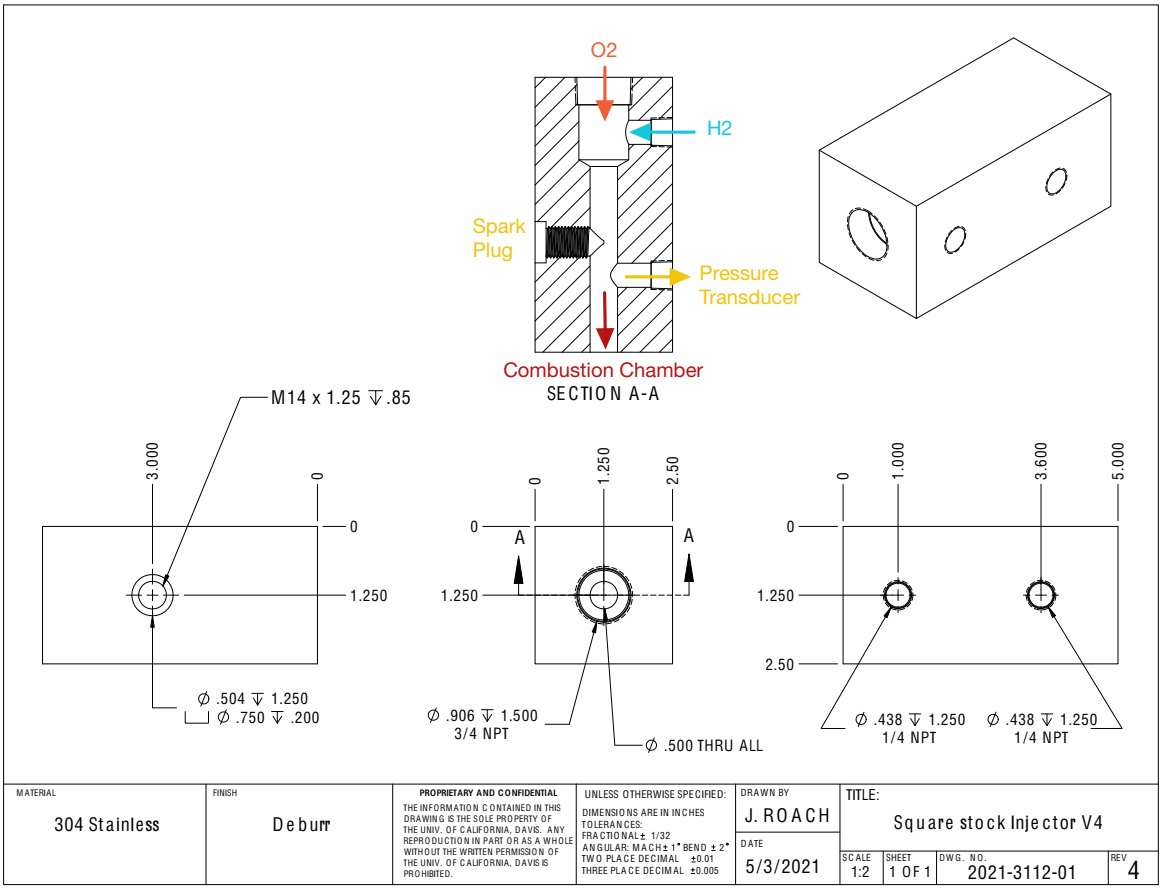

Figure 4.1. Hydrogen-oxygen torch igniter manifold.

As shown in Figure 4.1 the hydrogen-oxygen torch igniter is constructed from a 304 stainless steel block with four ports for the hydrogen, oxygen, spark plug, and pressure transducer. The steel block has a circular 1.27 cm (0.5 in) through hole for the gasses to travel in. The oxidizer port is along the axial direction while the hydrogen port is in the radial direction. The hydrogen enters a plenum-like chamber where the flow is forced to converge slightly. This was done in order to minimize swirl injection which is another method of increasing hybrid rocket performance. This experiment seeks to isolate how hydrogen affects the hybrid rocket combustion so utilizing a swirl injector may influence the results. The oxidizer port has a 1.27 cm (0.5 in) Swagelock fitting that has been

modified to allow a 0.635 cm (0.25 in) tube to pass through it. The oxidizer stream exits the 0.635 cm (0.25 in) tube approximately 2.54 cm (1 in) prior to the spark plug port. This was done in order to minimize the amount of thermal heat loss to the injector block, decreases the risk of flashback leading back into the gas tanks since the flame kernel is limited to the location of available oxygen, and allows for the hydrogen and oxygen to mix prior to the spark plug. The spark plug is an Bosch Iridium spark plug that is connected to a circuit containing common automotive ignition parts: a 12V battery, an ignition coil, and a condenser. The spark plug is operated by a manual toggle switch located next to the main operations terminal. Lastly, the pressure transducer port was designed to be close to the main combustion chamber in order to get accurate chamber pressures.

The hydrogen-oxygen torch igniter is then welded to a 304 stainless steel face plate that mates to the main combustion chamber, as seen in Figure 4.2.

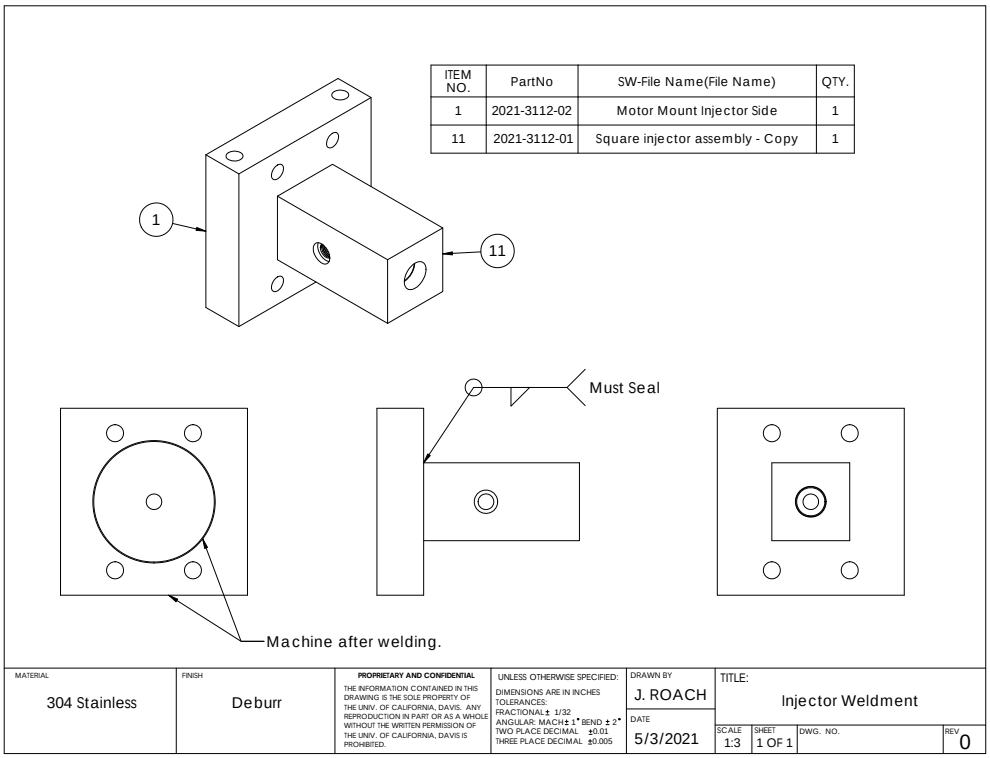

Figure 4.2. Full assembly of the hydrogen-oxygen torch igniter

By integrating the injector with the torch igniter, the walls can be cooled slightly by

the oxygen stream prior to entering the combustion chamber after the hydrogen flow is turned off. In addition, by integrating the two together there are less components that can fail such as pipe connections. Furthermore, this design minimizes the amount of thermal losses of the torch flame by decreasing the total distance from flame kernel to the ABS fuel grain.

4.1.2 Main Combustion Chamber

Illustrated in Figure 4.3, the main combustion chamber is a 10.16 cm (4 in) outer diameter by 30.48 cm (1 ft) 304 stainless steel pipe that houses the ABS fuel grain and is subject to high temperatures and pressures. On each end, the pipe tapers to allow for a male-female press fit with a groove for a Viton O-ring that helps seal the combustion chamber and the end plates.

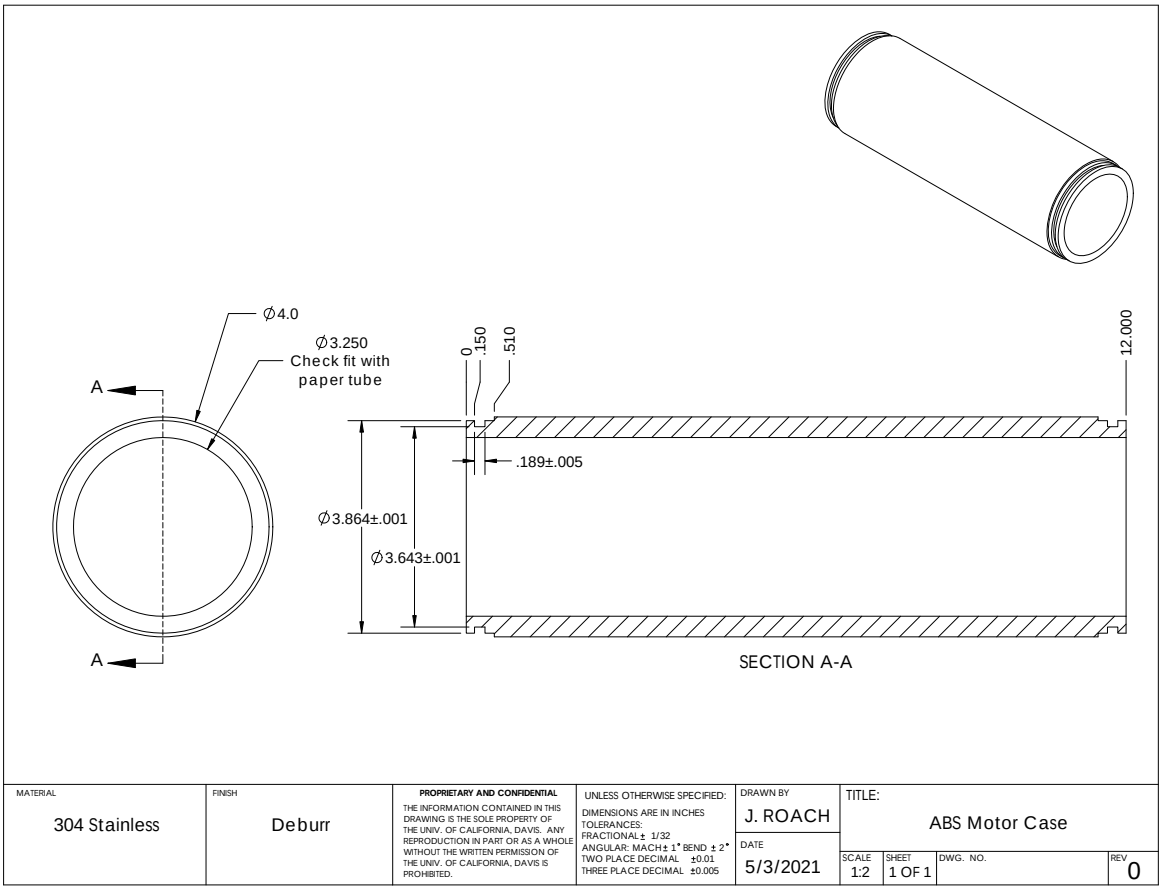

Figure 4.3. Motor case

The main combustion chamber is sealed by compression via the two end plates and four 16 inch threaded dowel rods. The combustion chamber is first press-fitted into both of the end plates, then the dowel rods are threaded through the holes in the end plates. Washers and nuts are then added to the outside of the dowel rods and installed to approximately 20.3373 N-m (15 ft-lbs) of torque. The ABS fuel grain is press fitted into a cardboard liner which allows for easy installation, sealing any gaps along the outer diameter of the fuel grain, and to ensure that the fuel grain does not melt to the combustion chamber. Thus the inner diameter of the combustion chamber must also account for both parts.

A pressure analysis was conducted for the main combustion chamber assuming no fuel grain to ensure the safety in the design. For this calculation, the main combustion chamber was assumed to be a capped pressure vessel with 266.893 N (60 lbf) applied axially, simulating the force applied via the compression plates that seal the rocket. This calculation did not use temperatures on the order of the rocket combustion temperatures. This is done because total run time of the rocket is low, the end plates are thick stainless steel that are significant heat sinks, and the ABS fuel grain will insulate a significant amount of heat therefore the motor case's temperature should be cool. The Von Mises yield criterion was used in order to find at what stresses would cause failure. It was calculated for a factor of safety equal to 1, the combustion chamber would require 33.65 MPa (4880 psia) to induce failure. At chamber pressures equal to 2.07 MPa (300 psia), the factor of safety would be 16.3.

4.1.3 Nozzle

The nozzle is composed of isomolded graphite and has a cylindrical body with two conical cuts in the center where they meet in the center to form the throat of the nozzle, as seen in Figure 4.4. A conical nozzle was chosen because it is the easiest to manufacture. The half angle, α, was set to 15 degrees and the length of the converging section was 5.31 cm (2.09 in) and the length of the diverging section was 2.31 cm (0.91 in). The nozzle fits through the nozzle end plate and is pressed against the end plate via a ledge of material. The section of the nozzle that fits through the end plate hole features a groove for a Viton O-ring that seals the nozzle from the outside environment.

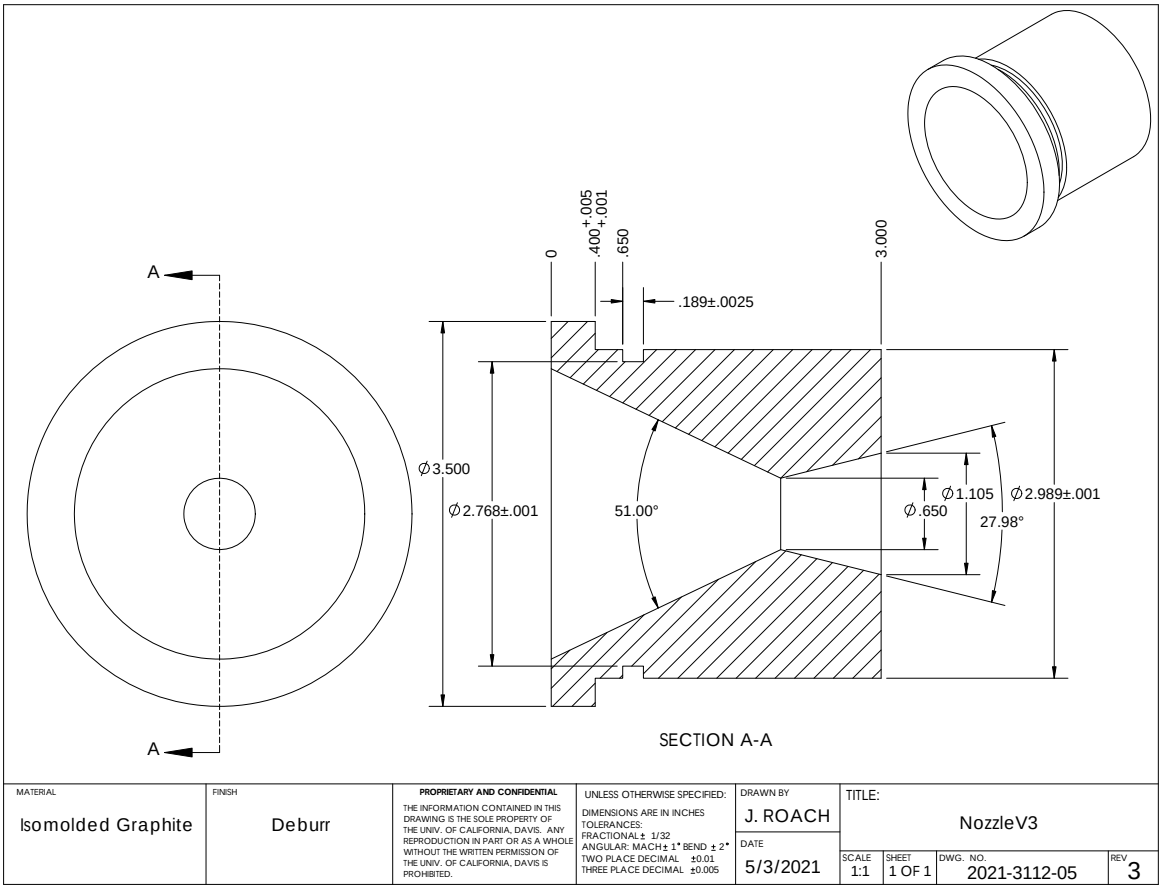

Figure 4.4. Nozzle drawing

The nozzle was designed for 1.72 MPa (250 psia) chamber pressure with an assumed ratio of specific heats, k, equal to 1.3. This resulted in an expansion ratio equal to 2.89. The nozzle throat diameter was chosen, but unfortunately this diameter was too large for the mass flow rates that were achieved in the experiment. This was an oversight of the design because at the time of design, the total propellant mass flow rate had not been determined and an arbitrary 1.65 cm (0.65 inch) diameter was chosen based on experiments found in the literature. However, the throat was able to reach sonic conditions, but resulted in an over-expanded flow. The nozzle throat diameter was measured after each run with several dowel rods at known sizes, however the nozzle throat had no measurable erosion.

4.2 ABS Fuel Grain Fabrication

ABS was ordered in 7.62 cm (3 in) nominal OD by 30.48 cm (1 ft) rod stock lengths via McMaster Carr (see Appendix D). The exact formulation of the ABS fuel grain is proprietary to the manufacturer. Because of inherent fabrication tolerances in the initial production of the ABS rod, it had to be machined down radially to about 7.59 cm (2.990 inches). However, due to the COVID-19 pandemic, large fabricating machines were unavailable for student use and therefore an angle grinder with grit 120 was used.

The ABS was first marked on both ends with a circle denoting the desired diameter. The rod stock was then placed in a vice grip and even passes of the angle grinder were performed on the top of the fuel grain until the top part of the marked circle was no longer visible. The rod stock was rotated slightly such that a visible part of the marked circle was facing upwards in the path of the angle grinder passes. After grinding the ABS rod stock, a fitment check with the cardboard fuel liner was performed. The goal of this fitment check was to ensure that the fuel grain was able to fit inside the cardboard liner without slipping out. An example of a used fuel grain that is installed within the motor case next to a new fuel grain in its cardboard fuel liner is shown in Figure 4.5.

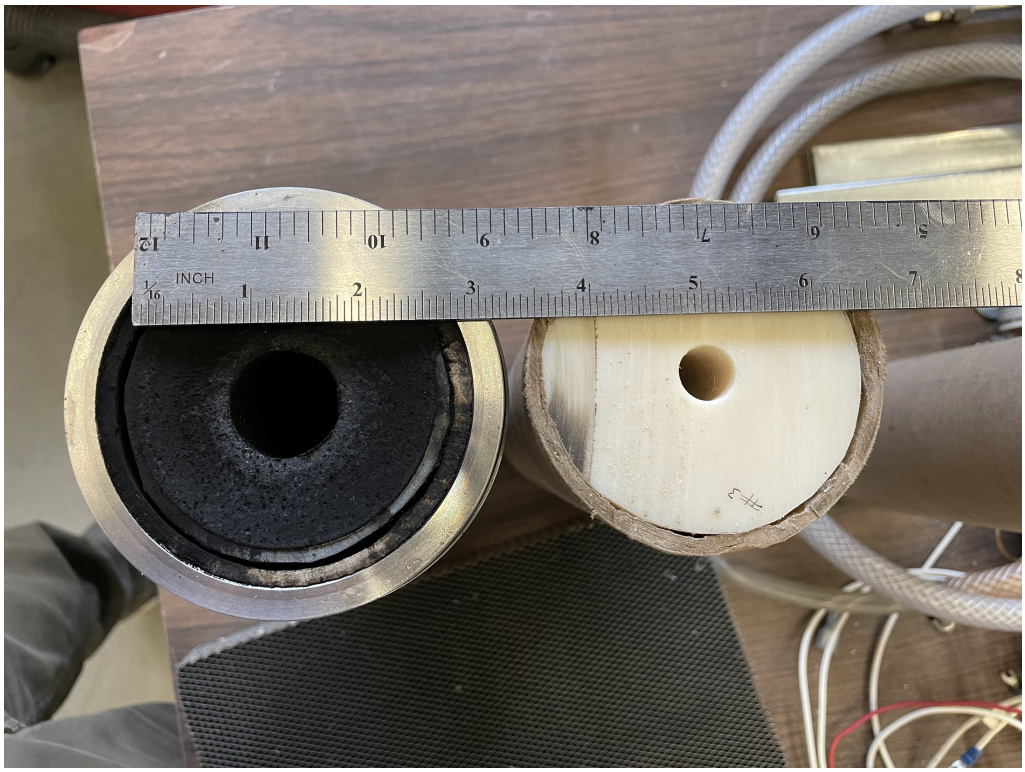

Figure 4.5. Used ABS fuel grain installed within the motor case and unused ABS fuel grain, left to right

Once the ABS rod stocks were inside the cardboard fuel liners, the next step was to insert a 1.27 cm (0.5 in) bore through hole. By using a 3D printed guide, marks were made on each face denoting the bore through point. Ideally, a lathe would be used to create a straight hole, however as mentioned above, large machinery was inaccessible to students. Thus a drill press with a 1.27 cm (0.5 in) by 60.96 cm (2 ft) long drill bit was used. Because of the unusual length of the drill bit, the drill press had to be modified in order to process the ABS rod stock. A linear rail system was installed using a long "L" bracket so that the operator could push the ABS rod stock against the linear rail and make consistent straight holes. Because of the relatively low melting point (compared to metals) of ABS, there is a danger of the drill bit casting radially during the cutting process. In order to alleviate this, the drill bit was frequently cooled and lubricated with water. Additionally, frequent small "pecks" of the drill bit were made to the surface. Once the through holes were made, the ABS fuel grains were weighed and a check of the ends' inner diameters were performed in order to verify that the inner diameter was 1.27

cm (0.5 in).

4.3 Experimental Equipment

4.3.1 Test Stand

The ABS/GOx/GH_2 rocket was situated inside of a 2.13 m by 2.13 m by 0.914 m (7 ft by 7 ft by 3 ft) deep fume hood within the Energy Research lab where the emitted exhaust gases were taken through a section of steel ducting before being released into the fume hood exhaust. The fume hood was chosen as a location for the firing tests because it can adequately evacuate the exhaust gases created and has a glass fume hood sash that acts as a barrier for potential projectiles and heat. Additionally, the fume hood has a pre-existing metal frame structure that could be used to mount a test stand, has ports for multiple circuits and data acquisition that can be controlled by the lab computer, and the test gases are located nearby eliminating the need to move them from their storage locations. The test stand was built to fit a pre-existing metal frame structure that was used to mount other experiments that were conducted in the Energy Research Lab. L brackets were mounted on the side of the metal frame where a platform was installed. The platform was constructed with wood sheets as a bottom support layer with a large piece of sheet metal on top. Two linear rails were mounted to the top of the platform which allowed the rocket to sit and move axially. An Omega 2224.11 N (500 lbf) button load cell was mounted to the metal frame structure and made contact with the front face of the injector block as shown in Figure 4.6.

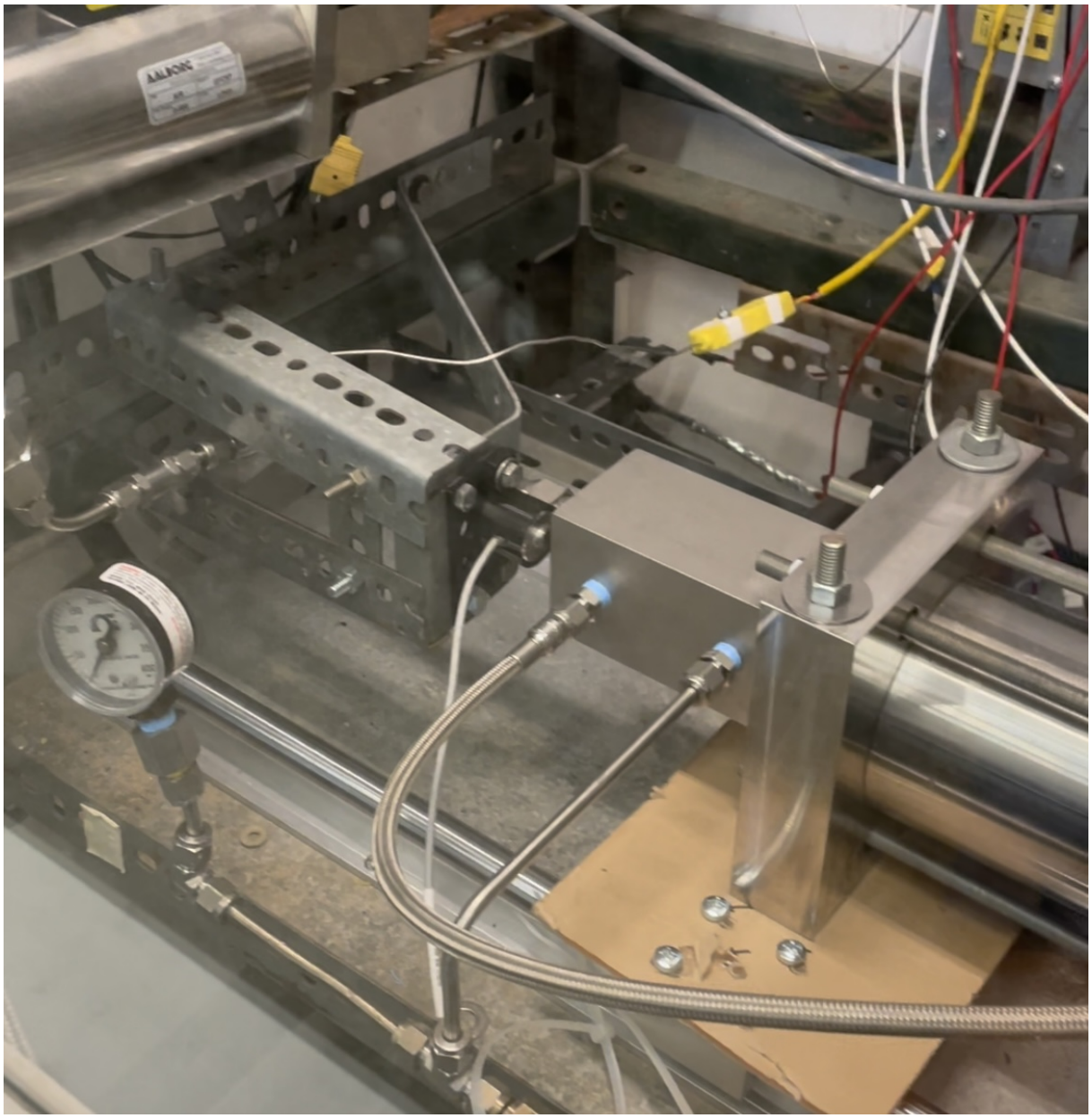

Figure 4.6. Button force transducer connection point

Since the burn impulse was low for each run, a blow-down propellant feed system was used. Gases were transported from their K-type bottles from Airgas through 1.27 cm (0.5 in) stainless steel braided flex hosing. Flex hosing was used in particular for the oxygen line because the rocket's linear movement where regular tubing would restrict its movement and would affect the thrust measurements. From the K-type bottles, the gases were flowed through 1.27 cm (0.5 in) normally closed solenoid valves.

A functional block diagram of the experimental setup is presented in Figure 4.7.

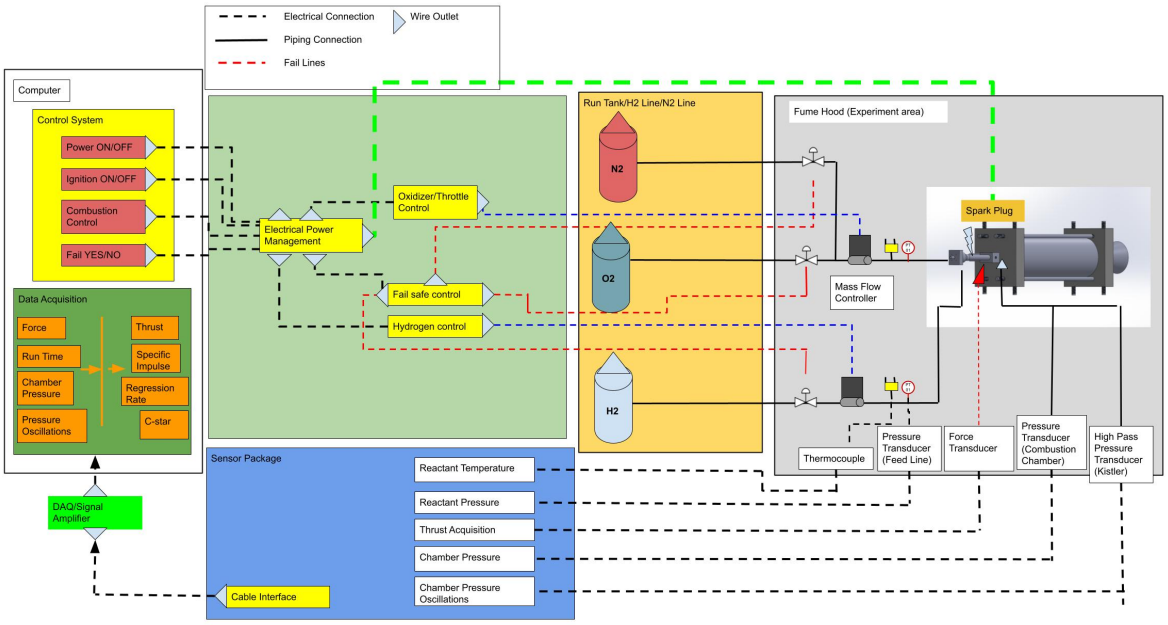

Figure 4.7. Functional block diagram of the test stand and operational systems

The solenoid valves were connected to the circuits within the hood and controlled via the lab computer. Solenoid valves were crucial to the experiment for timing and safety purposes. The solenoid valves were controlled on specific timing sequences that depended on the experiment and the actuation of these valves ensured that no additional flow from the tanks was allowed. Furthermore, the valves acted as safety mechanisms in the event of an emergency shutdown. Hybrid rockets' rate of combustion is directly controlled by the oxidizer mass flow rate, thus a complete shutoff of the oxidizer and any additional flammable gases ensures that no further combustion can ensue. In addition, a nitrogen gas line was added to the experiment in order to purge any leftover gases and completely halt any combustion within the rocket.

After the solenoid valves, the mass flow rate of each gas was controlled by Aalborg GFC67 500 liter per minute mass flow controllers which were mounted to the structural frame within the fume hood. The mass flow controllers are calibrated to air, thus when other gasses are used, calibration factors are used to find the actual mass flow rate. According to the manufacturer's guidelines, the value of the mass flow controller needs

to be multiplied by an empirically found 'k-factor' depending on the gas (see Appendix A). For oxygen, the k-factor is equal to 0.9926 and for hydrogen it is equal to 1.9. For example, if the mass flow controller reads 100 liters per minute for hydrogen, the actual volumetric flow rate is $100 * 1.9 = 190$ liters per minute. The mass flow controllers operate by a motorized valve which is opened and closed proportionally to the input voltage and deviations from the set point mass flow rate are automatically adjusted. Finally, the gases flow through a series of check valves to ensure no reverse flow and the temperatures of the flowing gases are checked by Omega K-type thermocouples before entering the rocket.

4.4 Run Procedure

Prior to installing the ABS fuel grain, the fuel grain's initial diameters and mass were measured. This is crucial for accurate regression rate calculations. The fuel grain was then placed within the motor case and the end plates were installed by tightening the nuts on the the four 0.953 cm (0.375 in) by 40.64 cm (16 in) threaded dowel rods to 20.3373 N-m (15 ft-lbs) of torque.

In order to minimize run to run variability and ensure the safety of all personnel, a pre-run procedure was followed. After personnel were cleared from the experiment area, the gas lines were 'pre-charged' by allowing the oxygen and hydrogen to flow separately then closing the mass flow controllers and solenoid valves. This ensures that the gases start flowing from the same place every run and that the safety mechanisms, namely the solenoid valves, were operating as intended.

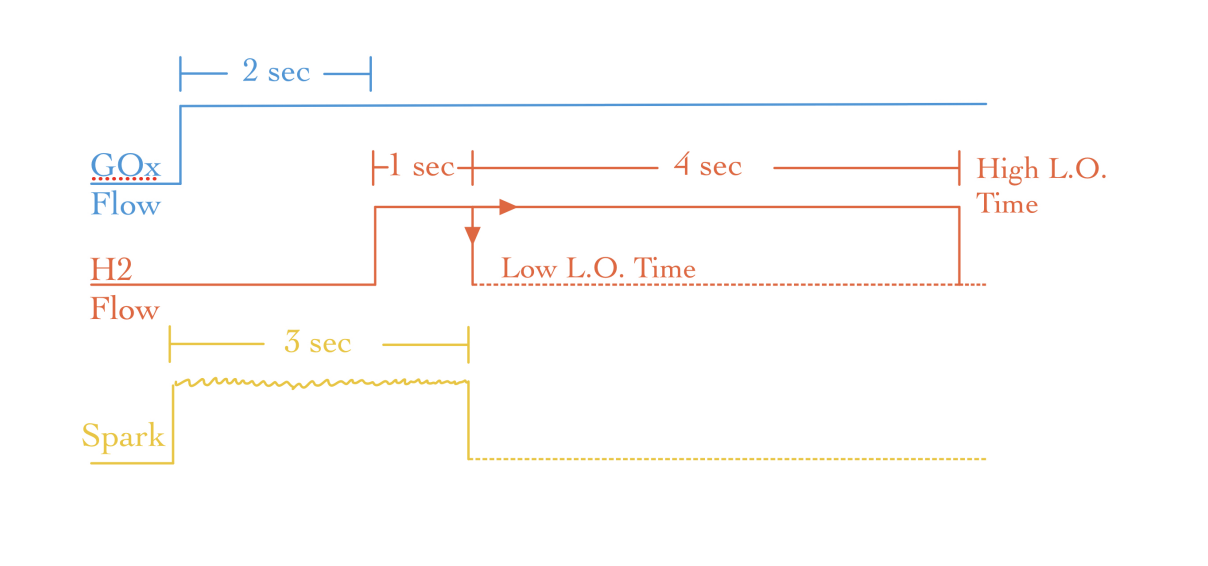

Figure 4.8. Ignition Sequence

After a final personnel check, the experiment began following the sequence outlined in Figure 4.8. This ignition sequence was modeled similarly to the NASA Lewis hydrogen-oxygen torch igniter [9]. At the start of the experiment, the oxygen flows for 2 seconds to ensure that there is no air within the rocket. At the same time, the spark plug is operated at a rate of about 100 hz. The spark plug is operated prior to the hydrogen flow to minimize hard starts or explosive ignitions that can occur if hydrogen and oxygen are allowed to mix well within the entire injector geometry. The hydrogen solenoid opens after 2 seconds and ignition is almost instantaneous. The spark plug continues to operate for an additional 1 second to ensure ignition before shutting off. The duration of time that hydrogen is allowed to flow is called the 'light-off time' (L.O. time) and it varies between the high condition of 5 seconds and the low condition of 1 second. After the L.O. time is elapsed, the hydrogen flow shuts off by closing both the mass flow controller and solenoid valve, allowing for pure GOx flow to enter the main combustion chamber.

At the end of the run, a nitrogen purge is performed for 15 seconds. This done in order to stop any combustion or smoldering within the rocket which would affect the end results. After a brief visual inspection to confirm no continued burning, the hydrogen and oxygen lines are purged separately by closing the quarter-turn run valves and opening the

solenoid valves and mass flow controllers. After about 30 minutes, a laser thermometer was used to ensure that the rocket has reached a safe handling temperature, then the ABS fuel grain was retrieved and its final diameters and mass were measured. See Appendix C

Chapter 5

Results

The hydrogen-oxygen torch igniter attained ignition for all test runs, across the varying O/F ratios, and with varying oxygen mass flow rate conditions. After careful inspection of the spark plug and internal components of the torch igniter, little to no degradation was found. Similarly the spark plug did not need to be replaced for the entire testing campaign. The torch igniter operated at oxidizer to fuel equivalence ratios, λ, of 1/2, 1, and 2 and was able to successfully ignite the ABS fuel grain 15 out of 16 tests. Despite being implemented into the system, the force transducer did not produce reliable outputs. It is believed that this is due to low oxygen mass flow rates leading to low nozzle performance resulted in low thrusts that are too small for the force transducer to reliably capture. Figure 5.1 shows an image of the ABS/GOx/GH_2 rocket in action.

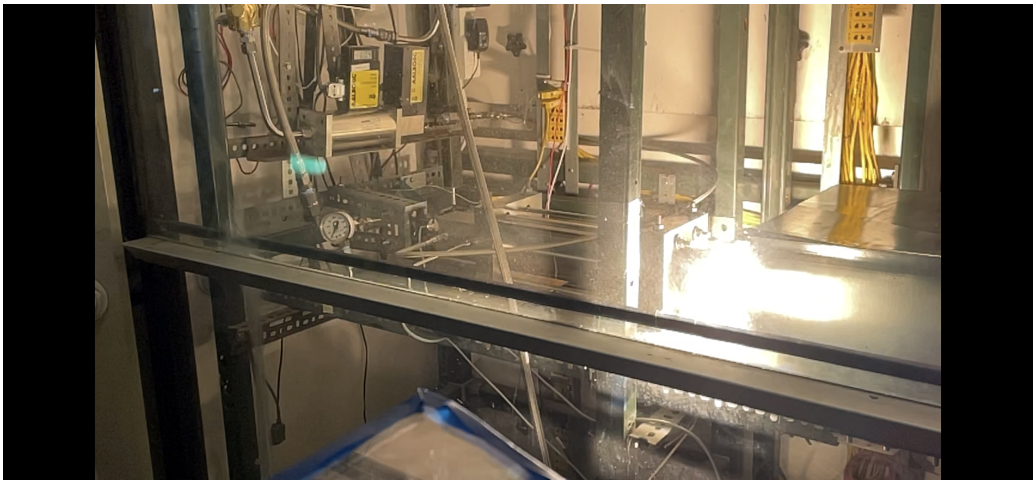

Figure 5.1. ABS/GOx hybrid rocket in action.

5.1 Pressures

The high oxygen mass flow rate resulted in the higher overall pressures as compared to the low oxygen mass flow rates. In Figure 5.2, the pressure plots for the high oxygen mass flow rate configurations are presented. 'Exp A' has the highest maximum pressure and highest pressure impulse due to the high light-off time and high hydrogen mass flow rate. The initial high pressure then drops suddenly at t=7 seconds, corresponding to the hydrogen mass flow stopping, and adjusts to the 'nominal' pressure, 240 kPa. 'Exp C' has a similar drop in pressure as 'Exp A', but since the mass flow rate of the hydrogen is low, the pressures within the L.O. time are similar to the low L.O. time 'Exp B' and 'Exp D'.

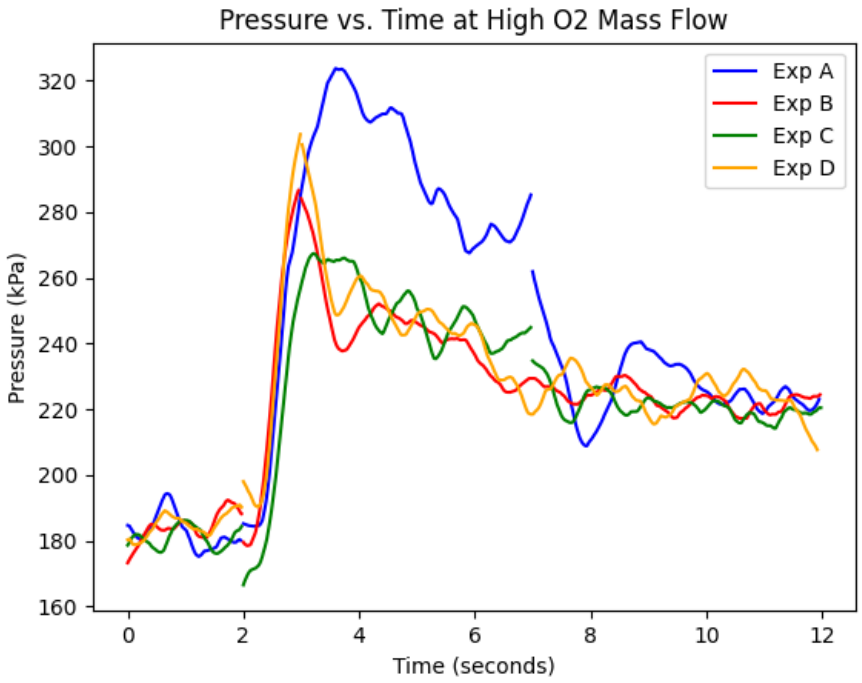

Figure 5.2. High oxygen mass flow rate pressure plots.

In Figure 5.3, the pressure plots for the low oxygen mass flow rate configurations runs are presented. At low O2 mass flow rate condition, the runs exhibited similar pressure curves to each other. Notably, 'Exp E' had a late pressure increase at about t=7 seconds, when the hydrogen mass flow rate shut off. This run exhibited a small 'sputter' at this

moment in the flame before returning to a more normal flame structure. It is believed that there was significant competition for oxygen between the ABS and the hydrogen for this run. This will be discussed in more detail in the following section.

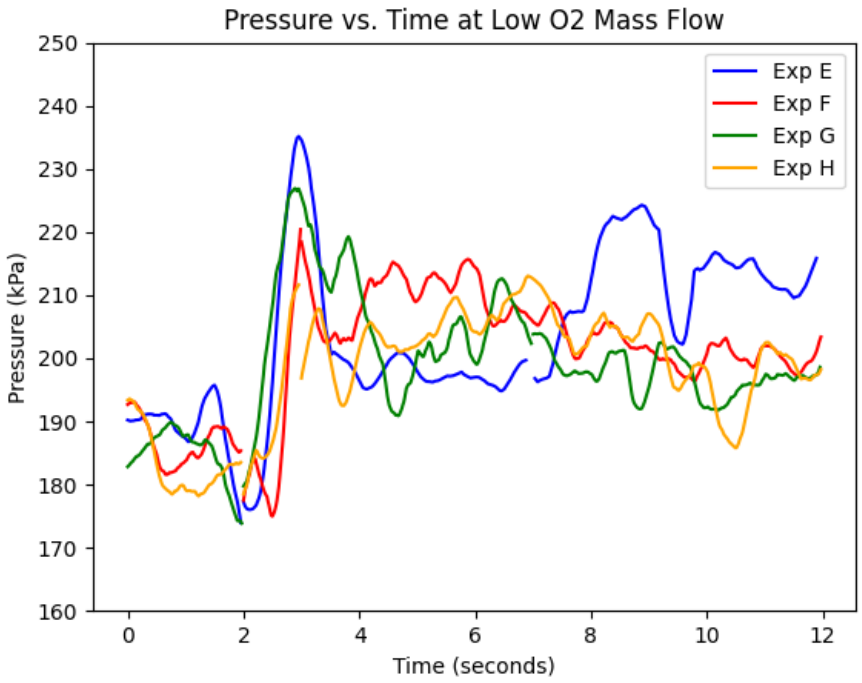

Figure 5.3. Low oxygen mass flow rate pressure plots.

5.2 Regression Rate

Low regression rates are frequently discussed within hybrid rocket literature. Researchers have attempted to address this problem in several ways such as complex grain geometries, fuel grain additives, and swirl injectors. This project looks to address how hydrogen may affect the regression rate by varying the duration the hydrogen mass flow and the hydrogen mass flow rate, at two different oxygen mass flow rates.

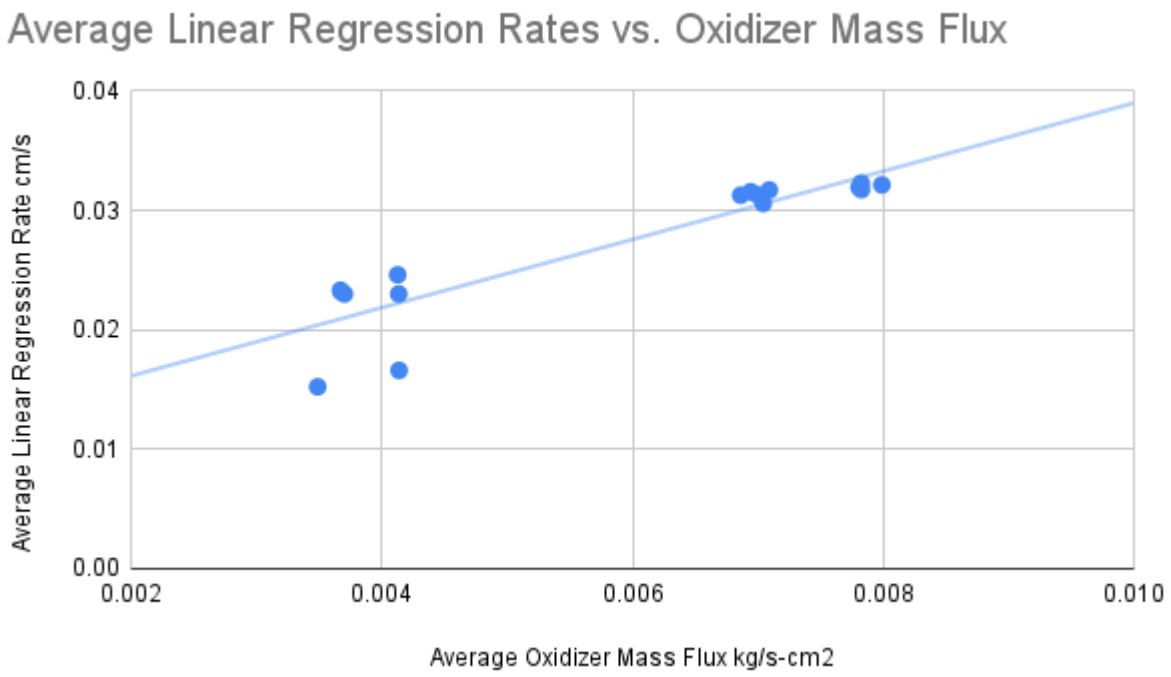

Figure 5.4. Average linear regression rates vs. oxidizer mass flux.

The average linear regression rate for all the test runs are plotted in Figure 5.4 as a function of the oxidizer mass flux $[\frac{kg}{cm^2 s}]$. As previously stated, the designed rocket nozzle required more mass flow rate than what the experiments had and as a result performed sub-optimally. However the regression rate is still valid despite this, since the regression rate for hybrid rockets is not a strong function of the pressure [1, 3, 28, 81].

In Table 5.1, the signal-to-noise ratios, t^*, are listed for each effect and interaction. As discussed previously, in order for the effect or interaction to be considered as statistically significant, t^* must be greater than 2.306. According to the factorial experiment design, based on a Student's t-distribution at a 95% confidence level, all the values are considered statistically significant.

	$E_{L.O.time}$	E_{H2}	E_{O2}	
t^*	-4.435561489	-6.402756283	35.70318756	
	$I_{L.O.,H2}$	$I_{H2,O2}$	$I_{L.O.,O2}$	$I_{L.O.,H2,O2}$
t^*	-6.920649562	7.976581074	7.41803399	6.679954642

Table 5.1. Signal-to-noise table for average linear regression rates.

As presented, the effects of Light-Off time and hydrogen mass flow rate are negative indicating that an increase in either one will decrease the average linear regression rate. However, since all of the interactions are also statistically significant, in-depth analysis is required. Since the oxygen mass flow rate directly effects the average linear regression rate as established by Marxman and Gilbert [1, 29] (see Section 2.1.4), the discussion of the results are split between high and low oxygen mass flow rates. This is done in order to more precisely analyze the effects and interactions of L.O. time and hydrogen mass flow rate.

Exp. Config.	L.O. Time (s)	$\dot{m}_{H_2}$ $[\frac{L}{min}]$	$\dot{m}_{O_2}$ $[\frac{L}{min}]$	$\bar{r}_{mass}$ $[\frac{cm}{s}]$
A	5	950	500	0.0322
B	1	950	500	0.0314
C	5	475	500	0.0318
D	1	475	500	0.0309

Table 5.2. Average linear regression rates for the high oxygen mass flow rate configuration.

The average linear regression rates for the high oxygen mass flow rate configuration are presented in Table 5.2. At the high oxygen mass flow rate condition, the average linear regression rate was found to increase for both an increase in the light-off time and an increase in the hydrogen mass flow rate. When isolating the effect of L.O. time, the regression rate increased 2.43% at the high hydrogen mass flow rate. At the low hydrogen mass flow rate, the regression rate increased by 2.9%. Likewise, when isolating the effect of hydrogen mass flow rate, at the high L.O. time condition, the average linear regression rate increases by 1.17%. At the low L.O. time condition, the regression rate increases by

1.64%.

As a result, at the high oxygen mass flow rate, the run configuration that had the largest regression rate was experiment configuration A. At configuration A, the hydrogen-oxygen torch operates at a stoichiometric O/F ratio (λ =1) which can attain a higher adiabatic flame temperature, about 3100K, when compared to a more fuel lean O/F ratio,(low hydrogen, high oxygen mass flow rate condition) about 3000K (λ =2). It is theorized that the higher torch flame temperature leads to higher temperature of the ABS fuel grain which results in higher pyrolysis rates. Furthermore, it is postulated that the increase in L.O. time led to an increase the regression rate due to longer exposure to high heat flux, thus increasing the overall amount of heat absorbed by the ABS fuel grain. Likewise, the increased regression rate due to an increase in hydrogen mass flow rate may be attributed to a difference in adiabatic flame temperatures. These results are further elucidated by the previously discussed Equation 2.1, where the regression rate of a turbulent boundary layer combustion can be increased with an increase in the convective heat transfer from the flame to the surface of the fuel grain, $h_{comb} - h_{wall}$ $[\frac{kj}{kg}]$. The hydrogen may also be aiding in the combustion mechanism of the ABS and GOx, however further testing is required to test this hypothesis.

Exp. Config.	L.O. Time (s)	$\dot{m_{H_2}}$ $[\frac{L}{min}]$	$\dot{m_{O_2}}$ $[\frac{L}{min}]$	$\bar{r_{mass}}$ $[\frac{cm}{s}]$
E	5	950	250	0.0159
F	1	950	250	0.0231
G	5	475	250	0.0238
H	1	475	250	0.0233

Table 5.3. Average linear regression rates for the low oxygen mass flow rate configuration.

The average linear regression rate for the low oxygen mass flow rate condition are listed in Table 5.3. The effect of the light-off time and the effect of hydrogen mass flow rate change for the low oxygen mass flow rate configuration. Here, the average linear regression rate only increased when the L.O. time was increased at the low hydrogen mass flow rate. This resulted in a linear regression rate increase of 2.09%, from 0.0233

$\frac{cm}{s}$ to 0.0238 $\frac{cm}{s}$. However, when the hydrogen mass flow rate is increased, for both high and low L.O. times, the average linear regression rate decreased by 39.73% and 0.95%, respectively. Similarly, when the L.O. time was increased at the high hydrogen mass flow rate condition, the linear regression decreased by 36.8%, from 0.0231 $\frac{cm}{s}$ to 0.0159 $\frac{cm}{s}$. It is important to note that when the oxygen mass flow rate is at the low condition and the hydrogen mass flow rate is at the high condition, the torch O/F ratio operates at fuel rich GH_2/GOx flame conditions ($\lambda = \frac{1}{2}$). When considering the location of where the two torch gasses meet, it is theorized that the initial flame kernel resides just before the main combustion chamber of the rocket. Therefore, when the torch operates at rich flame conditions, the oxygen will most likely react with the hydrogen rather than reacting with any pyrolyzed volatile hydrocarbons, creating a competition between the two fuels.

In Figures 5.5-5.7, mole fraction graphs as a function of O/F for the available oxidizer molecules in a hydrogen-oxygen flame at varying pressures. It can be seen that at steady state conditions and equivalence ratio equal to 1/2 (O/F=4), little to no oxidizer molecules are available. This elucidates the importance of the G_{ox} term in Equation 2.1 since the ABS fuel grain does receive high heat flux from a hot hydrogen-oxygen flame, but because available oxygen is near zero, the regression rate remains low.

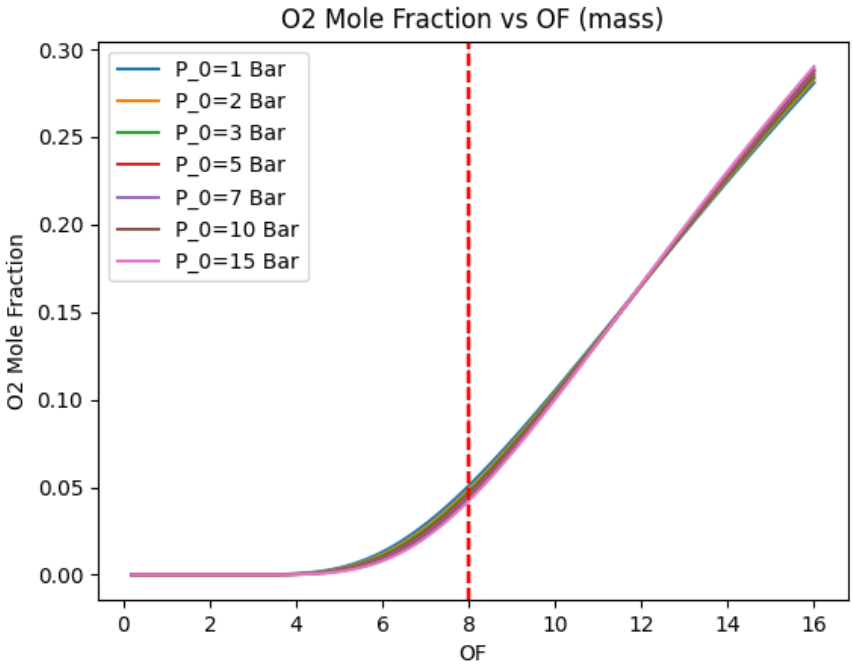

Figure 5.5. O2 mole fraction as a function of O/F ratio (mass) for different pressures for a hydrogen-oxygen flame

[10]

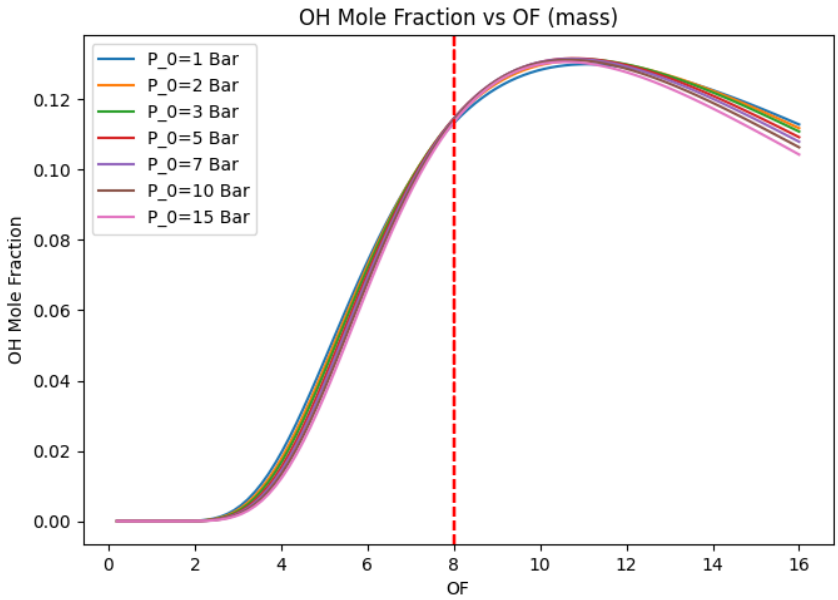

Figure 5.6. OH mole fraction as a function of O/F ratio (mass) for different pressures for a hydrogen-oxygen flame

[10]

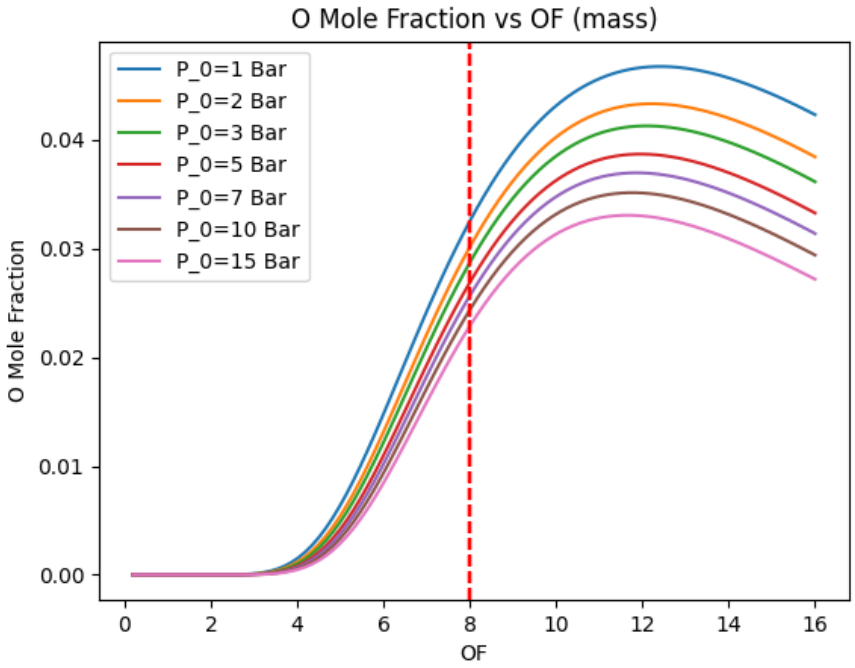

Figure 5.7. O mole fraction as a function of O/F ratio (mass) for different pressures for a hydrogen-oxygen flame

[10]

The competition for available oxygen was particularly notable for the second of the two runs at configuration E (high L.O. time, high GH_2 mass flow rate, and low O_2 mass flow rate). The torch igniter was unable to produce combustion with the ABS fuel grain after achieving ignition between the hydrogen and oxygen. It was observed that as the hydrogen mass flow was turned off, short 'sputtering' occurred followed by the flame being extinguished. Interestingly, this flame extinguishment was not experienced during the first test with the same experimental configuration, however similar sputtering was experienced at the point when hydrogen was completely shutoff. Upon flame extinguishment, the system was allowed to cool for 30 minutes, as per safety protocol, and the fuel grain was examined and weighed. It was found that the fuel grain lost only 5 grams, a very small amount compared to the normal mass losses, usually over 40 grams. Additionally, port diameters were also measured and found to have changed by only 0.04572cm (0.018 in), nearly an order of magnitude smaller than other completed runs. Since the fuel grain's weight and port diameters were within the same range of initial values for the other tests,

this fuel grain was reused for the same test configuration. In the subsequent test, the fuel grain experienced the same sputtering event when the hydrogen mass flow was turned off, but was able to keep the flame and resulted in a mass regression of 25.5 grams, about 3 grams different than the first of the two tests.

Because the changes in weight and port diameters were measured for half of a designed burn time, where the hydrogen and oxygen combustion was at fuel rich conditions for the entirety of the half burn, insights can be made about the interactions between the torch igniter and the ABS fuel grain. As seen in the first iteration, when the hydrogen mass flow rate begins to stop, the oxygen becomes more and more available to diffuse toward the ABS fuel grain, resulting in a transition period characterized by the flame sputtering, followed by an established ABS/GOx flame. Full burn time runs lost an average of 24.2 grams while the half burn time had a mass loss of 5 grams, under the same experimental conditions. Therefore, for this experimental configuration, it can be shown that fuel rich proportion of hydrogen and oxygen combustion results in extremely small regression of the ABS fuel grain and that the pyrolysis occurs when oxygen becomes available, in agreement with Equation 2.1. In contrast, for the low oxygen mass flow rate condition, the configuration that achieved the largest regression rate was the high L.O. time and low hydrogen mass flow rate, $\lambda = 1$. Here, the ABS fuel grain received a high total amount of heat from the hydrogen-oxygen torch, overcoming the endothermic pyrolysis step, and received enough oxygen to produce its own combustion which also applies heat back to the surface.

5.3 Characteristic Ignition Time

The characteristic ignition time, τ_{ign}, is a measure of the amount of time required to reach 63.2% of the maximum pressure within the light-off stage. This is an attempt to see how the hydrogen mass flow rate may affect the rapid build in pressure for the ABS/GOx hybrid rocket. In Table 5.4, the calculated signal-to-noise ratios are presented. The statistically significant values are: effect of light off time, effect of oxygen mass flow rate, interaction between hydrogen mass flow rate and oxygen mass flow rate, and the

interaction of all three effects.

	$E_{L.O.time}$	E_{H2}	E_{O2}	
t^*	6.89660166	-1.676509702	9.518993726	
	$I_{L.O.,H2}$	$I_{H2,O2}$	$I_{L.O.,O2}$	$I_{L.O.,H2,O2}$
t^*	1.821412485	3.699776106	0.5554704561	2.409614553

Table 5.4. Signal-to-noise table for characteristic ignition time

Here, the effect of a change in light-off time is not focused on because the L.O. time at almost all conditions increased τ_{ign} by about 30%. The exception is the high oxygen, high hydrogen mass flow rate configuration where an increase in L.O. time resulted in an 11% increase. It is believed that because the increases are similar in magnitude to each other, the change in L.O. time drives the characteristic ignition time increases. In order to demonstrate this phenomena, a pressure graph for a high L.O. time, high GH_2, high O_2 mass flow rate configuration is presented in Figure 5.8.

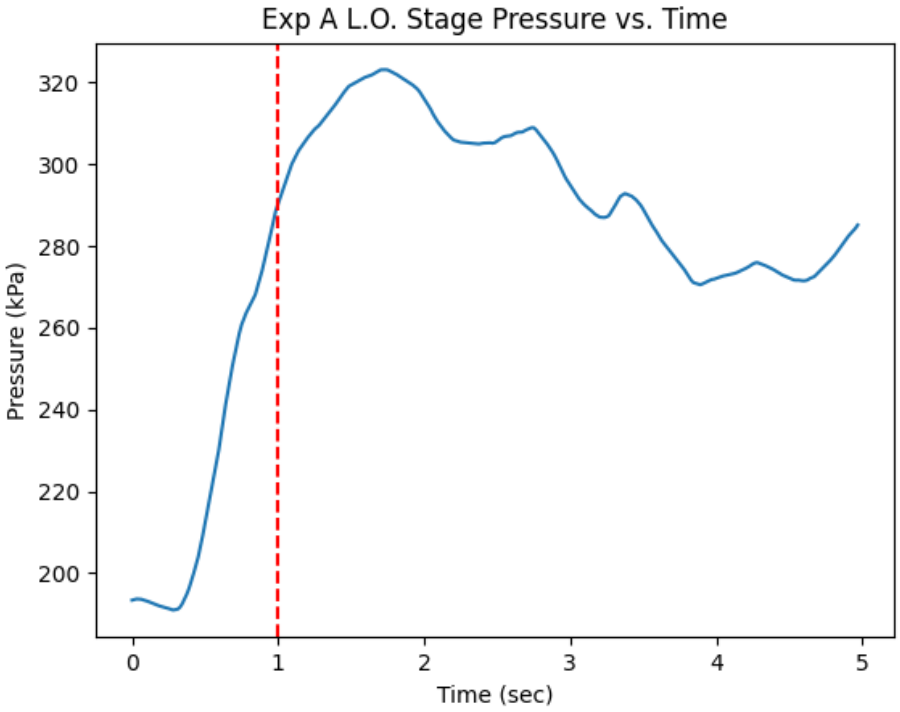

Figure 5.8. Example pressure graph for configuration A where the red line indicates the end of the low L.O time

The red line indicates the time location where the hydrogen flow is turned off in the low L.O. time configurations. It can be seen from this graph that the maximum pressure is achieved at about t=2 seconds. It is posited that the other experimental configurations were not able to achieve the same maximum pressure because they either lacked the time or the mass flow rate to do so. When given a longer duration of hydrogen mass flow rate, the pressure slopes begin to taper in magnitude as the pressure approaches the nominal maximum pressure for the given oxygen and hydrogen mass flow rate, t=1-2 sec. Conversely, for short L.O. time runs, there is no pressure slope tapering thus the 'true' pressure maximum is not reached because it is not given enough time to do so. Therefore, since the maximum pressure achieved in high L.O. time configurations is not reached by the low L.O. time configurations under the same conditions, the change in L.O. time drives the characteristic ignition time increases.

Exp. Config.	L.O. Time (s)	$\dot{m}_{H_2}$ $[\frac{L}{min}]$	$\dot{m}_{O_2}$ $[\frac{L}{min}]$	$\tau_{ign}(s)$
A	5	950	500	0.6186805
B	1	950	500	0.416237405
C	5	475	500	0.510306985
D	1	475	500	0.45449317

Table 5.5. Characteristic ignition time at the high oxygen mass flow rate configuration

Presented in Table 5.5, are the τ_{ign} for the high oxygen mass flow rate configuration. At this mass flow rate condition, an increase in hydrogen mass flow rate led to two different results. For the low light-off time configuration, τ_{ign} decreased by 8.79%. However, τ_{ign} increased by 19.2% for the high L.O. time runs. Even though the adiabatic flame temperature is higher for the high hydrogen mass flow rate condition ($\lambda = 1$), when operated for extended periods of time, there appears to be competition for oxidizer molecules between the ABS and hydrogen. It is theorized that the high adiabatic flame temperature aids in increasing the rate of pyrolysis from the initially cold ABS fuel grain. However as the surface pyrolyzes, the hydrogen and volatilized hydrocarbons begin to compete more and more against each other for available oxygen molecules. Therefore, when the hydrogen-

oxygen combustion is allowed to operate for a longer duration of time, the characteristic ignition time increases. In contrast, when the L.O. time was short, the ABS fuel grain receives the benefit of higher adiabatic flame temperature from the torch resulting in an increase in regression rate while also benefiting from little to no competition for oxidizer molecules.

Exp. Config.	L.O. Time (s)	$\dot{m}_{H_2}$ $[\frac{L}{min}]$	$\dot{m}_{O_2}$ $[\frac{L}{min}]$	$\tau_{ign}(s)$
E	5	950	250	0.338248945
F	1	950	250	0.238563
G	5	475	250	0.44160075
H	1	475	250	0.32153024

Table 5.6. Characteristic ignition time at the low oxygen mass flow rate configuration

Presented in Table 5.6, are the τ_{ign} for the high oxygen mass flow rate configuration. At this mass flow rate condition, an increase in the hydrogen mass flow rate led to a decrease in τ_{ign} by 26.51% and 29.63% for both high and low light-off times, respectively. As established by the regression rate section, the low oxygen and high hydrogen mass flow rates operate at a fuel rich combustion which leaves little to no available oxidizer molecules for the ABS fuel grain. This results in low regression rates for the duration of the burn. Thus when the hydrogen mass flow rate is increased at high L.O. times and the low oxygen mass flow rate, τ_{ign} decreases because there is little to no volatile hydrocarbons to compete against the hydrogen molecules. However, the low L.O. time's decrease in τ_{ign} is attributed to the same reasons as given in the high oxygen, low L.O. time configuration. Even though the torch operates at a fuel rich condition, because the L.O. time is low, the ABS fuel grain receives the benefit of increased heat flux which induces the regression of the fuel grain. This overcomes the endothermic step of pyrolysis without competition between the hydrogen and ABS.

5.4 Average Characteristic Exhaust Velocity

As explained in 4.1.3, the total mass flow rate through the nozzle throat is too low to achieve the chamber pressures that the nozzle was optimized for. This led to an interesting

phenomena with the characteristic exhaust velocity, c^*. By definition, c^* is defined as:

$$c^* \equiv \frac{P_c A_t}{\dot{m}} \tag{5.1}$$

with units of $[\frac{m}{s}]$ where P_c [Pa] is the chamber pressure , A_t $[m^2]$ is the area of the throat, and $\dot{m}$ $[\frac{kg}{s}]$ is the mass flow rate through the throat are empirically found. From NASA CEA, the maximum c^* value for the experimental pressures is about 1800 $\frac{m}{s}$ for ABS/GOx and about 2500 $\frac{m}{s}$. The minimum average c^* value in this experiment was 2955 $\frac{m}{s}$, significantly higher than theoretical. Because the mass flow rate was only a fraction of the required mass flow rate for optimal operation and the area of the throat was too large, the c^* value explodes. This is an unfortunate result of a design error, but it is believed that even though the values are not realistic, the trends that they exhibit are still valid.

In Table 5.7, the calculated signal-to-noise ratios for the effects and interactions are presented. The statistically significant effects and interactions are: effect of hydrogen mass flow rate, effect of oxygen mass flow rate, interaction of L.O. time and hydrogen mass flow rate, interaction of hydrogen mass flow rate and oxygen mass flow rate, and the interaction between all three effects.

	$E_{L.O.time}$	E_{H2}	E_{O2}	
t^*	0.2403684549	3.799759506	-32.24196338	
	$I_{L.O.,H2}$	$I_{H2,O2}$	$I_{L.O.,O2}$	$I_{L.O.,H2,O2}$
t^*	3.842178281	-3.224964199	-2.144099873	-2.991072443

Table 5.7. Signal-to-noise table for average c^*

In Table 5.8, the c^* values for all run configurations are presented. As explained earlier, the low oxygen mass flow rate configurations, E-H, exhibit the highest c^* values. This is due the large c^* increase from low total $\dot{m}$ that is exacerbated by low oxygen mass flow configurations. It was found that an increase in the light-off time led to a decrease in the average characteristic exhaust velocity for all but one comparison. At the high oxygen mass flow rate, c^* decreased by 1.8% and 4.76% for the high and low hydrogen mass flow rate conditions, respectively. A similar decrease of 5.12% was calculated for

the low oxygen, low hydrogen mass flow rate configuration. However, for the low oxygen, high hydrogen mass flow rate configuration, when the L.O. time increased, the average c^* value increased by 9.82%.

Exp. Config.	L.O. Time (s)	$\dot{m}_{H_2}$ $[\frac{L}{min}]$	$\dot{m}_{O_2}$ $[\frac{L}{min}]$	$\bar{c^*}$ $\frac{m}{s}$
A	5	950	500	3029.855813
B	1	950	500	3084.949605
C	5	475	500	2955.225002
D	1	475	500	3099.411533
E	5	950	250	5154.945376
F	1	950	250	4672.495488
G	5	475	250	4429.627304
H	1	475	250	4662.473907

Table 5.8. Characteristic exhaust velocities for all experimental configurations

It is believed that because these two runs operated with the hydrogen-oxygen torch at fuel rich combustion, the average c^* value increases because the ABS fuel grain does not receive enough oxygen, therefore resulting in a GH_2/GOx dominated combustion process. Thus, during the L.O. stage at fuel rich torch conditions, the hybrid rocket does not operate like a hybrid rocket, but rather more similarly to a GH_2/GOx bipropellant rocket. This is further elucidated by the flame extinguishment experienced, presented in the regression rate analysis. Since the GH_2/GOx combustion has a higher theoretical c^* value at fuel rich conditions, given no competition for oxygen molecules, hydrogen dominates the burn and the resulting average c^* value for the entire burn will increase when GH_2/GOx is allowed to burn longer. Conversely, when oxygen molecules are available for the ABS fuel grain, competition for oxidizer will occur. Thus, when the competition occurs for longer periods of time, the average c^* value decreases as seen in the other run comparisons.

The characteristic exhaust velocity was found generally to increase when the hydrogen mass flow rate was increased. However, the changes are negligible for low light-off time

at both high and low oxygen mass flow rate conditions since they resulted in less than 1% changes in average c^*. At the high L.O. time, the average c^* value increased by 2.49% and 15.14% for high and low oxygen mass flow rates, respectively. When the hydrogen mass flow rate increases for the high oxygen mass flow rate condition, λ decreases from 2 to 1. Thus it is believed that the average c^* increases as a result of higher combustion temperature and higher achievable c^*, as seen in Figures 3.1-3.1. However, as seen earlier, due to the change in equivalence ratio from stoichiometric to fuel rich combustion, the increase in c^* for the low oxygen mass flow rate is attributed to the hydrogen dominated combustion where GH_2/GOx combustion c^* maximum is fuel rich (O/F = 2.43).

5.5 Fuel Grain Inner Diameters and Qualitative Analysis

The ABS fuel grains were cut in half longitudinally to measure the inner diameters and to observe any qualitative characteristics. All fuel grains have 3 distinct regions, discernible by coloration and wave-patterns. Figure 5.9 is a representative example of used fuel grain that was cut in half axially. This particular fuel grain was from experimental configuration 1 with the length of each region marked. Region 1 (far left) is where the hydrogen-oxygen torch stream enters the ABS fuel grain initially. It has dark coloration with a slightly rough surface whose inner diameter decreases as it approaches the second region. The region 2 is characterized by lighter grain coloring with distinct wave patterns where the initial portion starts with short wavelengths that increase until the third region.

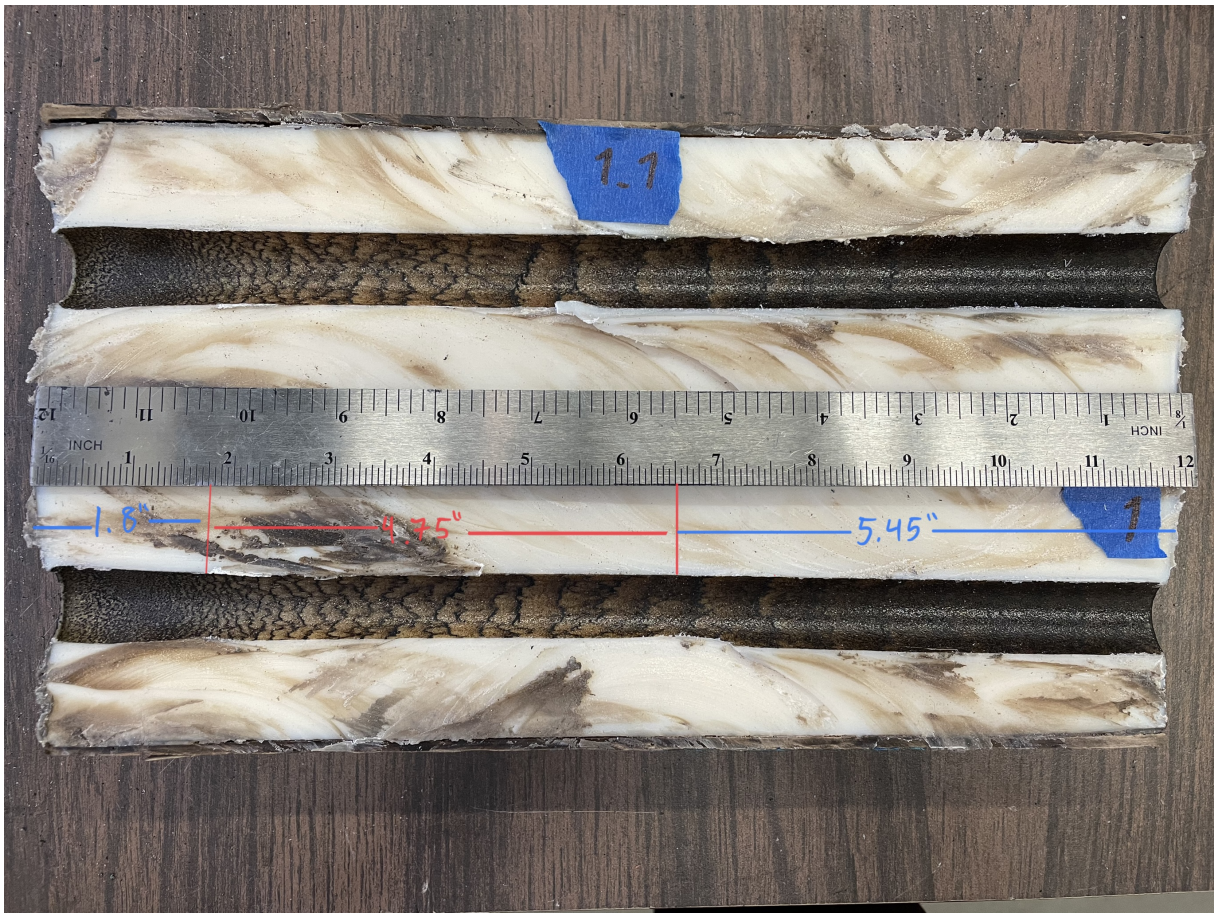

Figure 5.9. ABS fuel grain from experimental configuration 1. Flow goes left to right. Measurements are in inches

Region 3 is where the grain color returns to the dark coloration similar to the first region. This region has periodic bands on the surface that start from the ending of the second region and are consistent in length. The wave patterns are theorized to be products of pressure oscillations where the black lines of built up material are high pressure nodes and the lighter regions in between are high velocity, low pressure areas. It appears that the pressure waves during the combustion process have interference patterns that vary with longitudinal fuel grain position where the frequencies are high at region 1 and progressively decrease in frequency as it approaches region 3.

The inner diameters of each fuel grain were measured in one inch intervals along the fuel grain, Figures 5.10 and 5.11. The described regions have different inner diameters where the first and third regions have the largest inner diameters while the second region

consistently has the lowest. Therefore the regression rate was the lowest at region 2.

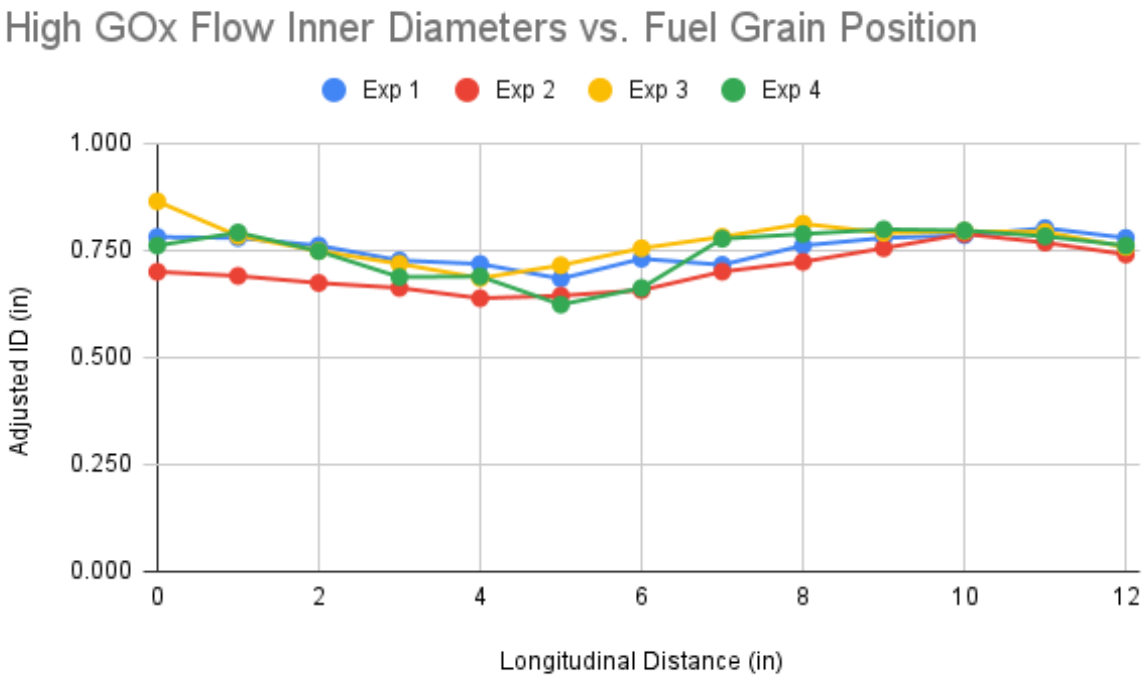

Figure 5.10. High GOx mass flux fuel grain inner diameters vs. fuel grain position

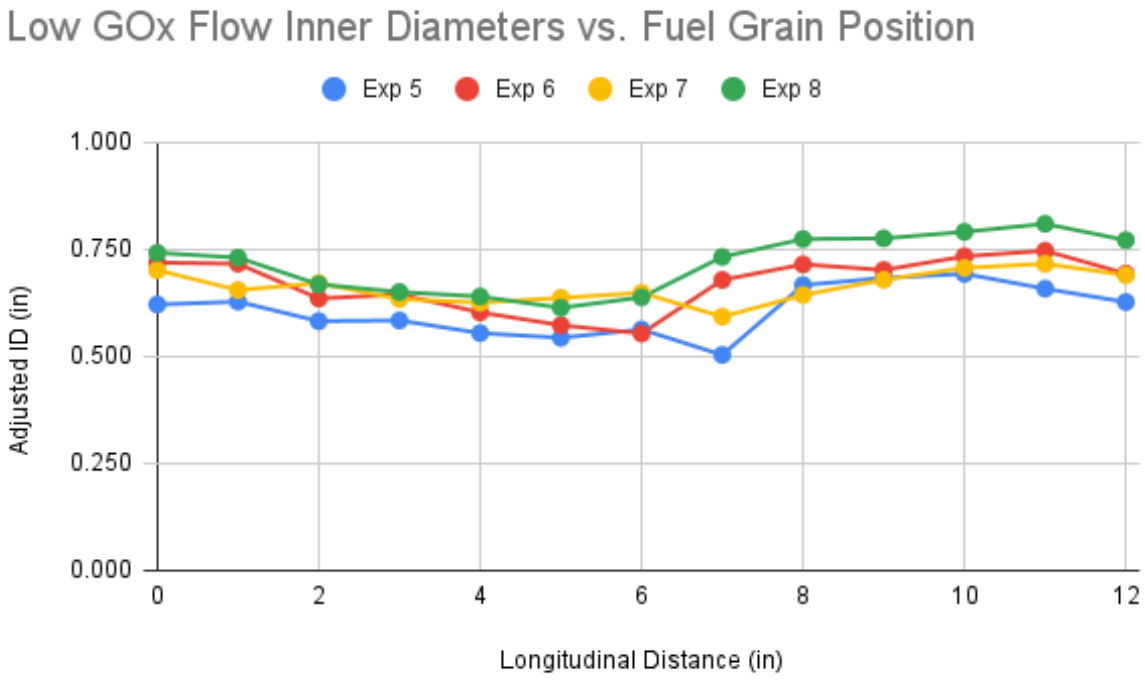

Figure 5.11. Low GOx mass flux fuel grain inner diameters vs. fuel grain position

These figures elucidate that the qualitative features for the burn patterns follow generally with the inner diameters for each region. Regions 1 and 3 are far darker in color than region 2 and the figures show that the darker regions also have more regression of the ABS fuel grain. This suggests that regions 1 and 3 have a combustion zone closer to the surface of the fuel grain, which allows for greater heat transfer from the flame to the ABS causing the surface to blacken and have larger inner diameters. In addition to the , the consistent changes in inner diameter from large to small to large suggests that there may also be low frequency instabilities in this system that are well documented in hybrid rocket literature [82–84].

Chapter 6

Conclusions and Recommendations for Future Works

6.1 Conclusions

A hydrogen-oxygen torch igniter was designed, built, and tested for use in a hybrid rocket with ABS as the solid fuel grain. The effects of the hydrogen-oxygen torch igniter operation to the combustion of ABS-oxygen is not currently found in literature. The effects of the duration of hydrogen flow (light-off time), hydrogen mass flow rate, and oxygen mass flow rate were tested in a factorial design of experiment based on a Student's t-Distribution at a 95% confidence interval. The hydrogen-oxygen torch igniter was able to reliably operate for all tests performed and had one failure to ignite the ABS fuel grain. This failure to ignite the ABS fuel grain is attributed to fuel rich combustion which results in little to no available oxygen for the ABS to combust with. Subsequently, this fuel grain was inspected and measured before performing a successful run at the same conditions. This serendipitous occurrence is what led to the conclusion that at fuel rich torch combustion, the majority of the regression rate occurs when the ABS fuel grain was exposed to oxidizer, after the shutoff of the torch igniter.

It was observed that hydrogen can significantly benefit hybrid rocket systems since it was shown to have statistically significant increases the average linear regression rate of the fuel grain, a frequently cited detriment to hybrid rocket propulsion. For the high oxygen mass flow rate condition, the average linear regression rate increased by 1-3%

when the hydrogen mass flow rate or the light-off time was increased. The increase in regression rate is attributed to higher total heat absorption from the hydrogen-oxygen flame which lead to higher regression rates. However, it was found that hydrogen and ABS compete with each other for available oxidizer molecules resulting in up to 40% decreases in regression rate for fuel rich torch conditions when the hydrogen mass flow rate or the light-off time was increased. These results corroborate the turbulent boundary layer combustion model as described by Marxman et al. [1, 81], since the regression rate was shown to change with different heat fluxes from the hydrogen-oxygen flame to the surface and that pyrolysis is significantly reduced with reduced oxygen mass fluxes.

To address ignition timings of the hydrogen-oxygen igniter, characteristic ignition times were calculated. The characteristic ignition time was defined as the amount of time for the chamber pressure to build to 63.2% of the maximum pressure. It was shown that the characteristic ignition time generally decreased with an increase in the hydrogen mass flow rate. However, for the high light-off time and high oxygen mass flow rate condition, an increase in the hydrogen mass flow rate lead to an increase in the characteristic ignition time. Furthermore, for every run configuration, an increase in the light-off time led to an increase in the characteristic ignition time. It is theorized that the increase in characteristic ignition time is potentially due to increasing oxidizer competition where an increase in hydrogen content and the longer period of torch operation allows for more competition. Thus, for the design space, it is observed that short duration, high hydrogen mass flow rate 'bursts' are optimal for achieving low characteristic ignition times.

The characteristic exhaust velocity, c^*, was also calculated, however the values are most likely unrealistic due to too large of a nozzle throat and low oxygen mass flow rates. Despite this, it is believed that because these values are empirically found, the trends are still valid. Generally, an increase in the light-off time led to a decrease in the characteristic exhaust velocity. Similar to the aforementioned results, this is theorized to be a product of oxidizer competition. This is further elucidated when no oxidizer competition is experienced as is the case for rich torch flame conditions ($\lambda = 1/2$). For this run configuration c^* increased when the light-off time increased. At these O/F ratios,

the system is dominated by hydrogen-oxygen combustion and its average c^* across the whole run time increases when the torch is allowed to operate longer. For low light-off times, an increase in the hydrogen mass flow rate led to negligible changes in c^*, but at high light-off time, the characteristic exhaust velocity increased. At high light-off time, an increase in the hydrogen mass flow rate produces higher pressures resulting in higher c^*.

These results show that the hydrogen-oxygen torch igniter conditions can significantly contribute to the overall performance of the hybrid rocket. It is shown that for increasing the performance of the solid fuel grain, fuel lean operation of the igniter with a short duration, high hydrogen mass flow is preferable. This configuration blends the benefits of increased regression rate, low characteristic ignition time, and no significant detriment to characteristic exhaust velocity. Furthermore, operating the hydrogen-oxygen torch igniter at optimal c^* is not optimal for overall solid fuel grain performance due to fuel rich torch operation inducing competition for oxidizer molecules.

In conclusion, the hydrogen-oxygen torch igniter is believed to be a reliable and effective solution to hybrid rocket ignition. The hydrogen-oxygen torch igniter presented was able to establish ignition of all but one of the runs and through the data it is seen that this torch igniter can also improve the performance of the hybrid rocket system by decreasing characteristic ignition time, increasing regression rates, and increasing the characteristic exhaust velocity. It is believed that the added build complexity and cost will be outweighed by the benefits of this ignition system and should be further researched to test its full capabilities for hybrid rocket propulsion.

6.2 Recommendations for Future Works

6.2.1 Confirmation Experiments

As noted in previous sections, the overall performance of the system was hampered by low mass fluxes created by a large throat in the nozzle. The results in this work, while still valid, could be improved by further testing with a nozzle that is more suited to the mass fluxes that are capable. Specifically, thrust profiles, specific impulses, and more accurate

characteristic exhaust velocity measurements are desired to make better comparison with other systems in the literature. Leaner torch O/F ratios should also be tested as the fuel rich stoichiometry may result in troubles with fuel grain ignition and regression rate. Potentially using the hydrogen-oxygen igniter near the fuel lean operating limits may be preferable since the heat flux is still high while also avoiding competition for oxidizer molecules.

6.2.2 Comparison with Other Torch Fuels and Solid Fuel Grains

A comparison of hydrogen versus other torch fuels would be an insightful addition to the body of literature. Even though hydrogen is a frequent and historic propellant choice, the storage requirements it necessitates is still a significant problem. Therefore testing other fuels, such as methane, and comparing their performances to hydrogen would be beneficial to the body of knowledge. Performing similar experiments as to this body of work with torch propellants with differing flame speeds, carbon content, and energy density could elucidate trends that may influence the choice in propellants.

As eluded to, testing a number of solid fuel grains with a number of different torch fuels could show trends among propellant configurations. For example, a fuel grain that requires a high enthalpy of vaporization may benefit more from hydrogen-oxygen torches versus a fuel grain with lower enthalpy of vaporization since hydrogen is able to apply high heat fluxes at the expense of propellant storage. These results would greatly inform propulsion designers, allowing for concrete knowledge of the interactions between torch propellants and solid fuel grains.

6.2.3 Emissions and Combustion Enhancement via Co-Firing

Emissions is a subject that is increasingly pertinent as the space industry increases the number of launches per year while global warming and emissions of greenhouse gasses remain a serious topic to consider. Measuring an emission profile of a rocket burn would be insightful information that would benefit the literature significantly. This would potentially be a novel subject in the rocket combustion field since measuring the emissions of extremely high temperature combustions is difficult. The results could be insightful

and may lead to further discussion in how the propulsion field can reduce emissions while retaining the well documented hydrocarbon combustion based systems.

In addition, similar to previous works performed at the ERL, it has been shown that co-firing with hydrogen can decrease the emissions and improve performance of a spark ignition Wankel engine. As shown in [64, 68, 77], hydrogen can significantly extend the lean limits of the combustion which allows for lower carbon content, leading to reduced carbon emissions. Furthermore, it has been shown that additional hydrogen and hydrogen radicals can improve the reactivity of the main hydrocarbon combustion process. This would require a full burn length co-firing of hydrogen rather than the 10% and 50% of total burn times conducted in this work.

References

[1] M. Gilbert G. Marxman. "Turbulent Boundary Layer Combustion in the Hybrid Rocket". In: *Symposium of Combustion* 9 (1 1963).

[2] Derrick M. Arnold. "Formulation and Characterization of Paraffin-Based Solid Fuels Containing Swirl Inducing Grain Geometry and/or Energetic Additives". In: *The Pennsylvania State University* 15 (2014).

[3] Oscar Biblarz and George P. Sutton. *Rocket Propulsion Elements*. Wiley and Sons, 2000.

[4] George Story. "Large-Scale Hybrid Motor Testing". In: *Fundamentals of Hybrid Rocket Combustion and Propulsion*. Ed. by Martin J. Chiaverini and Kenneth K. Kuo. American Institute of Aeronautics and Astronautics, 2007. Chap. 13, pp. 513–552.

[5] Zachary W. Peterson Stephen A. Whitmore and Shannon D. Eilers. "Comparing Hydroxyl Terminated Polybutadiene and Acrylonitrile Butadiene Styrene as Hybrid Rocket Fuels". In: 29 (2013).

[6] Daniele Pavarin Francesco Barato Nicolas Bellomo. "Integrated approach for hybrid rocket technology development". In: 128 (2016).

[7] Giordano Pinarello Alessandro Mazzetti Laura Merotto. "Paraffin-based hybrid rocket engines applications: A review and a market perspective". In: 126 (2016).

[8] B. Persons D. F. Pennington T. Man. "Rocket Propulsion Hazard Summary: Safety Classification, Handling Experience and Application to Space Shuttle Payload". In: *NASA* 69 (1977).

[9] George A. Repas. "Hydrogen-Oxygen Torch Igniter". In: (1994).

[10] Bonnie J Mcbride Sanford Gordon. "Computer program for calculation of complex chemical equilibrium compositions and applications. Part 1: Analysis". In: (1994).

[11] Nick G. Glumac Irvin Glassman Richard A. Yetter. *Combustion*. Elsevier, 2015.

[12] Robert K. Masse Robert L. Sackheim. "Green Propulsion Advancement: Challenging the Maturity of Monopropellant Hydrazine". In: (2014).

[13] Dietmar Welberg Daniel Fiot Pierre Michaud Christian Desaguie Santiago Casu Bastian Geiger Rainer Kiemel Ulrich Gotzig Stefan Krauss. "Development and Test of a 3D printed Hydrogen Peroxide Flight Control Thruster". In: (2015).

[14] Vigor Yang Matthew J. Casiano James R. Hulka. "Liquid-Propellant Rocket Engine Throttling: A Comprehensive Review". In: (2010).

[15] Victor J. Giuliano et al. "CECE: Expanding the Envelope of Deep Throttling Technology in Liquid Oxygen/Liquid Hydrogen Rocket Engines for NASA Exploration Missions". In: (2012).

[16] Jr. Erin M. Betts Dr. Robert A. Frederick. "A Historical Systems Study of Liquid Rocket Engine Throttling Capabilities". In: (2012).

[17] A.G. Galeev. "Review of engineering solutions applicable in tests of liquid rocket engines and propulsion systems employing hydrogen as a fuel and relevant safety assurance aspects". In: 42 (2017).

[18] Weidong Cai, Piyush Thakre, and Vigor Yang. "A Model of AP/HTPB Composite Propellant Combustion in Rocket-Motor Environments". In: (2008).

[19] Pragnesh N. Dave Shalini Chaturvedi. "Solid propellants: AP/HTPB composite propellants". In: *Arabian Journal of Chemistry* (2019).

[20] Jean-Francois Guery et al. "Solid propulsion for space applications: An updated roadmap". In: 66 (2010).

[21] Merrill W. Beckstead et al. "Modeling of combustion and ignition of solid-propellant ingredients". In: 33 (2007).

[22] Donald H. Barrett. "Solid Rocket Motor Igniters". In: (1971).

[23] Jason R. Gabl Alicia Benhidjeb–Carayon and Dr. Timothée L. Pourpoint. "Hypergolic Ignition and Relights of a Paraffin-based Hybrid Grain". In: (2018).

[24] David Altman and Allen Holzman. "Overview and History of Hybrid Rocket Propulsion". In: *Fundamentals of Hybrid Rocket Combustion and Propulsion*. Ed. by Martin J. Chiaverini and Kenneth K. Kuo. American Institute of Aeronautics and Astronautics, 2007. Chap. 1, pp. 1–37.

[25] Guobiao Cai Hui Tian Xintian Li. "Ignition theory investigation and experimental research on hybrid rocket motor". In: 42 (2015).

[26] Hui Tian et al. "Three-dimensional numerical and experimental studies on transient ignition of hybrid rocket motor". In: 140 (2017).

[27] Kenneth K. Kuo and Martin Chiaverini. "Challenges of Hybrid Rocket Propulsion in the 21st Century". In: *Fundamentals of Hybrid Rocket Combustion and Propulsion*. Ed. by Martin J. Chiaverini and Kenneth K. Kuo. American Institute of Aeronautics and Astronautics, 2007. Chap. 15, pp. 593–635.

[28] Martin J. Chiaverini et al. "Pyrolysis Behavior of Hybrid-Rocket Solid Fuels Under Rapid Heating Conditions". In: 15 (1999).

[29] R. J. Muzzy G. A. Marxman C. E. Woolridge. "Fundamentals of Hybrid Boundary Layer Combustion". In: (1963).

[30] E. D. Casillas, C. W. Shaeffer, and J. C. Trowbridge. "Cost and Performance Payoffs Inherent in Increased Fuel Regression Rates". In: (1997).

[31] Virgin Galactic. *Virgin Galactic*. URL: `https://www.virgingalactic.com` (visited on 02/27/2022).

[32] B. Nufer. "Hypergolic Propellants: The Handling Hazards and Lessons Learned From Use". In: (2010).

[33] Cameo Chemicals and NOAA. *Ammonium Perchlorate*. URL: `https://cameochemicals.noaa.gov/chemical/103`.

[34] Delphine Salgues et al. "Shear and Swirl Coaxial Injector Studies of LOX/GCH4 Rocket Combustion Using Non-Intrusive Laser Diagnostics". In: (2006).

[35] Stephen A. Whitmore. "Three-Dimensional Printing of "Green" Fuels for Low-Cost Small Spacecraft Propulsion Systems". In: 55 (2018).

[36] Stephen A. Whitmore et al. "High Regression Rate Hybrid Rocket Fuel Grains with Helical Port Structures". In: 31 (6 2015).

[37] Stephen A. Whitmore et al. "Consumable Spacecraft Structure with Integrated, 3-D Printed Acrylonitrile Butadiene Styrene (ABS) Thrusters". In: 53rd (2017).

[38] Victoria Coverstone Cagri Oztan. “Utilization of additive manufacturing in hybrid rocket technology: A review”. In: 180 (2021).

[39] Grant A. Risha Michael R. Weismiller Terrence L. Connell Jr. and Richard A. Yetter. “Characterization of Ammonia Borane (NH3BH3) Enhancement to a Paraffin Fueled Hybrid Rocket System”. In: (2010).

[40] P. M. Varkey Philmon George S. Krishnan and Lalitha Ramachandra M. Ravindra. “Fuel Regression Rate Enhancement Studies in HTPB/GOX Hybrid Rocket Motors”. In: (1998).

[41] Brendan R. McKnight. “Advanced Hybrid Rocket Motor Propulsion Unit for Cubesats”. In: (2015).

[42] Jean-Yves Lestrade Jérôme Anthoine and Santiago Casu Jérôme Messineo. “Performances of a Multi-Pulsed Hybrid Rocket Engine Operating with Highly Concentrated Hydrogen Peroxide”. In: 53rd (2017).

[43] Stephen A. Whitmore et al. “High-Performing Hydrogen Peroxide Hybrid Rocket with 3-D Printed and Extruded ABS Fuel”. In: (2018).

[44] Jan-Erik Rønningen and Johanne Husdal. “Nammo Hybrid Rocket Propulsion TRL Improvement Program”. In: (2012).

[45] Brian Evans Arif Karabeyoğlu Elena Toson. ““O/F Shift” in Hybrid Rockets”. In: 50th (2014).

[46] Kohei Ozawa and Toru Shimada. “Effects of O/F Shifts on Flight Performances of Vertically Launched Hybrid Sounding Rockets”. In: (2017).

[47] Stephen A. Whitmore and Stephen L. Merkley. “Effects of Radiation Heating on Additively Printed Hybrid Fuel Grain O/F Shift”. In: (2016).

[48] Nadir Yilmaz Stephen M. Davis. “Advances in Hypergolic Propellants: Ignition, Hydrazine, and Hydrogen Peroxide Research”. In: 2014 (2014).

[49] A. Santana Jr. M. Niwa and K. Kessaev. “Torch with Oxidizer Augmentation for LOX/LH2 Engine Ignition”. In: (2000).

[50] Sanders D. Rosenberg. “Ignition System for Oxygen/Hydrogen Auxiliary Propulsion Systems”. In: 10 (1983).

[51] Brian J. Cantwell David M. Dyrda. “Development of a Laser Ignition Scheme for Hybrid Rocket Motors”. In: (2018).

[52] Nicolaie Pavel et al. “Laser ignition - Spark plug development and application in reciprocating engines”. In: 58 (2018).

[53] Aristides M. Bonanos et al. “Dual-Mode Combustion Experiments with an Integrated Aeroramp-Injector/Plasma-Torch Igniter”. In: 24 (2 2008).

[54] Timothy C. Wagner and James M. Egges Walter F. O’Brien G. Burton Northam. “Plasma Torch Igniter for Scramjet”. In: (1989).

[55] Ichiro Nakagawa. “Plasma Torch Igniter for Hybrid Rockets”. In: 80 (2 2018).

[56] Juyoung oh, Seung-gyo Jang, and Jack J. Yoh. “Towards understanding the effects of heat and humidity on ageing of a NASA standard pyrotechnic igniter”. In: 9 (2019).

[57] Carl Hohmann, Bill Tipton Jr., and Maureen Dutton. “Propellant for the NASA Standard Initiator”. In: (2000).

[58] Spencer D. Mathias, Stephen A. Whitmore, and Richard Harvey. “High Voltage Breakdown and Arc-Tracking Mechanism of Thermoplastics with Applications to Hybrid Rocket Arc-Ignition”. In: *AIAA Propulsion and Energy Forum* (2017).

[59] Michael I. Judson Jr. “Direct Electrical Arc Ignition of Hybrid Rocket Motors”. In: (2015).

[60] Luis Eduardo Sanchez. “Development and Testing of Oxygen/Methane Torch Igniter Technologies for Propulsion Systems”. In: (2016).

[61] Antonietta Conte et al. “Design, Modeling and Testing of a O2/CH4 Igniter for a Hybrid Rocket Motor”. In: (2018).

[62] Steven J. Schneider, Jeremy W. John, and Joseph G. Zoeckler. “Design, Fabrication, and Test of a LOX/LCH4 RCS Igniter at NASA”. In: (2007).

[63] Timothy Charles Wagner. “Ignition and Flameholding in Supersonic Flow By Injection of Dissociated Hydrogen”. In: (1987).

[64] F. Amrouche et al. “An experimental investigation of hydrogen- enriched gasoline in a Wankel rotary engine”. In: *International Journal of Hydrogen* 39 (2014).

[65] Ibrahim Dincer. "Green Methods for Hydrogen Production". In: *International Journal of Hydrogen Energy* 37 (2012).

[66] A. Ingenito D. Cecere E. Giacomazzi. "A review on hydrogen industrial aerospace applications". In: 39 (2014).

[67] Engineering Toolbox. *Air - Diffusion Coefficients of Gases in Excess of Air*. URL: https://www.engineeringtoolbox.com/air-diffusion-coefficient-gas-mixture-temperature-d_2010.html (visited on 06/25/2021).

[68] Marissa Brower et al. "Ignition Delay Time and Laminar Flame Speed Calculations for Natural Gas/Hydrogen Blends at Elevated Pressures". In: 135 (2013).

[69] J.B. Greenwood et al. "Experimental results of hydrogen enrichment of ethanol in an ultra-lean internal combustion engine". In: 39 (2014).

[70] Sen Nieh Michael Seibert. "Simulation of dual firing of hydrogen-rich reformate and JP-8 surrogate in a swirling combustor". In: 38 (2013).

[71] Office of Energy Efficiency and Renewable Energy. *Hydrogen Storage*. URL: https://www.energy.gov/eere/fuelcells/hydrogen-storage (visited on 02/27/2022).

[72] James M. Margolis. *Engineering Plastics Handbook*. McGraw-Hill, 2006.

[73] James E. Mark. "Physical Properties of Polymers Handbook". In: (2007).

[74] Ian Tiseo. *Production capacity of acrylonitrile butadiene styrene worldwide from 2013 to 2023*. URL: https://www.statista.com/statistics/856670/acrylonitrile-butadiene-styrene-global-production-capacity/ (visited on 03/23/2022).

[75] Stephen A. Whitmore et al. "Estimating the Enthalpy of Gasification of Acrylonitrile–Butadiene–Styrene Hybrid Rocket Fuels". In: *Journal of Propulsion and Power* 31 (2015).

[76] James R. Wilson. "Pyrolysis of Acrylonitrile-Butadiene-Styrene ABS Under High Heat Flux Conditions". In: (2013).

[77] F. Amrouche et al. "An experimental analysis of hydrogen enrichment on combustion characteristics of a gasoline Wankel engine at full load and lean burn regime". In: 43 (2018).

[78] Richard S. Figliola and Donald E. Beasley. *Theory and Design for Mechanical Measurements*. Wiley, 2005.

[79] John S. Lawson and John Erjavec. *Modern Statistics for Engineering and Quality Improvement (Statistics Series)*. Duxbury, 2000.

[80] Brian J. Cantwell M. Arif Karabeyoglu. "Development of Scalable Space –Time Averaged Regression Rate Expressions for Hybrid Rockets". In: 23 (4 2007).

[81] G. Marxman and M. Gilbert. "Turbulent Boundary Layer Combustion in the Hybrid Rocket". In: 9 (1963).

[82] Changjin Lee Kyung-Su Park. "Low frequency instability in laboratory-scale hybrid rocket motors". In: 42 (2015).

[83] M. Arif Karabeyoglu et al. "Modeling of Hybrid Rocket Low Frequency Instabilities". In: 21 (2005).

[84] Arif Karabeyoglu. "Combustion Instability and Transient Behavior in Hybrid Rocket Motors". In: *Fundamentals of Hybrid Rocket Combustion and Propulsion*. Ed. by Martin J. Chiaverini and Kenneth K. Kuo. American Institute of Aeronautics and Astronautics, 2007. Chap. 9, pp. 351–411.

Appendix A

K-Factors for Aalborg Gas Flow Controllers

ACTUAL GAS	K FACTOR Relative to N_2	Cp [Cal/g]	Density [g/l]
Deuterium D_2	1.00	1.722	1.799
Diborane B_2H_6	.4357	.508	1.235
Dibromodifluoromethane CBr_2F_2	.1947	.15	9.362
Dichlorodifluoromethane (Freon-12) CCl_2F_2	.3538	.1432	5.395
Dichlofluoromethane (Freon-21) $CHCl_2F$	.4252	.140	4.592
Dichloromethylsilane $(CH_3)_2SiCl_2$	.2522	.1882	5.758
Dichlorosilane SiH_2Cl_2	.4044	.150	4.506
Dichlorotetrafluoroethane (Freon-114) $C_2Cl_2F_4$	.2235	.1604	7.626
1,1-Difluoroethylene (Freon-1132A) $C_2H_2F_2$	.4271	.224	2.857
Dimethylamine $(CH_3)_2NH$	.3714	.366	2.011
Dimethyl Ether $(CH_3)_2O$	.3896	.3414	2.055
2,2-Dimethylpropane C_3H_{12}	.2170	.3914	3.219
Ethane C_2H_6	.50	.420	1.342
Ethanol C_2H_6O	.3918	.3395	2.055
Ethyl Acetylene C_4H_6	.3225	.3513	2.413
Ethyl Chloride C_2H_5Cl	.3891	.244	2.879
Ethylene C_2H_4	.60	.365	1.251
Ethylene Oxide C_2H_4O	.5191	.268	1.965
Fluorine F_2	.9784	.1873	1.695
Fluoroform (Freon-23) CHF_3	.4967	.176	3.127
Freon-11 CCl_3F	.3287	.1357	6.129
Freon-12 CCl_2F_2	.3538	.1432	5.395
Freon-13 $CClF_3$	.3834	.153	4.660
Freon-13B1 $CBrF_3$	.3697	.1113	6.644
Freon-14 CF_4	.4210	.1654	3.926
Freon-21 $CHCl_2F$	.4252	.140	4.592
Freon-22 $CHClF_2$	.4589	.1544	3.858
Freon-113 CCl_2FCClF_2	.2031	.161	8.360
Freon-114 $C_2Cl_2F_4$	.2240	.160	7.626
Freon-115 C_2ClF_5	.2418	.164	6.892
Freon-C318 C_4F_8	.1760	.185	8.397
Germane GeH_4	.5696	.1404	3.418
Germanium Tetrachloride $GeCl_4$	.2668	.1071	9.565
Helium He (=<10/Lmin) Helium He-1 (>50 L/min) Helium He-2 (>10-50 L/min)	1.454 2.43 2.05	1.241 1.241 1.241	.1786 .1786 .1786
Hexafluoroethane C_2F_6 (Freon-116)	.2421	.1834	6.157
Hexane C_6H_{14}	.1792	.3968	3.845
Hydrogen H_2-1 (=<10/Lmin) Hydrogen H_2-2 (>10-100 L) Hydrogen H_2-3 (>100 L)	1.0106 1.35 1.9	3.419 3.419 3.419	.0899 .0899 .0899

ACTUAL GAS	K FACTOR Relative to N_2	Cp [Cal/g]	Density [g/l]
Hydrogen Bromide HBr	1.000	.0861	3.610
Hydrogen Chloride HCl	1.000	.1912	1.627
Hydrogen Cyanide HCN	.764	.3171	1.206
Hydrogen Fluoride HF	.9998	.3479	.893
Hydrogen Iodide HI	.9987	.0545	5.707
Hydrogen Selenide H_2Se	.7893	.1025	3.613
Hydrogen Sulfide H_2S	.80	.2397	1.520
Iodine Pentafluoride IF_5	.2492	.1108	9.90
Isobutane $CH(CH_3)_3$	.27	.3872	3.593
Isobutylene C_4H_8	.2951	.3701	2.503
Krypton Kr	1.453	.0593	3.739
Methane CH_4 Methane CH_4-1 (>10 L/min)	.7175 .75	.5328 .5328	.715 .715
Methanol CH_3	.5843	.3274	1.429
Methyl Acetylene C_3H_4	.4313	.3547	1.787
Methyl Bromide CH_3Br	.5835	.1106	4.236
Methyl Chloride CH_3Cl	.6299	.1926	2.253
Methyl Fluoride CH_3F	.68	.3221	1.518
Methyl Mercaptan CH_3SH	.5180	.2459	2.146
Methyl Trichlorosilane $(CH_3)SiCl_3$	.2499	.164	6.669
Molybdenum Hexafluoride MoF_6	.2126	.1373	9.366
Monoethylamine $C_2H_5NH_2$	.3512	.387	2.011
Monomethylamine CH_3NH_2	.51	.4343	1.386
Neon NE	1.46	.246	.900
Nitric Oxide NO	.990	.2328	1.339
Nitrogen N_2	1.000	.2485	1.25
Nitrogen Dioxide NO_2	.737	.1933	2.052
Nitrogen Trifluoride NF_3	.4802	.1797	3.168
Nitrosyl Chloride NOCl	.6134	.1632	2.920
Nitrous Oxide N_2O	.7128	.2088	1.964
Octafluorocyclobutane (Freon-C318) C_4F_8	.176	.185	8.397
Oxygen O_2	.9926	.2193	1.427
Oxygen Difluoride OF_2	.6337	.1917	2.406
Ozone	.446	.195	2.144
Pentaborane B_5H_9	.2554	.38	2.816
Pentane C_5H_{12}	.2134	.398	3.219
Perchloryl Fluoride ClO_3F	.3950	.1514	4.571
Perfluoropropane C_3F_8	.174	.197	8.388
Phosgene $COCl_2$	.4438	.1394	4.418
Phosphine PH_3	.759	.2374	1.517

Appendix B

Piping and Instrumentation Diagram

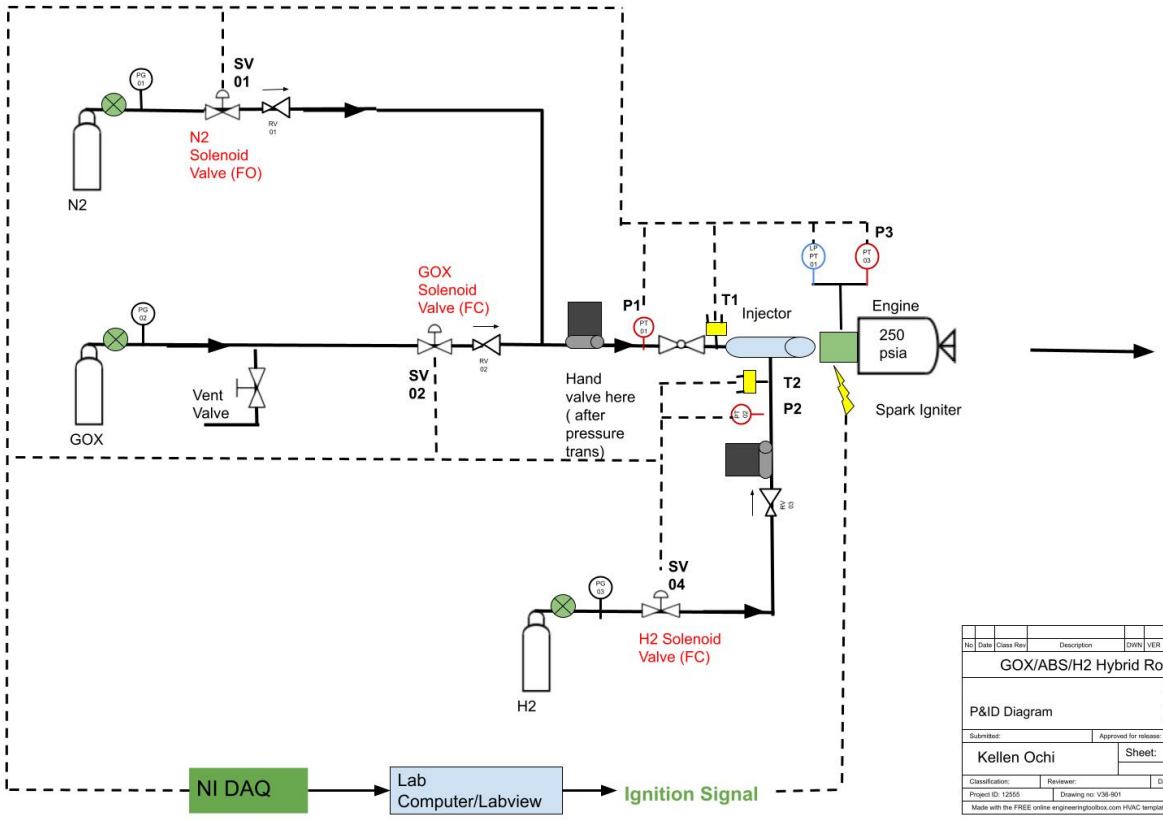

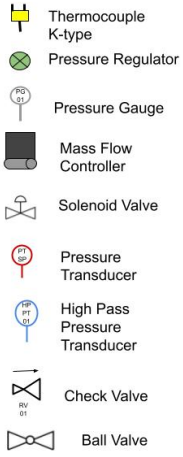

No	Date	Class Rev	Description	DWN	VER	CHKD	SUB	APP

GOX/ABS/H2 Hybrid Rocket

P&ID Diagram

Drawn: 02/11/21
Design:
Checked:
Date:

Submitted:
Approved for release:

Kellen Ochi

Sheet: S-0001
of

Classification:
Reviewer:
Date:

Project ID: 12555
Drawing no: V36-901
Rev. 1

Appendix C

Standard Operating Procedures

Rocket Assembly (May Require 2 People):

1. Install o-rings: Smaller ones -232 go on Nozzle, 2 of the larger -239 go on both ends of the motor case. O-rings will require lubricant such as Super Lube Silicone Lubricating Brake Grease
2. Weigh fuel grain and measure the two ends' opening diameter:
    a. Fuel Grain Weight: _____
    b. Injector Side Diameter:_____
    c. Nozzle Side Diameter:_____
3. Measure the diameter of the nozzle throat and exit by inserting dowel rods with known diameters (it is difficult to get calipers or a ruler into the throat)
    a. Nozzle Throat Diameter:_____
    b. Nozzle Exit Diameter:_____
4. Insert ABS fuel grain into cardboard liner and insert into the motor case
5. Insert the nozzle with installed -232 o-ring into the nozzle-end faceplate. Will require some force to push in. **Do not use any impact or tools, graphite is a brittle material and impact can significantly damage the nozzle**
6. Attach injector faceplate and nozzle-end faceplate to slide rail plate via threaded dowel rods
7. Fasten nuts and washers to both ends and tighten just past finger tight. ~5 ft-lbf torque
8. Insert one end of the motor case into the injector side. Will require some force (but not too much ~25 lbf) and some gentle wiggling in order to have a "snug" fit
9. Repeat for nozzle-end faceplate
10. Insert dowel rods through the horizontal holes in the faceplates
11. Fasten nuts and washers to both ends and tighten to 10 ft-lbf torque
12. Apply Teflon tape to spark plug and to tube adapter fittings (fitting between rocket injector block and tubing)
13. Install and tighten adapter fittings
14. Place a grounding wire between the spark plug and its first washer
15. Tighten spark plug with an additional spacing washer, requires 10 ft-lbs torque

Pre-Test Pressure Containment Check:

1. Using 3 or 4 clamps, attach a square piece of rubber gasket and a solid metal disk to the end of the nozzle (Nozzle -> gasket -> metal disk). The clamps attach to the metal disk and the nozzle end faceplate. This is in order to contain the air within the combustion chamber
2. Connect the fume hood air line to either the O2 or H2 line. Both will need to be checked
    a. It may be easier to work in sections of the tubing as some leaks will not occur until significant pressure is achieved (~100 psig)
3. Open building air valve until 100 psig is achieved on the attached strain gauge
4. Listen for any leaks, use soapy water when necessary
5. Use Teflon tape on any non-compression fittings when necessary
    a. Compression fittings are ***not*** supposed to have Teflon tape and if there is a leak, the tube/ferrule may have to be replaced
6. If no leaks are detected, remove the clamps, rubber gasket, and solid metal disk then move on to "Test Setup Procedure"

Test Setup Procedure:

1. **(if using) 1 hr prior:** Turn on the CalAnalytics gas analyzer. **Note:** The start up sheet requires 1 hr
2. **15 minutes prior**: Plug in MFC cords and plug power strip "Top" into hood outlet
3. Verify sufficient reserves of nitrogen, hydrogen, and oxygen in bottles by opening the bottle valve without opening the regulator.
4. Plug in pressure transducer and force transducer's power adapters into the hood
    a. Nitrogen pressure: _____
    b. Hydrogen pressure:_____
    c. Oxygen pressure:_____
5. Turn on the hood lights and ensure that the flow out of the hood is at **~ 220 fpm**
6. Ensure that the MFC cables are connected to MFC's.

7. Ensure that the solenoid, force transducer, and pressure transducer leads are secured and the circuit layouts are correct
8. Turn on SCXI module for thermocouples
9. Turn on computer (if not already on)
10. Open LabView program (if not already up)
11. Ensure that the MFC's are closed:
    a. In the Labview program, turn off the "Starter Button" and turn on the "MFC/Solenoid Manual Control" button. This will allow the user to actuate solenoids and MFC's as desired.
    b. In the "MFC Control & Timing Control Panel" page 4, set all the values to 0.
    c. Hit the "Manual Control Stop Button" to exit the manual control operation
12. Verify that the sampling is occurring at about 0.02 sample/second
    a. Press "Starter Button" to "on" position
    b. Press "Save data to file?" button to "on" position
    c. In the "File Path" box, specify the location of where the data should be saved
    d. Click on the run button to run a "psuedo"-test
    e. Resulting file should have data points at about 0.02 second intervals
    f. Ensure pressure transducer, force transducer, and thermocouples show appropriate baseline values on the data acquisition system.
13. **Gas Flow Check (Probably requires 2 people): Nitrogen, Oxygen, Hydrogen**
    a. **Nitrogen:**
        i. Ensure that the low pressure side of the regulator and the run valve are closed
        ii. Slowly open the tank, the high pressure gauge should display the remaining amount of gas in psig
        iii. Slowly open the low pressure side of the regulator to 200 psig
            1. If there is a leak, note the location and close the low pressure side. Fix leak before continuing
        iv. Open the run valve, check for any leaks
            1. If there is a leak, note the location and close the run valve. Fix leak before continuing
        v. On the LabView program, press the "Starter Button" to the "off" position
        vi. Press the "MFC/Solenoid Manual Control" to the "on" position

vii. On the “MFC Control & Timing Control Panel” switch to “page 4” on the top

viii. Turn on the “Red” wall circuit starting with the experiment side switch then the computer side. The red light bulb should illuminate indicating a live circuit

ix. Under the “H2, N2 Solenoid Manual Control” click on the right box and insert a “4” to open the N2 solenoid valve, “0” to close

1. Flow of N2 should be observed, if not check that the correct lines are being used and that the solenoid valve is connected correctly

x. Leave run valve for N2 open as it will be used in the other gases as a purge

b. Oxygen & Hydrogen:

i. Repeat the above steps i->ix except for O2 or H2

ii. Under the MFC Manual Control insert a value between 1-5 to open the MFC

1. Flow of gas should be observed, if not check that the correct lines are being used and that the solenoid valve and MFC are connected correctly

iii. Close MFC and solenoid then open N2 solenoid to purge

1. Purge for 7-10 seconds then close the solenoid

iv. Close run valve

v. Turn off Wall circuit on the computer side(must do between each gas to ensure that the solenoid valves are closed before opening the regulators)

Test Procedure (Requires at least 2 people):
Must have lab coats, ear protection, and face shields on for entirety of this section

1. Open garage door
2. Setup and turn on cameras
    a. One from the nozzle pointed towards the injector, ideally with the pressure gauge, MFC’s and force transducer in view
    b. One from the injector side pointed toward the nozzle
3. Bring fire extinguisher to computer side and have ready (pin doesn’t need to come out)

4. On the LabView program, click the “Save data to file?” button to the “on” position and set a file path
5. On Page 1 of the “MFC Control & Timing Control Panel” set the “Initial O2 only MFC Setpoint”, “ABS/GOx/H2 MFC Setpoint”, and “ABS/GOx Only Setpoint” to the desired values
6. Set timing values to desired values
    a. “O2 Initial Time On” should be set to 2 sec
    b. “H2 ON Time” + “ABS/GOX ON Time” should = 10 sec
    c. “N2 Purge time” Should be about 20 seconds
7. Connect spark plug circuit together
    a. Attach the flip switch leads to the circuit
    b. Attach the spark plug wire to the spark plug and the ignition coil
    c. Attach the negative then positive leads to the battery terminals
    d. Check all connections and that the spark plug grounding wire is still attached to the spark plug
8. Turn on the **Red** wall circuit on the experiment side of the wall (if not already flipped on)
9. Slowly open the nitrogen, oxygen, and hydrogen bottles (if not already completed in the earlier section)

    a. Oxygen Regulator Pressure:_____

    b. Nitrogen Regulator Pressure:_____

    c. Hydrogen Regulator Pressure:_____

10. Turn on the **Red** wall circuit on the computer side of the wall.
11. Open N2, O2, H2 run valves
12. Ensure all non-testing personnel are clear from the test cell and fenced-in area.
13. Make an announcement for starting the test firing: “We will be conducting a motor firing in the testing area. Please stand clear of the test cell and the fenced-in area.”
14. Have second person ready at the spark plug toggle switch, ready to start toggling the switch at about a rate of 100 bpm
    a. Spark plug operator will start the spark plug when the computer operator says “start” until ignition is established visibly
15. Click the “Starter Button” to the “on” position

16. Call out “3, 2, 1, start” and run the LabView Program

Test Concluded:

1. Click the “Starter Button” to the “off” position
2. Click the “MFC/Solenoid Manual Control” to the “on” position
3. Verify that there is no residual smoldering, opening the N2 solenoid valve if needed
4. Announce “Test completed”
5. Check that auto valves have shut
6. Turn off video cameras
7. Unplug the battery leads of the spark plug circuit
8. Unplug the toggle switch leads of the spark plug circuit
9. Remove the spark plug wire from the spark plug then remove the spark plug out of the injector block
10. Close the hydrogen, oxygen, and nitrogen bottles and close the regulator valves
11. Open the relief valves to purge the lines
    a. Once gas has escaped, close the relief valve
12. Close the run valves
13. Turn off “Red” Circuit
14. Using a handheld laser temperature meter, verify that the temperatures of the injector and outside motor casing are below 100F before handling (may need to wait 1hr prior to starting again)
15. Loosen the horizontal compression rods and disassemble the motor case from the faceplates.
16. Remove fuel grain from the motor case
17. If additional tests are to be completed, insert a new fuel grain to the motor case and move to “Test Setup Procedure”.
18. Turn off remaining circuits.
19. Turn off the gas analyzer (if using).
20. Quit the LabView program.
21. Turn off the SCXI board

Misfire situation types:

No ignition

Ignition with mid-test failure

Misfire procedure (Ignition with mid-test failure) :

1. Press EMERGENCY STOP on the Labview program; this will start nitrogen flow while stopping the flow of oxygen.
2. Announce “Misfire has occurred, stay clear of the test cell until directed otherwise”.
3. Continue nitrogen flow for at least 15 seconds.
4. Continue recording event on the video camera.
5. Verify if there is any smoldering or residual smoke appearing from the nozzle
    a. If smoldering is observed, continue to purge the system using the manual control.
6. Once no smoldering has been verified, close the hydrogen, nitrogen, and oxygen tanks.
7. Close the oxygen run valve manually (valve located inside of the hood)
8. On the control program; restart and turn on manual mode and ensure all relays are in the shut position.
9. Check line pressures from the computer to ensure that there are no residual gases flowing.
10. Record time and any abnormalities of the misfire.
11. Announce “Test completed”.
12. Gather evidence and determine the cause of the problem.

Misfire with no ignition (spark plug operational):

1. Hit stop on the control program.
2. Ensure that the flows have subsided and the pressures have returned to nominal values.
3. Check that all tank regulators are open and have sufficient pressures.
4. Press “Stop” on the data acquisition system and camera.
5. Reset camera and the data acquisition system.
6. Return to “Test Procedure” #4
7. If misfire continues, continue to “Test Concluded” section and diagnose the problem further.

Post Test Analysis (After Test Concluded section)

Fuel Grain Analysis:

1. Weigh fuel grain and measure the two ends:

a. Fuel Grain Weight: _____

b. Injector Side Diameter:_____

c. Nozzle Side Diameter:_____

2. Using a (insert method of cutting this thing in half), measure the inner diameter at ¼ ft intervals (injector to nozzle; i.e. from injector measure ¼ ft then measure inner diameter):

    a. ¼ ft ID:_____

    b. ½ ft ID:_____

    c. ¾ ft ID:_____

3. Inspect surface characteristics:
    a. Ablation?
        i. YES
        ii. NO
    b. Chugging?
        i. YES
        ii. NO
    c. Smooth or Rough

Appendix D

ABS Safety Data Sheet

Safety Data Sheet

Tecaran® Natural & Black

ISSUE DATE: 06/08/2015

1. PRODUCT AND COMPANY IDENTIFICATION

PRODUCT NAME:	Tecaran®
SYNONYMS:	Acrylonitrile Butadiene Styrene
PRODUCT COLORS:	Natural & Black
MANUFACTURER:	Ensinger Inc.
DIVISION:	Stock Shapes
ADDRESS:	365 Meadowlands Blvd., Washington, PA 15301
EMERGENCY PHONE:	(724) 746-6050
OTHER CALLS:	(856) 227-0500
CHEMICAL NAME:	Acrylonitrile Butadiene Styrene
CHEMICAL FORMULA:	basic formula $(C_8H_8)_x \cdot (C_4H_6)_y \cdot (C_3H_3N)_z$
PRODUCT USE:	Stock Shape for Machining
PREPARED BY:	Allyson M. Crouse, Technical Resource Manager
SECTION 1 NOTE:	Revised June 8, 2015

2. HAZARDS IDENTIFICATION

EMERGENCY OVERVIEW: Mechanical injury only.

ROUTES OF ENTRY: Eyes

POTENTIAL HEALTH EFFECTS

EYES: Solid or dust causes irritation or corneal injury due to mechanical action.

SKIN: Essentially nonirritating to skin. Mechanical injury only. Molten material may burn skin.

INGESTION: Single dose oral LD50 has not been determined. Single dose oral toxicity is believed to be very low. Now hazards anticipated from ingestion incidental to industrial exposure.

INHALATION: Dust may cause irritation to upper respiratory tract. At room temperature, exposure to vapors are unlikely due to physical properties, normal processing temperatures may generate vapors, which may cause irritation if ventilation is inadequate.

ACUTE HEALTH HAZARDS: None Known

CHRONIC HEALTH HAZARDS: None Known

MEDICAL CONDITIONS GENERALLY AGGRAVATED BY EXPOSURE: None Known

CARCINOGENICITY: None Known

Carbon Black, CAS: 1333-86-4

OSHA: (PEL, 8HR) 3.5 mg/m^3 (FRL_TWA)
OSHA: (PEL, 8HR) 3.5 mg/m^3 (TL_PEL)
ACGIH: TWA: 3.5 mg/m^3 (Inhalable Fraction); Notations: Not Classifiable as a Human Carcinogen

Styrene, CAS: 100-42-5

OSHA: (PEL, 8HR) 425 mg/m^3 (FRL_STEL)
OSHA: (PEL, 8HR) 215 mg/m^3 (FRL_TWA)
ACGIH: STEL: 40 ppm
ACGIH: TWA: 20 ppm
Notations: Not Classifiable as a Human Carcinogen , BEI ; Crit Eff: CNS impairment ,Peripheral neuropathy , Upper respiratory tract irritation

Particulates:

OSHA: Particulates not otherwise regulated/OSHA (PEL) 15 mg/m^3 (TWA, Total Dust)
Particulates not otherwise regulated/OSHA (PEL) 5 mg/m^3 (TWA, Respirable Dust)
ACGIH: Particulates not otherwise regulated/ACGHI (TLV) 10 mg/m^3 (TWA, Total Dust)

3. COMPOSITION/INFORMATION ON INGREDIENTS

INGREDIENT:

CAS NO.	% WT
Modified Poly (acrylonitrile-butadiene-styrene), 9010-94-0]/ Poly (styrene-acrylonitrile), 9003-54-7 blend	
Carbon Black, 1333-86-4	0 – 1.0
Styrene, 100-42-5	0.1 – 0.3

The non-hazardous components and exact percentage (concentration) of the composition have been withheld as a trade secret.

This product consists primarily of high molecular weight polymers which are not expected to be hazardous. The ingredients in this product are present within the polymer matrix and are not expected to be hazardous.

This product contains a proprietary blend of components encapsulated within a polymer matrix. These components are not regarded as hazardous under 2012 OSHA Hazard Communication Standard; 29CFR Part 1910.1200.

4. FIRST AID MEASURES

EYES: Rinse cautiously with water for several minutes. Remove contact lenses, if present and easy to do. Continue rinsing for at least 15 minutes. Mechanical effects only.

SKIN: Wash off in flowing water or shower.

INGESTION: No adverse effects anticipated by this route of exposure incidental to proper industrial handling. If ingested, induce vomiting; if patient is conscious. Call a poison control center/physician, if patient feels unwell.

INHALATION: Remove to fresh air, if effects occur. Consult a physician.

NOTES TO PHYSICIANS OR FIRST AID PROVIDERS: No specific antidote. Supportive care. Treatment based on judgment of the physician in response to reactions of the patient.

5. FIRE FIGHTING MEASURES

AUTOIGNITION TEMPERATURE: Not Available

EXTINGUISHING MEDIA: Dry chemical, carbon dioxide, water spray or “alcohol’ foam.

SPECIAL FIRE FIGHTING PROCEDURES: Do not use a solid water stream as it may scatter and spread fire. Water is the best extinguishing medium. Carbon dioxide and dry chemical are not generally recommended, because of their lack of cooling capacity may permit re-ignition on larger fires.

UNUSUAL FIRE AND EXPLOSION HAZARDS: None Known

HAZARDOUS DECOMPOSITION PRODUCTS: Carbon oxides, hydrogen fragments, hydrogen cyanide, nitrogen oxides.

SECTION 5 NOTES: Wear full protective suit. In case of combustion, use a suitable breathing apparatus. Dust particles in the atmosphere are combustible and may be explosive.
Keep away from heat and sources of ignition.

6. ACCIDENTAL RELEASE MEASURES

ACCIDENTAL RELEASE MEASURES: Ventilate the area and prevent access to unauthorized people. Wear suitable personal protective equipment. Do not allow entry to drains, water courses or soil. Prevent spreading by use of suitable barriers. Take up with suitable equipment, fill up in air-tight containers and give further treatment as soon as possible.

7. HANDLING AND STORAGE

HANDLING AND STORAGE: Avoid accumulation of dust in enclosed space. Use in well-ventilated area. Static discharge (spark) in high dust environments may be explosive. Electrostatic charge may build up during handling. Equipment should be grounded and bonded. Metal containers involved in the transfer of this material should be grounded and bonded. All electrical equipment should be grounded and conform to applicable electric codes and regulatory requirements. Material creates dangerous slipping hazard on hard surfaces. After handling, always wash hands thoroughly with soap and water. Keep away from strong oxidizing compounds. Store in a well-ventilated place. Provide ventilation and wear necessary protectors.

OTHER PRECAUTIONS: Obtain special instructions, before use. Do not breathe dust. Wash hands thoroughly after handling. Do not eat, drink or smoke; when machining this product. Use personal protective equipment as required.

8. EXPOSURE CONTROLS/PERSONAL PROTECTION

ENGINEERING CONTROLS: Standard ventilation required

VENTILATION: Good general ventilation should be sufficient for most conditions. Local exhaust ventilation may be necessary for some operations.

RESPIRATORY PROTECTION: For most conditions a dust mask is sufficient; however, if handling at elevated temperatures without sufficient ventilation, use an approved air-purifying respirator.

EYE PROTECTION: Safety glasses should be sufficient for most operations; however, for dusty operations wear chemical goggles. If vapor exposure causes eye discomfort, use a full-face respirator

SKIN PROTECTION: No precautions other than clean body-covering clothing should be needed.

OTHER PROTECTIVE CLOTHING OR EQUIPMENT: None Known

Special Precautions to be taken in Handling and Storage: Store in sealed containers. Protect from atmospheric moisture. Molten material can produce thermal burns. Avoid skin contact. Fumes released during normal processing may cause irritation. Provide adequate ventilation. Heating the resin above normal processing temperatures may cause hazardous decomposition products. Do not overheat. Handling and fabrication of plastic resins can result in the generation of dust. Dust results from sawing, filing, and sanding of plastic parts in post-molding operations. Quantities of dust in air may be combustible and may cause respiratory irritation.

EXPOSURE GUIDELINES:

Carbon Black, CAS: 1333-86-4

OSHA: (PEL, 8HR) 3.5 mg/m^3 (FRL_TWA)
OSHA: (PEL, 8HR) 3.5 mg/m^3 (TL_PEL)
ACGIH: TWA: 3.5 mg/m^3 (Inhalable Fraction); Notations: Not Classifiable as a Human Carcinogen

Styrene, CAS: 100-42-5

OSHA: (PEL, 8HR) 425 mg/m^3 (FRL_STEL)
OSHA: (PEL, 8HR) 215 mg/m^3 (FRL_TWA)
ACGIH: STEL: 40 ppm
ACGIH: TWA: 20 ppm
Notations: Not Classifiable as a Human Carcinogen , BEI ; Crit Eff: CNS impairment ,Peripheral neuropathy , Upper respiratory tract irritation

Particulates not otherwise regulated:

OSHA: Particulates not otherwise regulated/OSHA (PEL) 15 mg/m^3 (TWA, Total Dust)
Particulates not otherwise regulated/OSHA (PEL) 5 mg/m^3 (TWA, Respirable Dust)
ACGIH: Particulates not otherwise regulated/ACGHI (TLV) 10 mg/m^3 (TWA, Total Dust

9. PHYSICAL AND CHEMICAL PROPERTIES

APPEARANCE:	Opaque color stock shape
ODOR:	None
PHYSICAL STATE:	Solid
AUTOIGNITION TEMPERATURE:	Not Available
MELTING POINT:	Not Available
SPECIFIC GRAVITY (H2O = 1):	>1

SOLUBILITY IN WATER: Insoluble

10. STABILITY AND REACTIVITY

STABILITY: Stable under normal conditions.

CONDITIONS TO AVOID (STABILITY): To avoid thermal decomposition, avoid elevated temperatures. Heating can result in the formation of gaseous decomposition products, some of which may be hazardous. Do not exceed melt temperature recommendations in product literature.

INCOMPATIBILITY (MATERIAL TO AVOID): None Known

HAZARDOUS DECOMPOSITION OR BY-PRODUCTS: Process vapors under recommended processing conditions may include trace levels of hydrocarbons, styrene, acrylonitrile, acrolein, acetaldehyde, acetophenone, ethyl benzene, cumene, alpha methylstyrene, 4-vinylcyclohexene, phenols.

HAZARDOUS POLYMERIZATION: Not Applicable

11. TOXICOLOGICAL INFORMATION

TOXICOLOGICAL INFORMATION: No data – In solid state, this material is not considered as being harmful to human health.

Acute Toxicity Resin
LD50/oral/rat: >5000 mg/kg (estimated)
LD50/dermal/rabbit: >2000 mg/kg estimated

IARC: Not listed Styrene: Group 2B (possible human carcinogen) - In subsequent reviews in 1994 and 2002, IARC chose to maintain its classification for styrene. In chronic inhalation studies, mice, but not rats develop lung tumors following styrene exposure, even though both species form DNA adducts.

OSHA: Not regulated

NTP: Not tested Styrene: is reasonably anticipated to be a human carcinogen based on limited evidence of carcinogenicity from studies in humans, sufficient evidence of carcinogenicity from studies in experimental animals, and supporting data on mechanisms of carcinogenesis (2011).

Special Studies:
Styrene: A reproduction study in rats exposed to 125 and 250 ppm in drinking water (approximately 14-21 mg/kg/day) produced no treatment-related effects on reproductive performance over 3-generations. The only treatment related findings were reduced pup survival index in the F1 and

F2 offspring. There was no evidence of developmental effects and no other effects were reported. The parental NOEL was 250 ppm and the NOEL for the F1 and F2 offspring was 125 ppm. In developmental toxicity studies in rats, rabbits, and hamsters styrene was not a selective toxicant to the fetus and was toxic at only those doses that produced maternal toxicity. In humans, styrene is associated with central nervous system depression (headache, fatigue, nausea, and dizziness) at inhalation concentrations greater than 50 ppm. Styrene has also been reported to reduce sensory nerve conductions in occupation settings after exposure to 100 ppm or more. Styrene has also been reported to produce color vision deficiencies (dyschromatopsia) at concentrations greater than 8 ppm (averaging 24 ppm). Twelve epidemiology studies have been reported for styrene and half have supported the hypothesis that styrene produces lymphatic and hematopoetic cancers (LHC). However, those that show an increase of LHC has generally been small in size (limited statistical power), have shown no dose-response relationship, and/or had multiple chemical exposures. Of the six studies that have not shown an association with styrene and LHC, these studies tended to be larger in size (higher statistical power), had an older study population, and had good exposure data. Overall, the weight of evidence suggests that there is not an association of LHC and styrene exposure in humans. In a recent inhalation cancer bioassay, Sprague Dawley derived rats (70/sex/group) were exposed whole body to styrene vapor at 0, 50, 200, 500, or 1000 ppm 6 h/day 5 days/week for 104 weeks. Males exposed to 500 and 1000 ppm and females exposed to 200 ppm and higher gained significantly less weight than the controls. There were no changes of toxicologic significance in hematology, clinical chemistry, urinalysis, or organ weights. Styrene-related non-neoplastic histopathologic changes were confined to the olfactory epithelium of the nasal mucosa. The incidence and severity were related to dose. There was no evidence that styrene exposure caused treatment related increases of any tumor type in males or females or in the number of tumor bearing rats in the exposed groups compared to controls. In 2-year carcinogenicity bioassays conducted by the National Toxicology Program, rats and mice (50/sex/group) received 0, 500, 1000, or 2000 mg/kg/day and 0, 150, or 300 mg/kg/day, respectively, via oral gavage. In male or female rats and female mice there was no significant difference in tumor incidence when compared to the control groups. In male mice there was a positive association between styrene dose and the incidence of the combination of adenomas and carcinomas of the lung. However, due to the high background incidence of this tumor type in male mice, no firm conclusion was drawn for the carcinogenicity. In a study that administered styrene (125 and 250 ppm) in the drinking water of rats for 2 years, there was no evidence of carcinogenicity. In other chronic inhalation toxicity studies, rats were exposed to styrene via inhalation at concentrations up to 300 ppm for 4-6 hours/day, 5 days/week, for 1 year or up to 1000 ppm for 2 years. There was a slightly increased, but not statistically significant, incidence of mammary tumors in the females in both studies. Because the control incidence was also high and there was no dose-response relationship the studies were considered to be negative.

Carbon Black: The International Agency for Research on Cancer (IARC) has determined that carbon black is a class 2B known animal and possible human carcinogen by the route of inhalation. Rats exposed to high doses of carbon black by inhalation developed statistically significant increases in lung fibrosis and lung tumors. Carbon Black: The scientific discussions about the carcinogenic potential of inorganic low solubility particles (fine dust) including carbon black has not been concluded. Many inhalation toxicologists believe the lung fibrosis and tumors that developed in rats following exposure to carbon black result from massive accumulation of small dust particles that overwhelm the clearance mechanism

and produce what is termed "lung overload," an effect considered to be rat specific and not relevant to humans. In addition, based on epidemiological studies, no causal link between carbon black exposure and cancer risk in humans has been demonstrated.

12. ECOLOGICAL INFORMATION

ECOLOGICAL INFORMATION: No data – This material does not harm the environment, but is not biodegradable.

13. DISPOSAL CONSIDERATIONS

WASTE DISPOSAL METHOD: Dispose of contents/containers in accordance with local, regional, national and international regulations.

14. TRANSPORT INFORMATION

U.S. DEPARTMENT OF TRANSPORTATION
Not regulated

15. REGULATORY INFORMATION

U.S. FEDERAL REGULATIONS

TSCA (TOXIC SUBSTANCE CONTROL ACT): All ingredients are either exempt or listed on the TSCA Chemical Substance Inventory.

SARA (313) Title III of the Superfund Amendments and Reauthorization Act of 1986 (SARA):
This product contains a chemical or chemicals that are subject to the reporting requirements of the Act and Title 40 of the Code of Federal Regulations, Part 372.

Chemical Name	CAS Number	Weight %	CERCLA/SARA 313 de minimus:
Styrene	100-42-5	0.1 - 0.3	0.1

Canada - WHMIS Classification:
This product has been classified in accordance with the hazard criteria of the Controlled Products Regulations (CPR) and the SDS contains all the information required by the CPR. Unless noted below, this product is non-controlled. Some classifications may not apply to the entire product.

Chemical Name	Weight %	WHMIS hazard class:
Styrene, 100-42-5	0.1 - 0.3	0.1%; English Item 1473; French Item 1508 B2; D2A; F

California Proposition 65:
Components in this product known to the State of California to cause cancer and/or reproductive effects, are listed below:

Chemical Name	Weight %	California Proposition 65:
Carbon black,1333-86-4	0.3-1.0	Listed: February 21, 2003 Carcinogenic. (airborne, unbound particles of Respirable size)
Acrylonitrile, 107-13-1	0.01 - 0.10	Type of Toxicity: cancer

16. OTHER INFORMATION

ADDITIONAL INFORMATION
MEDICAL USE: CAUTION – Do not use in medical applications involving permanent implantation in the human body.

This Safety Data Sheet and the information it contains is offered to you in good faith as accurate. We have reviewed any information contained in this data sheet which we received from sources outside our company. We believe this information to be correct but cannot guarantee its accuracy or completeness. Health and safety precaution in this data sheet may not be adequate for all individuals and/or situations. It is the user's responsibility to evaluate and use this product safely and to comply with all applicable laws and regulations. No statement made in the data sheet shall be construed as a permission or recommendation for the use of any product in a manner that may infringe existing patents. No warranty is made, either expressed or implied.